# CONTENTS — A through G

**THE FORMATION PROCESS OF ADHERING AND CONSORTING COMPOUND CHONDRULES INFERRED FROM THEIR PETROLOGY AND MAJOR-ELEMENT COMPOSITION.** T. Akaki and T. Nakamura. Department of Earth and Planetary Science, Faculty of Science, Kyushu University, Hakozaki, Fukuoka 812-8581, Japan

**Introduction:** The mineralogical and isotopic properties of compound chondrules constrain the physicochemical conditions of chondrule formation events. The constraint cannot be obtained from the study of single chondrules. Therefore, we continue to study compound chondrules based on their major element concentration and oxygen isotopic composition.

Each compound chondrule was classified into three groups: adhering, consorting, and enveloping types according to the criteria given in [1]. The adhering and consorting types consist of two chondrules fused together, whereas the enveloping type has a core chondrule within a host chondrule. We have reported, from the electron microprobe analysis of the enveloping types that the host chondrules tend to have higher FeO and lower $Al_2O_3$ and CaO contents than the core chondrules [2]. The results are consistent with the enveloping-type formation model [1], which envisages the enveloping type was formed by a flash melting of a porous Fe-rich dust clump on a preexisting core chondrule. Thus, enveloping types need two times of heating for the formation.

On the other hand, it is less clear how the non-enveloping (adhering and consorting) type compound chondrules formed. They are presumed to have formed via collisions between totally or partially molten particles in the early solar nebula [3, 4]. However, this random collision model requires either much longer molten period that would lead to evaporation of large amounts of volatile elements such as Na and S or implausibly high mean density of chondrules in the nebula [1, 5]. Here, we report the results of further investigation of 29 non-enveloping compound chondrules from two CV3 chondrites (Allende CV3 and Axtell CV3) and three LL3 chondrites (Y790448 LL3.2, Y791558 LL3.1 and Y793596 LL3.0) based on their petrologic features and major element compositions.

**Results and Discussion:** The textural types of chondrules were classified into two groups: non-porphyritic types (those that formed by complete melting; C, RP, BP, BO) and porphyritic types (PO, POP, PPO, PP and GOP) [1]. According to this scheme, 29 non-enveloping compound chondrules can be classified into three categories: 12 pairs are non-porphyritic-non-porphyritic, 5 pairs are porphyritic-porphyritic, and 12 pairs are mixed. Each chondrule consisting compound chondrules were classified to primary chondrule and secondary one according to the criteria given in [1]. Primary chondrules are those that were rigid enough to retain their original shape during the formation of compound chondrules. On the other hand, secondary chondrules are those that had viscosities low enough to allow them to conform to the shape of the boundary to the primary.

Based on the petrologic observation, some non-enveloping compound chondrules, especially those having porphyritic chondrule, show clear evidence indicating the formation by a collision between two chondrules. For example in Fig. 1, it is composed of a PO chondrule and a BO chondrule. The olivine shell of the BO chondrule has been crushed and bended towards the center of the BO chondrule at the boundary to the PO chondrule (marked by arrows in Fig. 1). The texture indicates that the BO chondrule collided with the PO one, at the time when the BO chondrule had solid shell but its inner portion was still melted.

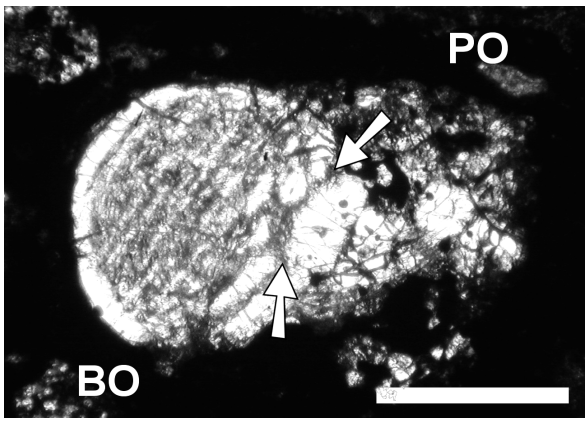


Fig. 1 Compound chondrule in the Allende CV3 chondrite composed of a barred olivine chondrule and a porphyritic olivine chondrule. Scale bar is 300 μm in length.

Next, we summarize the petrologic features of 12 non-porphyritic compound chondrules (6 BO-BO pairs and 6 RP-RP pairs). First, the constituent minerals of secondary chondrules such as barred olivine or radial pyroxene grow perpendicular to the surface of the

primary chondrules (Fig. 2). This indicates that the surface of the primary chondrules served as a nucleation site for barred olivine or pyroxene crystallizing from the melt of the secondary chondrule. Furthermore, the olivine or pyroxene bars in both primary and secondary chondrules tend to be in the same orientation. This striking feature is inconsistent with the formation process via collisions. Because a secondary chondrule melt collides with a primary chondrule from arbitrary direction, which is unrelated to the direction of mafic mineral bars in the primary, and then, the barred mafic minerals grow in the secondary melt on the surface of the primary chondrule. Therefore, the orientation of mafic mineral bars in the secondary does not need to be the same as that in the primary in the collision event.

The inconsistency with the formation process via collision event for non-porphyritic compound chondrules is also deduced based on their chemical compositions. In all 12 non-porphyritic compound chondrules (6 BO-BO pairs and 6 RP-RP pairs), the barred olivines or radial pyroxenes in secondaries tend to have slightly higher FeO contents than those in primaries. FeO enrichment of the secondary requires a high FeO concentration in a pre-chondrule melt of the secondary. During chondrule formation, FeO-rich and poor melts must have been heated to the same temperature and cooled in a similar way. Then, why only FeO-rich melt becomes to be the secondary? To explain this in a collision process, FeO-rich chondrule melt requires a longer time to solidify. In order to examine this condition, we evaluated the crystallization temperature of primary and secondary chondrules based on their bulk chemical compositions using a phase diagram of $SiO_2$-FeO-MgO [6]. The result showed that, in spite of differences in major element concentrations, liquidus temperature of primaries and secondaries is roughly similar to each other. Because the $SiO_2$ content is more effective on the liquidus temperature rather than the FeO content, and the difference of the $SiO_2$ contents between the primaries and the secondaries is small. Therefore, FeO-rich melt does not always solidify late and thus this condition is not verified.

Here, the formation process of non-enveloping compound chondrule is summarized. Some compound chondrules, especially having a porphyritic chondrule, were formed by a collision between totally or partially molten two chondrules. On the other hand, it cannot be made clear whether the non-porphyritic compounds were formed by a collision of two chondrules. We cannot argue further based solely on observations about the formation process of the non-porphyritic compounds, thus leave this issue in the future experiments for reproduction of compound chondrules.

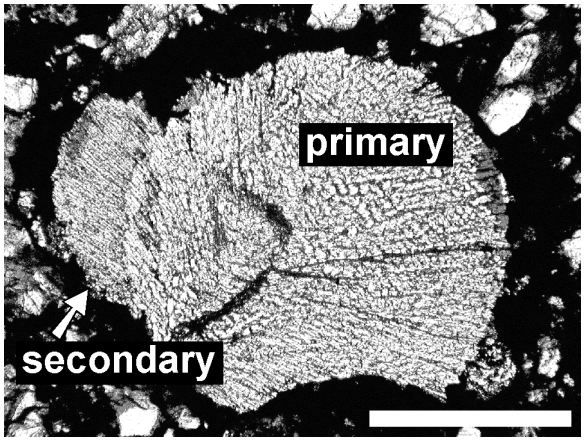


Fig. 2 Compound chondrule in the Y793596 LL3.0 chondrite composed of two radial pyroxene chondrules. Scale bar is 300 μm in length.

**References:** [1] Wasson *et al*. (1995) *Geochim. Cosmochim. Acta*. 59, 1847-1896. [2] Akaki and Nakamura (2002) Symp. *27th Antract. Meteorite, NIPR*, 1-3. [3] Lux *et al*. (1981) *Geochim. Cosmochim. Acta*. 45, 675-685. [4] Gooding and Keil (1981) *Meteoritics*. 16, 17-43. [5] Sekiya and Nakamura (1996) 20th *Proc. NIPR Symp. Antarct. Meteorites* 9, 208-217. [6] Bowen and Schairer (1935) *Amer. J. Sci.* 170, 151-217.

**THE PROSPECT OF HIGH-PRECISION PB ISOTOPIC DATING OF METEORITES.** Yuri Amelin, Geology Department, University of Toronto, and Geological Survey of Canada, 601 Booth St., Ottawa, ON, Canada, K1A 0E8 (yamelin@nrcan.gc.ca)

**Why Pb isotopes are now rarely used for dating meteorites:** From the classical studies by Patterson (1956) until the early 1980's, the Pb-Pb method remained the most widely used isotopic cosmochronometer. Subsequently, the use of the Pb-Pb method for dating meteorites declined, while the use of extinct nuclide chronometers increased, and now the systems based on short-lived nuclides are much more widely applied than Pb-Pb. Decreased utilization of the U-Pb system perhaps resulted from limitations to precision and accuracy commonly encountered in the earlier studies due to: U and Pb mobility, extensive contamination with terrestrial Pb, and the presence of excess radiogenic Pb of unknown origin. With these complications, it was rarely possible to obtain ages with a precision better than 5 to 10 m.y., and the accuracy of the dates was usually uncertain. This low precision severely limited the usefulness of the U-Pb method for studying the detailed chronology of the early solar system.

The techniques and methodology of terrestrial U-Pb geochronology have been greatly advanced over the past two decades. These new methods and concepts can be applied to cosmochronology in order to improve precision of the ages of meteorites and get better constrained age interpretations. Below I summarize some of the key issues of U-Pb geochronology and discuss their relevance to the studies of meteorites.

**The factors that control precision of Pb isotopic dates:** There are three main factors that limit the precision of a Pb-Pb isotope date: uncertainties related to common Pb correction, counting statistics, and uncertainty in correcting mass bias. Their relative contribution depends on the size of the sample, the concentrations of radiogenic Pb and common Pb, and uncertainty of mass bias. It is important to identify and deal with the biggest source of uncertainty first: for example, improving analytical precision and better control over mass bias would not significantly improve precision and accuracy of the age of a mineral that contains abundant common Pb with unknown isotopic composition.

**Importance of complete removal of common Pb:** Of all findings in U-Pb geochronology of the last 20-30 years, perhaps the most important one was the realization that only minerals that contain uranium but negligible common Pb are suitable for obtaining precise and interpretable dates. U-bearing minerals with negligible common Pb, such as zircon, monazite and baddeleyite in terrestrial rocks and Ca-phosphates and pyroxenes in meteorites, are the minerals of choice for dating, which yield precise and reproducible ages of geological processes.

There are two reasons why the negligible level of common Pb is important. First, it eliminates the major uncertainty in $^{207}Pb/^{206}Pb$ age calculations, using either model age or isochron approach. Second, it is much easier to recognize the patterns of multi-stage evolution in the systems containing radiogenic Pb only, than in the systems containing radiogenic Pb and common Pb mixed together.

The main step towards achieving low level of common Pb in analyses is choosing minerals that do no incorporate common Pb due to their structural properties and conditions of formation. Adhering phases rich in common Pb (e.g. chondrite matrix) are removed by a combination of air abrasion, ultrasonic agitation and acid leaching.

**Sensitivity:** The content of U in chondrites is low, about 10 ppb. Chondrules and CAIs have similar or only slightly higher U concentrations. As a result, the amount of radiogenic Pb produced in situ is low (ca. 10 ppb of radiogenic $^{206}Pb$ in a 4.56 Ga meteorite). An individual, relatively large, chondrule from a typical chondrite, with a weight of 1-10 mg, contains as little as ca. 10-100 picograms of radiogenic $^{206}Pb$. The amount of radiogenic Pb is further reduced by a factor of 2 to 5 by acid leaching, necessary for removing common Pb. This low content of Pb makes precise isotope analysis very sensitive to analytical blank and demanding to instrument sensitivity. Nevertheless, low electrometer noise and improved baseline stability of modern mass spectrometers, high ionization efficiency (total yield about 5-8%) achieved with the best available silica gel emitters, and low procedure blanks of about one picogram make precise analyses of samples containing about 20 pg or more of radiogenic $^{206}Pb$ possible. In more difficult cases, it may be necessary to combine several chondrules for each analysis in order to get a sufficient amount of Pb.

**Correction of mass bias** and its uncertainty becomes the main limiting factor for analyses of relatively large Pb samples (>50-100 pg) with low content of common Pb. There are several ways to tackle this problem. A conventional approach (applying fractionation factor determined from analysis of a standard to the analyses of geological samples) has limited precision of about 0.03-0.06% per amu, and involves an

uncertainty related to the presence of a residue of the sample matrix, which can shift the mass bias. Using a double spike is a much more accurate and precise way of correcting mass bias, however the double spike procedures developed so far are optimized for analysis of large amounts (several nanograms or more ) of common Pb, involve spiking with $^{204}$Pb and $^{207}$Pb (which are unacceptable for radiogenic Pb analysis because of extremely high sensitivity to memory and cross-contamination), and require splitting of samples for double spiking. These procedures in their present form are not suitable for analysis of sub-picomole quantities of radiogenic Pb. A double-spiking procedure using $^{202}$Pb-$^{205}$Pb has to be developed and optimized for analysis of radiogenic Pb, in order to achieve the best possible precision of Pb isotopic dating of meteorites.

**The uncertainty in the decay constants of uranium isotopes** is an additional factor that can contribute significantly to the total error of Pb-Pb dates. The question of whether the decay constant errors to be included in the total errors of the dates is not trivial. If Pb isotopic dates are compared to the dates obtained with another long-lived nuclide chronometer, then the decay constant errors should obviously be included for both isotopic chronometers. In determination of age intervals with the Pb-Pb method within a relatively short period of the early solar system evolution (ca. 4.57-4.40 Ga), the errors of decay constants almost completely cancel out, and should be excluded from the uncertainty of age intervals. However, decay constant errors must be considered in all other interpretations.

**The peril of multi-stage evolution:** Two-stage or three-stage evolution of U-Pb isotopic systems can produce linear arrays in Pb-Pb isochron coordinates (Gale and Mussett 1973). If these arrays are interpreted as single-stage (conventional) isochrons, then severely biased dates can be obtained. Possible redistribution of Pb during chondrite metamorphism, which leads to anomalously old Pb-Pb dates, has been discussed by Tera and Carlson (1999). It is important to note that anomalously old Pb-Pb dates can only be observed if a mineral has gained ancient radiogenic Pb. Minerals (e.g. zircon) that do not accommodate Pb during their growth typically do not gain Pb during secondary processes either, unless their lattice is damaged by radiation or another factor. The possible multi-stage evolution for such minerals therefore reduces to ancient Pb-loss, which leads to lower $^{207}$Pb/$^{206}$Pb apparent dates. For a set of mineral grains (or chondrules, CAIs, etc) that experienced ancient Pb-loss during the same secondary process, the $^{207}$Pb/$^{206}$Pb apparent date would vary with the fraction of radiogenic Pb lost. The variations in radiogenic $^{207}$Pb/$^{206}$Pb is therefore an indicator of multi-stage evolution. The consistency of radiogenic $^{207}$Pb/$^{206}$Pb, on the other hand, strongly suggests single-stage evolution, because there are many factors (e.g., grain size, mineral composition, fracturing) that make metamorphic or alteration-related Pb-loss vary, and there is no process known to stabilize the degree of secondary Pb-loss.

There is still a hypothetical possibility that the studied mineral could gain radiogenic Pb released from other minerals. Thus the best choice for dating are the minerals or mineral aggregates (CAIs, chondrules) with very high $^{238}$U/$^{204}$Pb, extracted from a medium with much lower $^{238}$U/$^{204}$Pb. Any mobile radiogenic Pb in such cases would be mixed with common Pb and would be detected by elevated $^{204}$Pb content. This emphasizes, once again, the importance of using only minerals with negligible common Pb for Pb-Pb dating. In Pb-Pb dating of chondrules and CAIs, the condition of much higher $^{238}$U/$^{204}$Pb in the studied mineral aggregate compared to its surrounding is usually satisfied. This is not always the case for achondrites (e.g., eucrites), which can have fairly high $^{238}$U/$^{204}$Pb in the whole rock. In the studies of such meteorites, it is important to identify and analyze all minerals – carriers of uranium and radiogenic Pb.

**Pb-Pb vs. U-Pb:** CAIs and chondrules are unfortunately not as resistant to acid attack as zircon. Intensive acid leaching, which is necessary for common Pb removal, is likely to disturb the ratio of U to radiogenic Pb in these objects, making accurate determination of $^{238}$U-$^{206}$Pb* and $^{235}$U-$^{207}$Pb* dates difficult or impossible. The capability of the U-Pb system to determine open-system behaviour, and the possibility of calculating both ages in a two-stage model, are therefore lost. The dates based on the ratio of radiogenic Pb isotopes are, however, not disrupted by leaching.

**Interpretation of Pb-Pb isotopic dates:** The $^{207}$Pb*/$^{206}$Pb* dates can yield either the timing of mineral formation, or the timing of cessation of Pb and U migration. An extensive set of experimental data for thermal diffusion of Pb and U in minerals is now available for interpretation of Pb isotopic dates in terms of diffusion models. The other mechanisms of U-Pb isotopic resetting: aqueous alteration and shock metamorphism, may be just as important as thermal metamorphism, but experimental data about redistribution of Pb and U in these processes are not available yet.

**References:** [1] Patterson C.C. (1956) *Geochim. Cosmochim. Acta 10,* 230-237. [2] Gale N. H. and Mussett A.E. (1973), *Rev. Geophys. Space Phys., 11*, 27-86. [3] Tera F. and Carlson R.W. (1999) *Geochim. Cosmochim. Acta 63,* 1877-1889.

# Evolution of UV-Irradiated Protoplanetary Disks

*John Bally*

Department of Astrophysical and Planetary Sciences
Center for Astrophysics and Space Astronomy
Center for Astrobiology
University of Colorado, Boulder
bally@casa.colorado.edu

Stars and planetary systems form from the gravitational collapse and fragmentation of dense and turbulent cores in giant molecular clouds[1] (GMCs). Typical GMCs contain around 100,000 times the mass of Sun and are 10 - 100 light years in extent.

Observations show that the majority (~90%) of all stars in the sky form in dense clusters containing from tens to many thousands of stars. However, most forming clusters are transient gravitationally unbound entities. They expand and dissolve on a time-scale of several million years, comparable to the time required for planet formation. In forming clusters, the mean separation between stars can be less than 1,000 AU.

Young clusters frequently contain massive stars which produce powerful stellar winds, intense UV radiation, and explode as supernovae soon after birth. These massive stars carve bubbles of hydrogen plasma (HII regions) in their surroundings by ionizing their parent molecular clouds. HII regions such as the Orion Nebula[2], one of the nearest and best studied celestial objects, are signposts of on-going star and planet formation. These clustered star forming environments and their massive stars pose hazards to nascent protoplanetary disks.

Protoplanetary disks around young stars in clusters are subjected to external dynamical perturbations by close-passages of sibling stars and high rates of UV-radiation induced mass loss. These processes can rapidly destroy the outer parts of protoplanetary disks. Observations of young disks surrounding low-mass stars in the Orion Nebula show that many disks lose the equivalent of Jupiter's mass every 10,000 years.

Nevertheless, HII regions may be ideal sites for planetary system birth. The central parts of most disks (to radii of tens of AU from the central star) can survive photo-erosion for many millions of years, longer than the survival time of unbound clusters and their most massive stars. Additionally, recent models show that the removal of light gases increases the concentration of heavy elements, rocks, and ices. UV radiation may facilitate the first steps toward planet formation. I will present new models in which photo-ablation, settling, and radial migration of millimeter to meter-scale solids promote rapid growth of planetisimals.

I will review recent observations of protoplanetary disks in the Orion Nebula. I will present preliminary results of calculations showing triggered planetisimal formation in UV-irradiated disks.

## REFERENCES:

1. *Physical Conditions in Regions of Star Formation* Neal J. Evans II, 1999, Annual Reviews of Astronomy and Astrophysics, **37**, 311-362

2. *The Orion Nebula and its Associated Population* C. R. O'Dell, 2001, Annual Reviews of Astronomy and Astrophysics, **39**, 99-136

# A MODEL FOR THE FORMATION OF E CHONDRITES

Milton Blander[1] and Arthur Pelton[2]
[1] Quest Research, 1004 E 167th Place, South Holland, IL 60473-3114
[2] Ecole Polytechnique, CP6079 Succ. Centre-Ville, Montreal (Quebec), Canada

## ABSTRACT

The purpose of this paper is to demonstrate that the formation of E chondrites from a gas of solar composition is consistant with the concepts of the "Constrained Equilibrium Theory" (Blander and Katz, 1967) which block the formation of metallic iron alloys and also forms metastable silicate liquid condensates which crystallize well below liquidus temperatures by more than 400 degrees or more. Constraints on iron condensation can be expected in terms of nucleation theories and leads to supersaturation of gaseous Fe which creates high iron chemical activities which increase as the temperatures decreases. This leads to the formation of FeO at activities much higher than the small equilibrium activities through the reaction

$$Fe + H_2O \leftrightarrow FeO + H_2$$

This reaction allowed us to determine from the FeO activities in Semarkona the relative temperatures of crystallization of all chondrule types which in turn allows us to calculate the compositions of each chondrule type accurately by the FACT computer program. All but one chondrule type theoretical calculations of compositions matched the measured chondrule compositions.within the accuracy of the data. The one chondrule type which did not match the composition probably has inaccurately measured data on the relative amounts of type IA and IAB-IB.

Our calculation proved that the concepts of the "Constrained Equilibrium Theory" had major roles in forming Semarkona, and provides the probability that similar applications can use them for other classes of of meteorites. Our theory is amazingly simpler and more accurate than so-called theories now believed. In this paper we will determine that the properties of E chondrules which are very different from ordinary chondrites, is consistent with the concept of the "Constrained Equilibrium Theory".

In the formation of metastable silicate droplets the FeO concentrations are higher than equilibrium concentrations (about 0.1 wt%). We calculate from data of Wiik and Keil (Keil, 1968) and Schneider et al. (2002) that the maximum concentration of FeO in type EH chondrules are 8.41 wt% and 1.78 wt% for type EL chondrules. These quantities are deduced by data on chemical analyses by Wiik and by Keil on measurements calculated from modal and mineral compositions of Fe. In addition, we also used the data of Schneider et al. on the average compositions of chondrules. Since the data is from different chondrule types (those known in 1968 by Keil and type 3 chondrules by Schneider) there will be some uncertainties. The differences do not seem to be very large.

At these compositions, because of the high concentrations of Fe in the nebula, the high temperatures for E chondrites at these pressures (1 atmosphere) and a large supersaturation of

iron, can lead to a high probability for the condensation of iron as Fe-Ni alloys as suggested by nucleation theory. The reduction starts at compositions of FeO of 8.70 wt% for EH chondrules and 1.78 wt% for EL chondrules. Our calculated reduction of FeO to unalloyed Fe is 7.85 wt% of FeO for EH chondrules and 1.03 wt% FeO for EL chondrules. The average residual iron oxide in the data of Schneider et al. is 0.85 wt% for EH chondrules and 0.75 for EL chondrules. Since the precursor chondrule droplets crystallize as the temperature decreases, the first crystals formed would freeze in a relatively high FeO droplet because the reduction is not likely to be rapid because the reducing hydrogen has a small solubility in the droplet. The highest FeO contents measured by Schneider et al. is 4.6 wt% for EH3 chondrules and 1.9 wt% for EL3 chondrules. The other chondrules measured were all lower than these two numbers and the lowest ones were slightly larger than the equilibrium composition of a little less than 0.1 wt% FeO. The lower the FeO content of a chondrule suggests a lower temperature of crystallization.

Our calculations and observations explain the observations by Weisberg et al. (1994) in which the environment forms relatively high FeO in the precursor droplets (stage 1) and the environment changes when Fe-Ni alloys precipitate and FeO reduces to Fe (stage 2). In our work, this is not a change of oxidation but is a change allowing metallic iron to condense as mostly Fe-Ni alloys and iron forms in the reduction of FeO. The chondrules are never (or seldom) reduced to equilibrium compositions of FeO in the minerals.

Three of the four compositions of E chondrites chemically analyzed by Jarosewich (1990) leads to ratios of $MgO/SiO_2$, $CaO/SiO_2$ and $Al_2O_3/SiO_2$ which are smaller than expected in a solar composition. Our calculations on removal of some of the condensates suggests a loss of a large fraction of the condensates possibly by a wind (Shu, 1996) or, more likely, if close to the sun, by gravitational movement of a large fraction of the condensates toward the sun.

**OXYGEN ISOTOPIC DIFFUSION AND EXCHANGE EXPERIMENTS ON OLIVINE AND CHONDRULE MELTS: PRELIMINARY RESULTS.** J. S. Boesenberg[1,2], R. H. Hewins[2] and M. Chaussidon[3] [1]Earth and Planetary Sciences, American Museum of Natural History, New York, NY 10024 (bosenberg@amnh.org), [2]Geological Sciences, Rutgers University, Busch Campus, Piscataway, NJ 08854, [3]CPRG-CNRS BP20, 54501 Vandoeuvre-les-Nancy, France.

**Introduction:** Chondrules are thought to have formed within hours to days based on textural features and zoning profiles (Fe-Mg) in olivines of experimentally produced chondrules [1, 2]. The diffusivity of oxygen in olivine is roughly four orders of magnitude slower than Fe-Mg in the temperature range chondrules likely formed (1400ºC-1900ºC) [3, 4, 5]. Because of these differences in diffusion rates, oxygen isotopic experiments were run in a vacuum furnace 1) to explore the oxygen isotopic exchange kinetics during chondrule formation, 2) to determine over what timescales chondrule formation could occur based on O-isotopic exchange rates and 3) to determine to what extent the isotopic composition of the solar gas at nebular pressures could alter the initial O-isotopic composition of the chondrule or its components. Isotopically distinct components were run and the components were 1) chondrule melt and olivine, 2) chondrule melt and CO gas and 3) olivine and CO gas.

**Chondrule melt-olivine exchange:** Refractory solids in chondrites, such as olivine, tend to be $^{16}$O-rich, possibly because they equilibrated with a silicate-enriched nebular gas at high temperature, and exchanged oxygen during melting [6]. Chondrule relict forsteritic olivine is $^{16}$O-rich in ordinary chondrites [7, 8] and mildly enriched in the carbonaceous chondrites [9]. Typical melt-grown chondrule olivine is moderately heterogeneous, with a 3-4‰ variation [9]. This variation might be explained by chondrule open-system behavior, or by the partial equilibration of relict olivine with the melt. A recent study by [10] seems to support the former rather than latter explanation. [10] found that olivine within two chondrules from the Mokoia CV3 carbonaceous chondrite have extreme oxygen isotopic heterogeneity ranging from (-50,-50) to (1,3), while their Fe-Mg compositions remain constant. No relict grains were detected.

The first set of experiments in this study explore the variations seen by [10] and their possible explanations. Eagle Station (ES) olivine (-7, -3 ‰) was mixed with an iron-rich IIAB chondrule melt analogue (isotopically close to terrestrial mantle) and placed in a vacuum furnace at temperatures of 1300ºC to 1515ºC and pressures of ~$10^{-3}$ torr. Although the experiments were run, ion microprobe and electron microprobe analysis are only partially complete at the writing of this abstract (Aug 2004). Our preliminary results from these experiments are below.

Following analysis, exchange rates between the IIAB melt and relict olivine will be determined and the likely paths of diffusion will be explored. Oxygen isotopic diffusion rates within olivine will be quantified and compared against Fe-Mg diffusion rates to investigate possible relict grain and chondrule histories. The thermal history required to erase the exotic oxygen signature may be within the range plausible for chondrule formation, or the ES signature may persist in some relict cores until evaporation effects, such as isotopic mass fractionation, become apparent.

**Chondrule melt-gas exchange:** [11, 12] developed the idea that nebular solids were $^{16}$O-rich when primitive and became $^{16}$O-poor by processing, especially during chondrule formation. [13] showed that 50% exchange of oxygen occurs between silicate and a $H_2/H_2O$ gas mixture after only 5 minutes of melting at one atmosphere. [13] argued that at nebular pressures (~$10^{-2}$ to $10^{-5}$ torr) 50% exchange could take 10 hours, depending on surface kinetics and exchange probability. These times might be consistent with the textural and Fe-Mg zoning experiments of [1] and [2].

The major oxygen-bearing gaseous species in the early solar nebula at high temperature (~1300 - 1600°C) is carbon monoxide (~50-60 vol%) [14]. For the experiments, isotopically labeled, $^{16}$O-enriched carbon monoxide ($C^{16}O$, +200 ‰ in $^{16}$O) gas at pressures between $10^{-2}$ to $10^{-3}$ torr were reacted with the IIAB chondrule melt analogue both above and below its liquidus (1504°C) for various times. Exchange rates between the IIAB melt and gas will be determined. The enormous contrast in oxygen isotopic composition between the gas and melt should make exchange easy to detect, and swamp any evaporation or contamination effects (the largest contamination is the possible exchange between the experimental charge and the alumina furnace muffle tube).

**Olivine-gas exchange:** Relict olivines are uncommon in most chondrules and are thought to have formed during condensation or around other stars, being incorporated into chondrules shortly after the flash heating event. Relicts are recognized by their high mg# and $^{16}$O-rich composition. Nearly all relict olivines plot along the slope one line in the three isotope oxygen diagram. Debate still continues concerning whether relicts (or other materials along this trend) result from mass dependent or independent fractionation [11, 15]. Perhaps, next month, when the Genesis mission returns with its payload of solar wind trapped particles this debate will begin to be resolved.

Terrestrial olivine spheres, purchased from a jeweler (Spheres were used to minimize problems with calculating crystal surface area or crystallographic orientation.) were reacted with the labeled $C^{16}O$ gas at 1500°C and 1400°C for up to four hours in the vacuum furnace. Diffusion rates will be calculated for the olivines three crystallographic axes.

**Experimental Procedure:** Charges were placed onto Pt or Re wire loops and suspended in a heavily modified Deltech vertical muffle tube furnace, which was converted into the presently unique "Angry Mountain" vacuum furnace. The furnace consists of a standard alumina 1.75 inch diameter muffle tube with customized stainless steel KF (Kwik flange) adapters bonded to either end using a ceramic-to-metal brazing technique (Brazing completed by Omley Industries - Grants Pass, Oregon). The KF adapters allow access to the sample from above and attach to turbo and mechanical pumps below. The experiments were run at pressures of $10^{-2}$-$10^{-3}$ torr. The maximum attainable vacuum is 8 x $10^{-7}$ torr near room temperature or 3 x $10^{-4}$ at 1550°C. Vacuum measurements were made in a cold (50°C) region of the furnace and recalculated for the temperature experienced by the sample. Vacuum gauge pressure readings were recorded by computer continuously throughout the experiment. Argon and/or CO gas was bled into the furnace at flowrates of ~$10^{-4}$ liters/min. through a gas valve. Argon was added for 30 minutes preceding each experiment to minimize atmospheric oxygen contamination. Because of equipment limitations, drop quenching is not possible in this furnace. Quenching is achieved by removing the sample from the furnace hotspot. Therefore, quench products, such as melt-grown olivines, are made.

**Preliminary results and discussion of chondrule melt-olivine exchange experiments:** General observations made of the data indicate that many of relict olivine cores remained isotopically unmodified and plot near previously published analyses of ES [16]. In short duration runs, the glass, which plots on the terrestrial fractionation line, appears to have a composition near $\delta^{18}O$~15. The melt grown olivines have isotopic compositions more $^{16}O$-rich than the original melt. Their compositions, which vary by duration and/or temperature, seem to reflect growth from a modified melt in which dissolved ES olivine has contributed to the isotopic composition of the melt. Relict olivines in the short duration runs do not appear to have diffusional profiles at the 5 µm spot size of the ionprobe. In the long duration runs (64-128 minutes), diffusional profiles are present, but have not yet been analyzed in detail. Most of the analyses plot on slopes of ~0.8 indicating mixing between the respective isotopic reservoirs.

In the high temperature (1500°C and 1515°C), short duration runs, the reaction of olivine core compositions with the melt is minimal. Pronounced reaction can be seen at a duration of 32 minutes, with the cores being distinctly 5-6‰ heavier than ES. The liquidus temperature of the analogue melt was determined to be 1504°C. ES olivine has a melting temperature over 1800°C. At temperatures exceeding the liquidus of the melt, the rate of dissolution of the olivine into the melt appears to be only slightly exceeded by the rate of oxygen diffusion into the crystal.

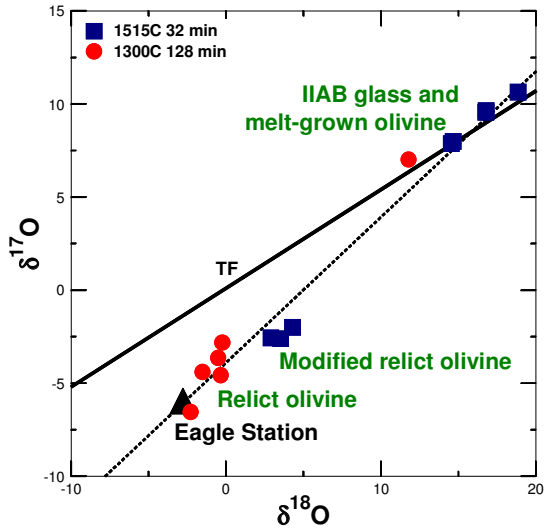


Both long duration (32 and 64 minutes) 1400°C runs have olivine relict cores which appear to have been modified. The shorter run contains more extreme compositional differences between the melt and olivine relicts.

The low temperature runs (1300°C) contain little melt. The melt analogue is made from oxides and not fused powdered glass. It appears that the relict ES olivine is reacting with individual oxide grains to variable degrees, resulting is very disparate and unpredictable compositions.

**References:** [1] Jones R. H. and Lofgren G. E. (1993) *Meteoritics* **28**, 213-221. [2] Weinbruch S., Buttner H., Rosenhauer M., and Hewins R. H. (1998) *MaPS* **33**, 65-74. [3] Ryerson, F. J. Durham W.B., Cherniak D. J. and Lanford W. A. (1989) *JGR.* **94**, 4105-4118. [4] Gerard O. and Jaoul O. (1989 *JGR.* **94**, 4119-4128. [5] Yurimoto H., Morioka M. and Nagasawa H. (1992) *Geochem J.* **26**, 181-188. [6] Cassen P. (2000) *LPSC* **XXXI,** #1141 (CD-ROM). [7] Saxton J. M., Lyon I. C., Turner G. (1998 *MaPS* **33**, 1017-1027. [8] Sears D. W. G., Lyon I., Saxton J. and Turner G. (1998) *MaPS* **33**, 1029-1032. [9] Leshin L. A., McKeegan K. D., Engrand C., Zanda B., Bourot-Denise M., and Hewins R. H. (1998) *MaPS* **33**, A93-A94. [10] Jones R. H., Leshin L. A., Guan Y., Sharp Z. D., Durakiewicz T. and Schilk A. J. (2004) *GCA* **68**, 3423-3438. [11] Clayton R. N., Grossman L., Mayeda T. K. (1973) *Science* **182**, 485-488. [12] Clayton R. N., Onuma N., Mayeda, T. K. (1976) *EPSL* **30**, 10-18. [13] Yu Y., Hewins R. H., Clayton R. N., and Mayeda T. K. (1995) *GCA* **59**, 2095-2104. [14] Ghiorso M. S. (1994) *GCA* 58, 5489-5501. [15] Thiemens M. H.(1996) In *Chondrules and the Protoplanetary Disk* (eds. R. H. Hewins, R. H. Jones and E. R. D. Scott), Cambridge University Press, 107-118. [16] Clayton R. N. and Mayeda T. K. (1978) *EPSL* **40**, 168-174.

**THE THREE-DIMENSIONALITY OF SPIRAL SHOCKS IN DISKS: DID CHONDRULES CATCH A BREAKING WAVE?** A. C. Boley[1], R. H. Durisen[2], M. K. Pickett[3], [1]Dept. of Astronomy, Indiana University (acboley@astro.indiana.edu), [2]Dept. of Astronomy, Indiana University (durisen@astro.indiana.edu), [3]Dept. of Chemistry & Physics, Purdue University Calumet (pickett@astro.calumet.purdue.edu)

**Introduction:** It is becoming evident that the thermal processing of chondrules occurred in shocks within the Solar Nebula. One-dimensional shock calculations with radiative physics have shown that, for shock speeds greater than about 7 km/s, flash melting of chondrule precursors by frictional drag heating, followed by the immersion of the chondrules in the slowly cooling post-shock gas, produces the requisite rapid cooling rates above the liquidus and subsequent moderate cooling rates during crystallization [1]. Wood [2] suggested that spiral arms in the Solar Nebula could be responsible for these shocks. Gravitational instabilities (GIs) in disks can produce transient spiral waves in the inner disk due to dense patterns or clumps in the outer disk and are the most promising mechanism for generating chondrule-producing shocks [3]. This can process copious amounts of material in the 2 to 3 AU region, and the transient nature of the GI induced waves may keep the arms from processing too much material, or providing too many heating events.

Although 3D hydrodynamics simulations [4] have demonstrated that transient GI features produce strong enough midplane shocks to form chondrules, spiral shocks in vertically stratified disks are intrinsically three-dimensional, and shock strengths vary with height [5]. Moreover, in a disk, compressions caused by a spiral perturbation can produce hydraulic jumps. Martos and Cox [6] have already shown that partial hydraulic jumps occur in galactic disks when the otherwise isothermal equation of state (EOS) is stiffened by a magnetic field. Since the EOS in protoplanetary disks is not generally isothermal, compressions should cause jumps in them as well. These jumps create very complex structures that result in multiple locations of shock compressional heating plus significant transport and mixing of material radially and vertically. We use 3D numerical hydrodynamics simulations of disks to characterize spiral hydraulic/shock-jump (hs-jump) morphologies, their implications for chondrule heating events, and their importance to mixing.

**Hydraulic jumps:** A classical hydraulic jump, or bore, occurs in incompressible fluids, where the only way to reduce the kinetic energy of fluid elements coming into the wave is to convert it to gravitational potential energy or dissipate it by the generation of turbulence [7]. The compressible gas of a protoplanetary disk can also be collisionally and compressionally heated. The result is that 3D spiral waves in disks can be a mixture of a shock and a hydraulic jump. The cause of the jump in a compressible gas disk can be understood if one considers the EOS. For an isothermal shock in a non-self-gravitating disk, the pressure increases exactly as the density increases and hydrostatic equilibrium in the z-direction is not lost. No vertical jump occurs. However, if the shock is adiabatic, with $\gamma > 1$, the post-shock gas pressure increases more than the gas density and hydrostatic equilibrium is violated. The post-shock gas will expand in the direction of the largest pressure gradient, which is perpendicular to the plane of the disk. Disk self-gravity complicates this picture, but, for strong adiabatic shocks, jumps will still occur.

**Methods:** To produce spiral waves in disks we use the Pickett et al. [8] 3D hydrodynamics code. A localized, corotating $\cos(2\varphi)$ potential perturbation with maxima located around r = 4 AU is applied to an equilibrium disk model. The perturbation stimulates the growth of a two-armed spiral that extends from 4 AU into the inner disk. The disk is forced to cool at a constant rate to balance the heating due to shocks. Except for breaking waves at the surface, cooling allows the spiral arms to settle into a quasi-steady state, near the midplane, long enough for a fluid element at r = 2 AU to pass through both arms.

**Preliminary Results:** For the simulations in this Abstract, we scaled the High-Q disk of Pickett et al. [8] from an outer radius $R_{out}$= 40 AU to $R_{out}$ = 4.8 AU with $M_{disk}/M_{total}$ = 0.130. Although this probably puts too much mass in the inner Solar Nebula, the simulation demonstrates the 3D character of the spiral waves. Additionally, the densities and the changes in velocity, corrected for pitch angle, at 2 AU do overlap the range of interest for shock production of chondrules [1]. Figure 1 shows velocity vectors superposed on density contours for a cylindrical cross section at r = 2 AU. The spiral arms are propagating in the positive $\varphi$ direction and the gas is overtaking the pattern. Upon encountering the spiral arm, the gas is compressed and a jump immediately follows. The second peak and portions of the primary peak are due to jumping gas that passes through this cross section from larger r. Figure 2 shows the same cross section as in Figure 1 but with contours representing heating by artificial viscosity. The strongest heating occurs in a nearly vertical but somewhat concave shock along the trailing edge of the arm. Heating also takes place after the hs-jump at higher z.

The complex 3D gas motions and resulting radial movements are demonstrated in Figure 3. The velocity vectors in the r-z plane for 2AU $\times$ $\varphi$ = 3 AU indicate that the spiral arms transport and mix mass efficiently over a large $\Delta$r, approximately 0.4 to 0.5 AU or more. When inward moving material encounters the spiral wave it develops a morphology that is analogous to a

breaking wave. These waves are large, several tenths of an AU, and result in widespread shock heating at high disk altitudes. The arrow labeled "A" in Figure 3 shows where a wave of jumping gas is breaking onto the surface of the disk. As in Figure 2, heating contours are superposed onto the velocity field.

Once we have gained a suitable understanding of hs-jumps in a quasi-steady state and their role in producing breaking waves, we will investigate spiral perturbations in the fully developed self-gravitating turbulence of GI active disks [9].

**References:** [1] Desch, S. J., Connolly, H. C, Jr. (2002) Meteor. Planet. Sci., 37, 183. [2] Wood, J. A. (1996) Meteor. Planet. Sci., 31, 641. [3] Boss, A. P., Durisen, R. H. (2004) This Volume. [4] Boss, A. P. Lunar Planet. Sci. Conf. XXXI, #1084. [5] Pickett, B. K., Cassen, P., Durisen, R. H., Link, R. (2000) ApJ, 529, 1034-1053. [6] Martos, M. A., Cox, D. P. (1998) ApJ, 509, 703-716. [7] Massey, B. S. (1970) Mechanics of Fluids: 2nd Edition, Van Norstrand Reinhold Company, London. [8] Pickett, B. K., Meja, A. C., Durisen, R. H., Cassen, P. M., Berry, D. K., Link, R. P. (2003) ApJ, 590, 1060-1080. [9] Meja. A. C., Durisen, R. H., Pickett, M. K., Cai, K. (2004) astroph /0407037.

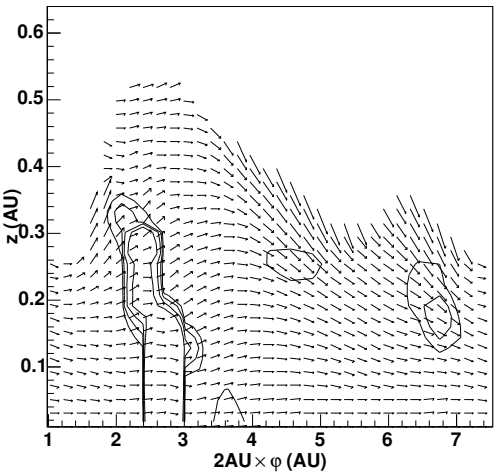


Fig. 2. Same as Fig. 1 except the contours now indicate regions of heating from artificial viscosity. The strongest heating occurs along the entire height of the disk at the trailing edge of the spiral arms. However, there are also regions of heating at higher z where gas is falling back onto the disk from a jump at larger r. The contours correspond to 1.15(-7), 2.31(-7), 4.61(-7), and 9.22(-7) erg/cc/s.

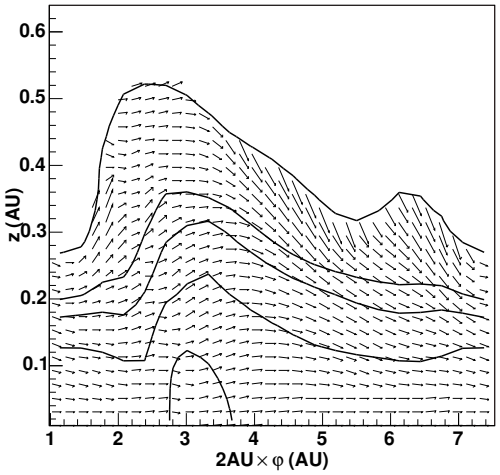


Fig. 1. Velocity vectors for a cylindrical cross section of the disk at r = 2 AU. Each component is scaled to its axis appropriately. Superposed onto the graph are density contours corresponding to 5.44(-12), 6.80(-10), 1.36(-9), 2.72(-9), and 5.44(-9) g/cc. Notice that immediately following the shock the gas is forced upwards in the z-direction.

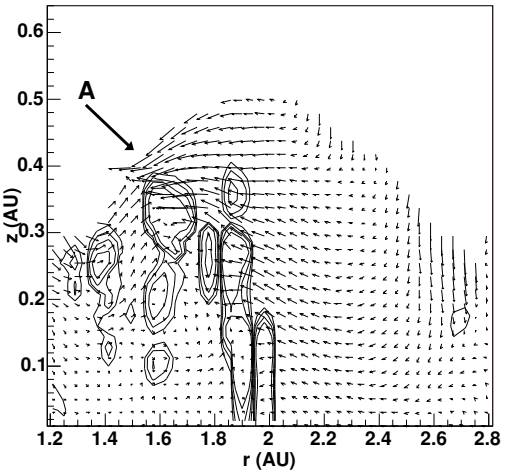


Fig. 3. Similar to Fig. 2 but for an r-z slice at 2AU × $\varphi$ = 3AU. Material is moved radially over large $\Delta$r and regions of very strong heating are present at high and moderate z. The "A" labels where a breaking wave is falling onto the disk; note the strong inflow in this region.

**SHOCK HEATING: ORIGIN OF SHOCK WAVES IN THE PROTOPLANETARY DISK.**
A. P. Boss[1], R. H. Durisen[2], [1]DTM, Carnegie Institution of Washington (boss@dtm.ciw.edu), [2]Dept. of Astronomy, Indiana University (durisen@astro.indiana.edu).

Finding an appropriate heat source for melting the chondrules that constitute the bulk of many primitive meteorites is perhaps the most outstanding problem in all of meteoritics [1]. The chondrule precursor dust grain aggregates appear to have been heated to the melting point through multiple flash heating events. Shock waves within the solar nebula are one possible means for accomplishing this. Such waves are able to melt suitable chondrule precursors provided that the shock waves move with respect to the precursor aggregates at a speed of about 7 km/sec [2]. However, a suitable mechanism for producing shock waves inside the solar nebula needs to be identified. Here we review the status of four different mechanisms which have been proposed as sources of such shock fronts. Wood [3] proposed that nebular spiral arms might be effective, a hypothesis which has been strongly supported by recent calculations of the evolution of gravitationally unstable disks. We shall see that Wood's mechanism appears to be the most likely source of the thermal processing of chondrules.

*Accretion shock:* Gas and dust grains falling onto the solar nebula from the presolar cloud must pass through the accretion shock at the surface of the nebula before being brought to rest inside the disk. The kinetic energy released during this process at all radii $< 15$ AU is more than sufficient to melt any dust grain. Pre-existing dust grains will be slowed down and heated by frictional gas drag [4]. However, it is unlikely that very many precursor dust aggregates of the needed size (mm-size or larger, for fluffy aggregates) could form in the relatively low density environment of the presolar cloud, or in even earlier phases of interstellar evolution. In addition, detailed calculations of the expected post-shock heating at 2 to 3 AU [5] have found that mass accretion rates onto the disk of at least $10^{-5}$ $M_\odot$ $yr^{-1}$ are necessary to produce melting of any infalling dust aggregates. Such high rates are not usually seen in young stars of solar mass.

*Infalling clumps:* It has also been suggested [6] that mass accretion onto the disk may have been punctuated by the infall of clumps of gas and dust whose impact with the disk accretion shock might have launched shock waves deep into the disk, down to where pre-existing dust aggregates could be thermally processed. However, detailed models of the clump impact process have found that observed clumps in collapsing protostars are much too low in mass to produce the desired strong shock waves [7].

*Bow shocks driven by planetesimals:* Once sizeable bodies have formed by collisional accumulation in the disk, they will create bow shocks in the disk gas, provided that they are moving at supersonic speeds with respect to the gas [8]. Detailed models of the process, which considered planetesimals 10 km to 1000 km in size, moving at speeds of 4 km $s^{-1}$ to 8 km $s^{-1}$ with respect to the gas, showed that only the 1000 km-size bodies moving at 8 km $s^{-1}$ produced bow shocks consistent with the melting of chondrule precursors [9]. Chondrule cooling rates could only be matched if the disk opacity was lower than expected for this early phase of disk evolution, however. This mechanism also requires the planetesimals to have significantly eccentric orbits, which is only likely to occur for planetesimals which are being driven by resonant gravitational interactions with a Jupiter-mass planet [10]. If Jupiter has already formed, then presumably planetesimals have also already formed throughout the asteroid region, perhaps making chondrule formation at this time too late.

*Spiral waves:* Finally, we turn to Wood's [3] suggested mechanism. Current models of the formation of gas giant planets, whether the mechanism is core accretion or disk instability, require the solar nebula to be at least marginally gravitationally unstable. Such a disk naturally becomes strongly nonaxisymmetric through the growth of spiral waves, which drive the evolution of the disk, whether or not they are able to form gas giant planets [11]. One common outcome of the evolution of such disks is the formation of strong, transient shock fronts in the inner disk, driven by spiral arms and clumps at greater distances [12]. The spiral pattern driven by clumps rotates at a speed governed by the Keplerian angular velocity at about 5 AU to 8 AU. As suggested by Wood [3], there can be a large difference in velocity between the spiral pattern and solid aggregates on Keplerian orbits at radii inside or outside that radius.

Figures 1 and 2 present the results of a new 3D radiative hydrodynamics model of an unstable disk. For one-armed ($m = 1$ modes) spiral density waves of the type seen in the midplane, the inner Lind-

blad resonance occurs at angular velocity $\Omega = \infty$, or zero radius. This means that a single clump can drive spiral density waves right down to the center of the solar nebula. The 3D model exhibits this behavior, showing the presence of a strong shock front between 2 and 3 AU. At that distance, the velocity difference between solids and the shock front should be on the order of 10 km $s^{-1}$, sufficient for melting chondrule precursor dust aggregates.

Multiple heating events are required to explain chondrule textures [13] and spiral density waves are clearly able to satisfy this constraint. It has also been pointed out that such a mechanism might produce *too* many heating events [14]. Global simulations of unstable disks integrated long enough for the gravitational instabilities to settle into an asymptotic turbulent behavior [15], as well as simulations like that in Figures 1 and 2, show, however, that nebula shock fronts with the required conditions (shock speed, and pre-shock and post-shock densities) are by no means a permanent feature. Rather, shocks which appear to have roughly the desired characteristics are transients in a chaotic environment. Future work needs to estimate how often such a disk is likely to produce a shock front suitable for chondrule formation.

Considering the problems that beset the three other suggested mechanisms, spiral waves [3] driven by gravitational instabilities seem to be the preferred mechanism for thermally processing the chondrule precursors.

**References:** [1] Hewins, R. H. (1996), in *Chondrules and the Protoplanetary Disk*, pp. 3-9, Cambridge Univ. Press. [2] Desch, S. J., Connolly, H. C., Jr. (2002), *Meteor. Planet. Sci.*, *37*, 183. [3] Wood, J. A. (1996), *Meteoritics Planet. Sci.*, *31*, 641. [4] Wood, J. A. (1984), *Earth Planet. Sci. Lett.*, *70*, 11. [5] Ruzmaikina, T. V., Ip, W. H. (1994), *Icarus*, *112*, 430. [6] Boss, A. P., Graham, J. A. (1993), *Icarus*, *106*, 168. [7] Tanaka, K. K., Tanaka, H., Nakazawa, K., Nakagawa, Y. (1998), *Icarus*, *134*, 137. [8] Hood, L. L. (1998), *Meteoritics Planet. Sci.*, *33*, 97. [9] Ciesla, F. J., Hood, L. L., Weidenschilling, S. J. (2004), *Meteoritics Planet. Sci.*, in press. [10] Weidenschilling, S. J., Marzari, F., Hood, L. L. (1998), *Science*, *279*, 681. [11] Boss, A. P. (1997), *Science*, *276*, 1836. [12] Boss, A. P. (2000), *Lunar Planet. Sci. Conf. XXXI*, #1084. [13] Hewins, R. H., Fox, G. E. (2004), *Geochim. Cosmochim. Acta*, *68*, 917. [14] Chiang, E. I. (2002), *Meteoritics Planet. Sci.*, *37*, 151. [15] Mejía, A. C., Durisen, R. H., Pickett, M. K., Cai, K. (2004), astroph/0312611

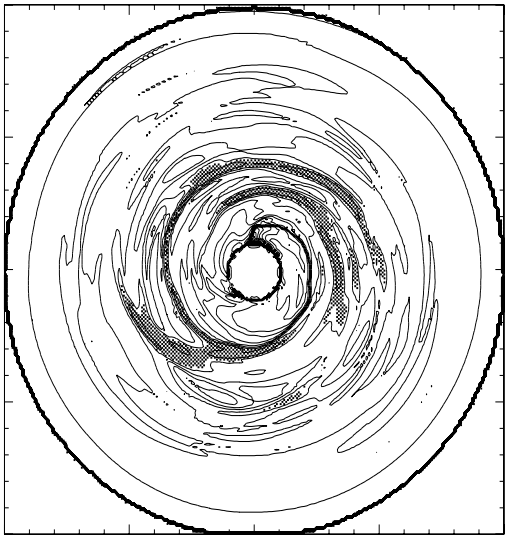

Fig. 1. Density contours in the midplane of a gravitationally unstable disk, showing a strong transient shock front located at 12 o'clock just outside the inner boundary of radius 2 AU. Radius of the entire region shown is 20 AU. Hatched regions denote regions with densities above $10^{-10}$ g $cm^{-3}$.

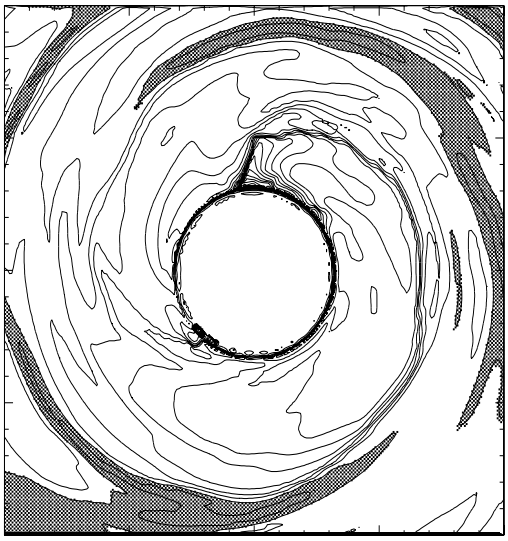

Fig. 2. Expanded view of Figure 1, showing a region of radius 6.7 AU. Solids rotating in the counterclockwise direction between 2 and 3 AU encounter the shock front at a speed of $\sim$ 10 km $s^{-1}$.

# Thermal Structures of Protoplanetary Disks

Nuria Calvet [1], Paola D'Alessio[2] and Dorothy S. Woolum[3],

(1) Center for Astrophysics, 60 Garden St., Cambridge, MA 02138, ncalvet@cfa.harvard.edu, (2) Centro de Radioastronomía y Astrofísica, Apartado Postal 3-72 (Xangari), 58089 Morelia, Michoacán, México, p.dalessio@astrosmo.unam.mx, (3) Physics Department, California State University, Fullerton, California 92834, USA, dwoolum@fullerton.edu

During their first $\sim 10^6$-$10^7$ years, a large fraction of stars of low and intermediate masses are surrounded by dusty disks, which are responsible for the observed near to far-IR SEDs. The standard view is that the inner disk is truncated by the stellar magnetosphere (near the co-rotation radius $\sim 2 - 4R_*$) and disk material is deviated toward high latitudes, merging into the star in accretion shocks. The disk accretion rate is inferred from the observed veiling luminosity produced by these shocks. Assuming steady state, this mass accretion rate is used to characterize the mass transport and the structure of the rest of the disk. We review present models of the thermal structure of these steady accretion disks irradiated by the central star and by the accretion shocks at the stellar surface. In these models, the dust at the disk surface is mostly heated by irradiation, favored by the curvature of the disk photosphere. The energy of the external radiation reprocessed by the upper layers of the disk atmosphere along with local viscous dissipation are the main heating mechanisms of the regions closer to the disk midplane. We study the effect of dust growth and settling on the disk thermal structure. A new ingredient, recently incorporated into the irradiated disk models is the existence of a "wall" at the dust sublimation radius. In the case of Classical T Tauri Stars, there is observational evidence that the wall is heated by both the stellar and the accretion shocks radiation, which places the sublimation radius (for $T_{sub} \sim 1400$ K) between 0.07 and 0.15 AU (10-25 $R_*$). The existence of the wall, supported by near-IR spectra and interferometry, implies that the dust cannot reach the magnetospheric radius, introducing a problem for the X-wind theory proposed to explain the origin of CAIs (Calcium-Aluminioum-rich inclusions) and chondrules in chondritic meteorites. We also present models for more evolved disks, called transition objects, such as TW Hya and Co Ku Tau/4. These disks show low density gaps in their inner regions ( $\lesssim$ 10 AU), probably produced by a massive body or a planet. The disk material in the gaps is more exposed to the external radiation.

**METEORITICAL ASTROPHYSICS: A NEW SUBDISCIPLINE.** A. G. W. Cameron, *Lunar and Planetary Laboratory, University of Arizona, Tucson, AZ 85721 (acameron@lpl.arizona.edu).*

A recent remarkable discovery by Katharina Lodders [1] showed that the abundances of extinct radioactivities (relative to reference nuclei) in chondrites, achondrites, and irons are proportional to the squares of their mean lives, whereas no such abundance-mean life relationship is apparent for the data of calcium-aluminum rich inclusions (CAIs) and a variety of other inclusion types. In this talk I shall interpret these results in terms of galactic and solar nebula processes.

The first step in organizing the data for interpretation is to require that both the abundance of the extinct radioactivity (as measured by its decay product abundance) and that of the reference nuclide should have the same nucleosynthesis history, or else that a correction to the ratio be made to compensate for the ratio of the two different production processes. The striking feature of this diagram is that the lower edge of the data (the Lodders Line) is remarkably straight; most of the data are derived from chondrites; and its slope on the log-log diagram is two. So the extinct radioactivities are present in proportion to the square of their mean lives. All the other data lie above the Lodders line in this diagam; the sources of that data are in general somewhat larger particles than those that have contributed to the Lodders Line.

A straight relationship between abundances of extinct radioactivities and their mean lives means that these radioactivities originated from a common reservoir, the interstellar medium (ISM), and that they were isolated from the rest of the ISM at some point in the past, which is when the solar nebula formed. If the extinct radioactive abundances had accumulated into the solar nebula gas at constant rates they would have become proportional to the first power of the mean lives, a relationship often assumed for this as a galactic process. Thus to find that they are proportional to the second power of the mean lives indicates that a major new process was involved. This relationship can be obtained if the injection of radioactive material into the patch of gas in the interstellar medium, that will form the solar nebula, starts and then increases in injection rate in proportion to the elapsed time since the beginning of the accumulation. Since the observed relation includes the abundance of $^{146}$Sm (mean life $1.49\times10^8$ years), which is very long compared to the lifetime of the solar nebula, one must conclude that a galactic process is involved, with the radioactive accumulation beginning much earlier than that mean life prior to formation of the solar system.

This relation is derived as follows. Assume that the abundance $N$ of a particular species increases proportional to the time $t$ for a total time $T$ with a proportionality constant $a$. Let this go on during the time $T$, with the species decaying with a mean life $\tau$. The total amount of a species injected is given by

$$N_{tot} = \int_0^T atdt = aT^2/2$$

The amount of the radioactive species surviving at the end of the period $T$ is

$$N = \int_0^T ate^{-t/\tau}dt = a\tau^2(1-(T/\tau+1)e^{-T/\tau})$$

If $T \gg \tau$, then $N \approx a\tau^2$. Hence

$$N/N_{tot} \approx 2\tau^2/T^2$$

One cannot directly know the total amount of radioactive material injected, so it is necessary to compare the surviving abundance to the abundance of a reference isotope of the same element that acts as a proxy for the total production of the radioactivity. Thus the reference isotope must be made in the same source(s) as the radioactive one, and be carried together with the radioactive one in small particles within the ISM, and the radioactive decay product must be lost from the small particles (by recoil, evaporation, or other means). It would also be helpful if the reference isotope had the same nucleosynthetic history as the radioactivity, but usually things cannot be that simple. If the particles carrying the radioactive isotope and its reference isotope are so big that the radioactive decay products cannot be lost while in the ISM, then the above derivation would not be applicable. However, the decay products must be retained once the particles are in the solar nebula by incorporation into larger bodies (meteorites).

For much of the last four decades the general paradigm in the meteoritical community has been that the solar nebula formed hot and that inclusions such as CAIs were chemical condensates from a cooling gas of solar composition. What should this picture be replaced by if instead the inclusions were not formed in the solar nebula? The great majority of relevant nucleosynthesis in the galaxy occurs in supernova explosions. The evolution of massive stars leading to such explosions occurs in a series of concentric thermonuclear burning shells, and it has been argued that condensations in such shells could not therefore form solids derived from a full solar composition. However, it has been found in numerical simulations that intense heating in the center of the star leads to neutrino heated bubbles that expand violently away from the center, and also that the supernova shock wave that propagates through the interior causes strong Rayleigh-Taylor instabilities at shell boundaries, so that violent Rayleigh- Taylor fingers shoot forward at such boundaries. Both proccesses induce strong mixing, and the work of Kifonidis *et al.* has shown that the result is a good approximation to a solar composition except in the outermost part of the stellar atmosphere [2]. Thus in an expanding supernova remnant the cooling will be of an approximately solar composition gas. The result is that chemical condensation will occur, but at something like seven orders of magnitude lower density than would be the case for a hot solar nebula. What difference does that make?

Chemical condensation calculations have been carried out by Katharina Lodders for a large range of pressures in a solar

composition gas. The results show that the chemical condensation in the supernova would occur at about 300 degrees C lower temperature than would be the case in the solar nebula, but the condensation lines of the individual chemical species are nearly parallel, and indeed the sequence is indistinguishable from a solar nebula case.

Does the solar nebula have a part to play in any of this? Yes. It has been apparent for some time that strong shock waves in the solar nebula heat chemically condensed materials, partially vaporizing some of them and in general melting the others and leading to recrystallization upon cooling. For this reason I call the condensed objects that become CAIs and AOAs in the nebula protoCAIs and protoAOAs while they are in the interstellar medium. The shock waves also melt "dust balls" of interstellar grains into chondrules. Where do such shock waves originate? The meteoritic community has apparently remained ignorant of the theory of the Rossby Wave Instability process in accretion disks developed in 2001 [3]. This process needs much further investigation, but the existing simulations show a group of 3 or 5 such elliptical vortices formed around a circle in an accretion disk, with shocks trailing each end of a vortex. We do not know how many such circles of vortices there can be, nor where they are most likely to be located in the nebula, so this is a subject needing much further investigation.

When the supernova initially expands, the higher pressure at the center causes it to expand more rapidly than the surface region, and so the exploding star comes to resemble an expanding uniform density sphere [4] (except for some central fallback), mixed throughout and closely approximating a solar composition. The surface layers of such a supernova expand at about 10,000 km/sec (3 percent of light velocity), whereas near the center the expansion is relatively slow. Prior to the explosion the star loses significant mass in the form of a Wolf-Rayet wind, expanding at about 3,000 km/sec, and this will slow down the supernova shock somewhat. But a chemical condensate of 1 cm radius ejected from the surface will be travelling fast enough so that in most cases it would escape from the galaxy and wander in intergalactic space. But such objects from near the center would remain locally in the ISM.

Recent submillimeter observations of the Cas A and Kepler supernova remnants [5,6] indicate that between 1 and 4 $M_\odot$ of micron-size grains were ejected. A similar amount of larger protoCAIs and protoAOAs (which I collectively call “interstellar marbles”) should also be ejected. When the solar nebula is formed it therefore is already filled with the variety of condensates needed to make meteorites.

Thus the conclusion follows that the interstellar medium is filled with supernova condensates in the size range from microns to several centimeters radius. These, together with other condensates from red giant star envelopes, form the subject matter of meteoritical astrophysics. There is a particularly important property of these objects: whereas the gas in the interstellar medium moves in response to local gas pressure, the interstellar marbles are largely decoupled from the gas because of their size and mass, and therefore they will fall through the gas in response to gravitational potential gradients, retarded somewhat by friction with the gas through which they move.

To gain some insight into this behavior, I constructed a numerical model of a Giant Molecular Cloud (GMC), central temperature 35 K, central density $10^6$ hydrogen molecules per cc, radius one parsec. Free fall velocity starting at 1 parsec reaches the center at $1.56 \times 10^5$ cm/sec after a fall time of 2.4 million years, well within the lifetime of a GMC. A 1 cm. radius marble reaches the center nearly as fast ($1.49 \times 10^5$ cm/sec), whereas a 1 micron radius marble takes twice as long and is slowly drifting. The larger marble thus acts like a damped pendulum; so do smaller marbles but their velocities are smaller. Unlike a pendulum, marbles falling from an initially smaller radius get to the GMC center sooner with smaller velocities, so a dense cloud of marbles will build up there and settle into a central object. Subsequent collisions will continue to build up a new type of stellar object that I call a *condensar*, composed of chemical condensates. My model GMC has a total mass of 65 $M_\odot$, of which a little over 1 $M_\odot$ would be condensates and grains, so allowing for inefficiencies the condensar formed at the center would have a mass of a few tenths of a solar mass. Lacking internal hydrogen, there would be no thermonuclear reactions, so the condensar would be nearly nonluminous.

This is a good match to the properties of MACHOs (MAssive Compact Halo Objects), which have been discovered by their microlensing effects on background stars in the Magellanic Clouds, amplifying their luminosity by a substantial factor as they pass through the line of sight. Until now, these MACHOs have been a mysterious form of dark matter, possessing a gravitational field but undetected by optical instruments. The MACHO Project has been a significantly large-scale effort to detect their unique signature in amplifying light from background objects, and a result of their investigation is the production of a maximum likelihood set of contours relating probable mass and the fraction of MACHO mass in the halo (about 0.2, probably representing condensars released in the halo when our galaxy captured other smaller galaxies in the course of its history). The maximum likelihood mass of the MACHOS ranges from 0.1 to 1.0 $M_\odot$ [7,8].

These studies suggest that the subject matter of meteoritical astrophysics goes well beyond the study of meteorites themselves. However, the study of meteorites and their components must be a vital part of the development of this subject. There also needs to be better intercommunication between meteoriticists, astrophysicists, and physical chemists concerned with condensation processes.

This work has been partially supported by NASA grant NAG5-11153.

References: [1] K. Lodders and A. G. W. Cameron, Lunar and Planetary Science Conf. XXXV, Houston (2004), abstract 1186; [2] K. Kifonidis *et al.*, Astron. Astrophys., **408**, 621 (2003); [3] H. Li *et al.*, Astrophys. J., **551**, 874 (2001); [4] D. Arnett, Supernovae and Nucleosynthesis, Princeton University Press, Princeton, N.J. (1996); [5] L. Dunne et al., Nature, **424**, 285 (2003); [6] H. L. Morgan et al., Astrophys. J., **597**, L33 (2003); [7] C. Alcock, Science, **287**, 74 (2000); [8] C. Alcock et al., Astrophys. J., **542**, 281 (2000).

**ORIGIN AND THERMAL HISTORY OF FeNi-METAL IN PRIMITIVE CHONDRITES.** A. J. Campbell[1], M. I. Petaev[2], A. Meibom[3], C. Perron[4], and B. Zanda[4,5], [1]Dept. of the Geophysical Sciences, University of Chicago (5734 S. Ellis Ave., Chicago, IL 60637 USA; a-campbell@uchicago.edu), [2]Dept. of Earth and Planetary Sciences, Harvard University (20 Oxford St., Cambridge, MA 02138 USA; mpetaev@cfa.harvard.edu), [3]Dept. of Geological and Environmental Sciences, Stanford University (Building 320, Lomita Mall, Stanford, CA 94305 USA; meibom@pangea.stanford.edu), [4]Laboratoire d'Etude de la Matiere Extraterrestre, Museum National d'Histoire Naturelle (61 rue Buffon, 75005 Paris, France; perron@mnhn.fr), [5]Dept. of Geological Sciences, Rutgers University (610 Taylor Rd., Piscataway, NJ 08854 USA; zandahew@rci.rutgers.edu).

**Introduction:** FeNi metal is commonly a major component in primitive chondrites, and is therefore a potentially important and useful constituent for investigating the high temperature history of chondritic components. In part, this is because of the mineralogical simplicity, relative to silicate systems, that metal exhibits at high temperatures in the range of compositions that are appropriate to chondrites. This reduced number of phases allows one to more easily interpret chemical variations in metal in terms of its thermal and chemical history. In addition, the siderophile elements span a wide range of chemical behaviors, so that analysis of an appropriate suite of siderophiles often can be employed to eliminate or confirm hypotheses regarding The more complex microstructures of the Fe-Ni system at low temperatures makes it also a very sensitive indicator of secondary thermal processes.

In the last few years there have been several important developments that have enhanced our understanding particularly of the high-temperature history of primitive chondrite metal. The first of these is the enormous increase in the number of specimens that has resulted from the systematic searches for meteorites, especially in Antarctica and the Sahara desert. Concomitant with the increase in number of meteorites available for study is a better recognition of the diversity among them; hence our classification schemes have improved, and the number of classes expanded. Several primitive chondrite groups, including the CR, CH, and CB classes, which are metal-rich, consist of a small number of quite rare meteorites, and were largely unrecognized until a number of their members were recovered from the Antarctic and the Sahara.

Another recent development that has facilitated insight into primitive chondrite metal is the improvement in microanalytical techniques that are sensitive to siderophile elements at trace abundance levels. Laser ablation ICP-MS has been particularly successful in this regard. This technique has been used to provide trace siderophile element analyses at spatial scales down to 15 μm, which allows a new way of approaching problems regarding chemical and thermal history of meteoritic metal, that is complementary to the much longer history of trace element analysis of lithophile elements by ion microprobe.

Finally, experimental studies continue to provide valuable support for, or tests of, proposed metal-forming processes. Recent experimental efforts have focussed particularly on better understanding the consequences of redox reactions, evaporation, and diffusion on the compositions and textures of primitive chondrite metal.

**CH and CB Chondrites:** These meteorites contain a variety of metal textures, and have attracted much recent attention in both analytical and theoretical studies [1,2]. The CH chondrites, and the $CB_b$ chondrites QUE 94411 and HH 237, contain zoned metal grains that have been interpreted as products of nebular condensation [3,4,5]. These interpretations are based on the zoning of minor elements (Ni, Co, Cr, P, Si) as well as trace elements (PGEs, Re, Au, Cu, Ga), and are supported by isotopic mass fractionations in Fe, Ni, and Cu [6]. The refractory elements (relative to Fe) are enriched in the cores of the zoned metal grains relative to the rims, whereas elements more volatile than Fe are depleted, but often less depleted toward the rims. Comparisons of the observed compositional zoning to calculations of metal condensation, grain growth, and diffusion have been used to constrain the high-temperature thermal history and timescales of formation of these grains [3,4,5,7]. The unzoned metal in CH and $CB_b$ meteorites also exhibits significant compositional variation, and trace element studies suggest that this metal formed under varying conditions of temperature and oxygen fugacity [7,8]. The origin of metal in Bencubbin and related $CB_a$ members remains uncertain, but seems to be different from that of the zoned grains of CH and $CB_b$ chondrites. The coexistence of metals of different origins in the same chondrites or chondrite groups is not the least puzzling characteristics of these meteorites.

**CAI Metal:** CAIs are generally enriched in refractory siderophiles, to levels similar to their refractory lithophile enrichments, indicating a high-temperature origin for both components. Low

temperature processes, including sulfidation and oxidation of the metal, has partly obscured the original compositions of CAI metal, at least in CV chondrites [9]. However, the distribution and relative abundances of trace siderophile elements indicate that not all of the variations in metal composition can be attributed to secondary processing. CAI metal reflects incomplete mixing of metal precursors that had a wide range of temperatures of formation [10,11]. The distributions of Mo and W in CV CAIs have been interpreted as evidence of relatively high oxygen fugacity conditions [10,12], in sharp contrast to the highly reducing conditions inferred from $Ti^{3+}/Ti^{4+}$ ratios and other indicators in the silicate phases [13]. There is a relative paucity of studies of CAI metal from chondrite classes other than CV.

**CR Chondrite Metal:** Renazzo and the other CR chondrites are unequilibrated and highly reduced, and offer excellent opportunity to study the relationship between metal and silicate evolution in chondrites. The formation of metal in CR chondrites was intimately connected with the chondrule-forming process [14]. The observed range of chondrule textures indicates that metal was expelled, usually incompletely, from the chondrule interiors. Variations in minor and trace element compositions in metal, between interior grains and grains on chondrule rims, serve as evidence that volatile loss during heating was followed by recondensation of volatile siderophile elements into the rim metal [15,16]. Redox effects are also observed in CR chondrule metal; these are possibly related to exchange between metal and silicate, and transport of oxidizable elements from interior metal to the vapor phase [14]. The bulk depletion of volatile siderophile elements from Renazzo chondrules may have been inherited from their precursors [15,16].

**Ordinary Chondrite Metal:** The chemistry of most ordinary chondrite metal is dominated by parent body low-temperature processing, specifically sulfidation and kamacite/taenite equilibration. Nonetheless, some pre-accretional history may be preserved in the least equilibrated specimens. As in the CR chondrites, it is evident from textural features and composition relationships between metal and silicates that the chondrule-forming process played an important role in ordinary chondrite metal evolution.

**Experiments:** Recent studies continue to yield interesting insights into chondrite metal chemistry. Some work has followed the trail of [17], pursuing possible redox mechanisms for metal formation in chondrules. Heating of a CI composition under a range of $P(H_2)$ conditions showed that Fe metal formation occurred primarily by FeS desulfidization, and not by FeO reduction under the experimental conditions [18]. However, TEM studies of experimentally produced dusty olivines indicate that in situ FeO reduction may have occurred [19]. Other studies have emphasized transport properties in the metal, to better elucidate the distributions of siderophiles and the timescales associated with observed diffusion [20,21]. These results, and the relative paucity of experimental efforts, suggest that greater emphasis on experimental strategies to understanding high-temperature processing of chondrite metal may prove rewarding.

**References:** [1] Weisberg M. K. et al. (2001) *MAPS, 36*, 401. [2] Krot A. N. et al. (2002) *MAPS, 37*, 1451. [3] Meibom et al. (1999) *JGR, 104*, 22053. [4] Campbell A. J. et al. *GCA, 65*, 163-180. [5] Petaev M. I. et al. (2003) *GCA, 67*, 1737. [6] Alexander C. M. O'D. and Hewins R. H. (2004) *Met. Soc. Meeting*, #5080. [7] Campbell A. J. and Humayun M. *GCA, 68*, 3409. [8] Hezel D. C. et al. (2003) *MAPS, 38*, 1199. [9] Blum J. D. et al. (1989) *GCA, 53*, 543. [10] Palme H. et al. (1994) *GCA, 58*, 495. [11] Campbell A. J. et al. *GCA, 67,* 3119-3134. [12] Fegley B. Jr. and Palme H. (1985) *EPSL, 72*, 311. [13] Beckett J. R. and Grossman L. (1986) *LPSC XVII*, 36. [14] Zanda B. et al. (2002) *LPSC XXXIII*, #1852. [15] Connolly H. C. Jr. et al. (2001) *GCA, 65*, 4567. [16] Humayun M. et al. (2002) *LPSC XXXIII*, #1965. [17] Connolly H. C. Jr. et al. (1994) *Nature, 371*, 136. [18] Cohen B. A. and Hewins R. H. (2004) *GCA, 68*, 1677. [19] Leroux H. et al. (2003) *MAPS, 38*, 81. [20] Watson H. C. and Watson E. B. (2003) *PEPI, 139*, 65. [21] Righter K. et al. (2003) *LPSC XXXIV*, #1373.

**THE COLLISIONS OF CHONDRULES BEHIND SHOCK WAVES.** F.J. Ciesla[1] and L.L. Hood[2], [1]NASA Ames Research Center; MS 245-3; Moffet Field, CA 94035; ciesla@cosmic.arc.nasa.gov; [2]Lunar and Planetary Laboratory; University of Arizona; 1629 E. University Blvd; Tucson, AZ 85721; lon@lpl.arizona.edu.

**Introduction:** One of the reasons that the mechanism(s) responsible for the formation of chondrules has remained so elusive is that each proposed mechanism must be able to explain a large number of features observed in chondrules. Most models of chondrule formation focus on matching the expected thermal histories of chondrules: rapid heating followed by cooling during crystallization at rates between ~10-1000 K/hr [1, and references therein]. Thus far, only models for large shock waves in the solar nebula have quantitatively shown that the thermal evolution of millimeter-sized particles in the nebula can match these inferred thermal histories [2-4]. While this is a positive step for the shock wave model, further testing is needed to see if other properties of chondrules can be explained in the context of this model.

One area of interest is understanding the collisional evolution of chondrules after they encounter a shock wave. These collisions could lead to sticking, destruction, or bouncing. Here we focus on understanding what conditions are needed for these different outcomes to occur and try to reconcile the seemingly contradictory conclusions reached by studies of compound chondrule formation and chondrule destruction by collisions behind a shock wave.

**Chondrule Collisions:** The observation of compound chondrules in meteorites has led to the realization that chondrules were susceptible to collisions while still in their molten state during the formation process [5,6]. The frequency of these objects has been used to put constraints on the density of chondrules in the nebula during a chondrule formation event [3,5,7]. By assuming a relative velocity between the chondrules and a time interval during which the chondrules were likely to "stick" upon experiencing a collision, previous workers have calculated that the ratio of chondrule mass density to gas density would be, on average, 0.15-0.30. These models have typically assumed a value for the relative velocity between the chondrules to be 100 cm/s, which has been constrained by estimates of chondrule surface tension [8]. This is roughly the relative velocity expected in a turbulent nebula with a value of $=10^{-4}$ (dimensionless turbulence parameter).

In the shock wave model, relative velocities between the particles will arise in a different way. As the particles enter the shock, they will be moving with some relative velocity with respect to the gas. It is this relative motion that leads to the heating of the particles and their subsequent deceleration. The force exerted on a particle by the gas will depend on its velocity, temperature, and size. Thus particles of different sizes will decelerate at different rates, leading to relative velocities between the particles.

This effect was studied by Nakamoto and Miura [9] who calculated the rate at which particles of different sizes would collide and the energy associated with those collisions. Assuming that those particles which experienced collisions such that the energy of the colliding particle ($m_2v^2/2$) was greater than the strength of the particle( $m_1/f$, where $=3x10^6$ erg/g, and $f$=0.3 is an efficiency factor) was destroyed, these authors explored how likely particles of different sizes were to survive behind a shock wave under various conditions. They concluded that in order to produce the observed chondrule size distribution, the ratio of chondrule mass density to gas mass density should be on the order of or less than 0.01 (close to the average value in a canonical solar nebula). If this ratio was exceeded, the larger chondrules observed in meteorites would not survive.

Thus the results of compound chondrule studies seem to be inconsistent with the survival of chondrules behind a shock wave. In order to produce the observed number of compound chondrules, the particles must have been concentrated at relatively high mass ratios. However, such high mass ratios may not allow those chondrules to survive the formation process. We are currently investigating ways that these contradicting calculations can be reconciled.

**Model Development:** By calculating the rate at which different particles are decelerated as they flow behind a shock wave, we can calculate the relative velocity between two particles of different sizes. Given the relative velocity between two particles (particle 1 with radius $r_1$ and particle 2 with radius $r_2$), we can then calculate what the number density of particles the same sizes as particle 2 would have to be to ensure that a given particle 1 would collide with one of these particles ($n_2=1/\ r_1^2vt$, where t is the time that the particles are susceptible to collisions and v is the relative velocity). If we limit ourselves to those velocities which would lead to the destruction of particle 1, based on the criteria described above, then we can calculate what the minimum number density would have to be to ensure that particle 1 would be destroyed in these collisions.

*Size Distribution of the particles.* In general, large relative velocities (large enough to lead to destruction of a particle) can be achieved between the particles

considered. However, when particle 2 has a radius which is close in value to that of particle 1, the velocities of the particles do not differ significantly at any point behind the shock wave. This means that the criteria for destruction would not be met—that is that the collisional velocity between the particles would be too small to lead to destruction. Thus, if the particle size distribution entering the shock wave is narrow, then very few particles may be destroyed due to collisions. Models of the redistribution of particles in the solar nebula by turbulence predict that particles of similar size (actually similar products of radius and mass density) are preferentially concentrated by turbulent eddies [10]. Thus this "window" of low relative velocity of the particles may be due to the size selection of turbulence in the nebula. We are investigating the dependence of the size of the window and the size distribution of particles in eddies on nebular parameters.

*Results of Collisions.* In the compound chondrule investigations described above, the velocity of the collisions was thought to be on the order of 100 cm/s or less, because surface tension arguments suggest that larger collisional velocities would disrupt the chondrules [8]. However, this velocity is much less than the disruption velocities for particles using the criteria outlined in [9]. While slight differences in the critical velocity for disruption can be expected due to large uncertainties, differences of several orders of magnitude will lead to the discrepancies described above. This must be examined more closely.

In [7], we outlined a simple model to describe the conditions needed for two viscous particles to stick based on Hertzian contact theory of two spherical particles. Specifically, the collisional time between two spherical particles must be less than the Maxwell time. The Maxwell time is a property of a given material: on timescales short compared to the Maxwell time, the material will behave elastically and collisions will lead to bouncing or disruption; on timescales long compared to the Maxwell time, the material will behave viscously and collisions will lead to flow or sticking of the chondrules. This model can be expanded to consider the variability of the Maxwell time with impact parameters as well as composition and temperature variations in the behavior of the chondrules. A more complex model will help to constrain what will happen when two chondrules collide at a given velocity.

*Compound Chondrule Formation at High Velocities.* Should large velocity collisions allow for the formation of compound chondrules, we can estimate the formation rate of compounds based on the relative velocities calculated above. In addition, we can improve upon previous compound chondrule calculations by considering particles of various sizes. In their investigation of compounds, Wasson et al. [6] detailed the various sizes of the different components of compound chondrules and showed that the primaries and secondaries may have very different sizes from one another. While these observations may be the result of uncertainties due to observing the compounds in thin-section [7], they may also be the result of the way the objects formed.

**Summary:** The collision of two chondrules can lead to a number of outcomes: the chondrules may stick and form a compound chondrule, one or both of the chondrules may be destroyed, or the two chondrules may simply bounce off of one another. Behind a shock wave the relative velocity between two chondrules may vary over many orders of magnitude. Understanding the conditions needed for each of these outcomes to be satisfied is important in evaluating if chondrules could have been formed by shock waves in the solar nebula.

**References:** [1] Jones, R. H. et al., (2000) in Protostars and Planets IV, V. Mannings et al., eds., pp. 927-946, Univ. of Arizona Press, Tucson. [2] Iida, A. et al. (2001) *Icarus*, 153, 430-450. [3] Desch, S. and Connolly, H. (2002) *Meteorit. Planet. Sci*., 37, 183-207. [4] Ciesla, F. and Hood, L. (2002) *Icarus*, 158, 281-293. [5] Gooding, J. and Keil, K. (1981) *Meteoritics*, 16, 17-43. [6] Wasson, J. et al. (1996) *Geochim. Cosmochim. Acta*. 59, 1847-1869. [7] Ciesla, F. et al. (2004) *Meteorit. Planet. Sci*., 39, 531-544. [8] Kring, D. (1991) *Earth. And Planet. Sci.,* 105, 65-80. [9] Nakamoto, T. and Miura, H. (2004) *LPS. XXXV*, Abstract #1847. [10] Cuzzi, J. et al. (2001) *Astrophys. J.,* 546, 496-508.

**PRIMARY SIGNATURES OF THE NEBULAR DUST PRESERVED IN ACCRETIONARY RIMS AND MATRICES OF CV CHONDRITES.** M. Cosarinsky[1] and L. A. Leshin[1,2]. [1]Department of Geological Sciences, Arizona State University, Tempe, AZ 85287-1404; [2]Center for Meteorite Studies, Arizona State University. E-mail: cosarinsky@asu.edu

**Introduction:** Fine-grained materials that occur in accretionary rims (ARs) around chondrules and Ca-Al-rich inclusions (CAIs) and in the matrix of CV chondrites provide a unique probe for understanding the origin of nebular dust and its subsequent modification by nebular and/or asteroidal processes. Isotopic studies of such materials are challenging due to their small grain size. Oxygen isotopic compositions of chondritic materials present large isotopic variations, with the most refractory components, CAIs and amoeboid olivine aggregates (AOAs), enriched in $^{16}$O by ~5% with respect to most chondrules and average matrix. Recent ion microprobe data have shown the existence of large $^{16}$O-enrichments in individual chondrule olivine grains [1,2] and AR olivine [3]. These results suggest a genetic link between chondrule precursors and CAIs. However, with few exceptions, matrix materials have been measured only by "bulk" methods and their small-scale isotopic variability has remained largely unexplored. Here we report *in situ* chemical and oxygen isotopic compositions of the finest components of CV chondrites present in ARs around CAIs and matrices in Leoville, Vigarano and Allende. These data will help constrain the environment of formation of the fine-grained nebular dust and establish possible relationships with other chondritic components.

**Results:** ARs around CAIs in CV chondrites form a structure consisting of two to three layers that differ in olivine grain size and/or chemical composition. In all cases, the inner layer (IL) is more compact and coarser grained, similar in texture to AOAs. It consists of forsteritic olivine ($Fa_{<10}$) that is $^{16}$O-rich ($\Delta^{17}O \sim -25$ to $-15$ ‰; $2\sigma \sim 3$ ‰) (Fig. 1). In Allende and Vigarano, olivine from this layer also presents strong enrichments in FeO ($Fa_{10\text{-}40}$) that correlate with relative depletions in $^{16}$O ($\Delta^{17}O \sim -20$ to $-5$ ‰) (Fig. 1). The middle (ML) and outer layers (OL) as well as the matrix of each chondrite are more porous and very fine-grained (<1 μm in Leoville and Vigarano and up to 10 μm in Allende). Olivine from the ML in Leoville is intermediate in mineral chemistry and isotopic composition ($Fa_{15\text{-}25}$; $\Delta^{17}O \sim -16$ to $-11$ ‰) (Fig. 1). In Allende, ML olivine is FeO-rich ($Fa_{\sim 35}$) and exhibits variable $\Delta^{17}O$ values from $-15$ to 0 ‰ (Fig. 1). OL and matrix olivine is mostly fayalitic ($Fa_{30\text{-}65}$), although variable in isotopic composition ($\Delta^{17}O \sim -17$ to 0 ‰) (Fig. 1). Larger grains in all the samples studied are generally $^{16}$O-rich, but even some of the finest olivine grains show $^{16}$O-rich values.

**Discussion:** Olivine from ARs and matrices in CV chondrites exhibit large correlated variations in chemical and isotopic compositions. There is a progressive enrichment in FeO and depletion in $^{16}$O (compared to the maximum values observed in CAIs and AOAs) seen in olivine from all layers and matrices, which suggests variable degrees of mixing between two end-member compositions: FeO-poor and $^{16}$O-rich with FeO-rich and $^{16}$O-poor. The textural and compositional similarities of IL olivine to AOAs suggest that this layer accreted $^{16}$O-rich forsterite that condensed from the nebula and was later sintered around CAIs during a heating event [3]. The fine-grained olivine from the outermost AR layers and from CV matrices may represent the same population of dust that escaped such thermal processing by nebular sorting. Alternatively, it may represent a second generation of dust that later accreted around CAIs and chondrules and as CV matrix. In any case, these fine-grained components also preserve some $^{16}$O-rich signatures, suggesting that the nebular dust was initially $^{16}$O-rich and later underwent variable degrees of isotopic exchange with and $^{16}$O-depleted reservoir. The observed progressive variation in chemical and isotopic compositions most likely resulted from variable degrees of exchange of initially $^{16}$O-rich forsterites with an FeO-rich and $^{16}$O-poor reservoir.

In Allende, olivine chemical and isotopic signatures also vary with grain size so that the finest grains are the most fayalitic and depleted in $^{16}$O. This grain size effect on composition suggests a diffusion-controlled exchange mechanism for the observed compositional mixing. Calculations based on Fe-Mg [4] and O diffusion [5] in San Carlos olivine yield closure temperatures that differ by approximately 300˚C, higher for O because of its slower diffusion rate. This temperature discrepancy may indicate that this was not a coupled exchange process or that the assumptions involved in the calculations do not properly reflect conditions during olivine alteration. An alternative explanation for our results could be the formation of FeO-rich and $^{16}$O-poor overgrowths around $^{16}$O-rich forsterite grains. In either case, however, the conclusion remains that the initial fine-

grained olivine in Allende ARs and matrix was enriched in $^{16}$O. After their accretion around CAIs and the agglomeration of the CV parent body, AR and matrix olivine most likely experienced chemical and isotopic exchange *in situ* in the parent body as inferred by a rock fabric control on the distribution of chemical and isotopic heterogeneities.

**Implications:** The preservation of $^{16}$O-rich signatures in the finest components of CV chondrites is strong evidence that even the finest nebular dust originated from the same isotopic reservoir as CAIs as well as AOAs and chondrule precursors. It is possible that the largest fraction of nebular dust that accreted as the outer AR layers and matrix was similar to chondrule precursor materials. This fraction of condensate dust largely escaped nebular processing and was later modified in the CV asteroid. Therefore, most chondritic materials apparently originated from a widespread –in time and/or space– gaseous reservoir enriched in $^{16}$O and later evolved differently, recording distinct nebular histories. In particular, the interaction with an $^{16}$O-poor nebular gas is recorded by the chondrule formation process and the variable melting of CAIs and isotopic exchange of individual minerals. This $^{16}$O-poor reservoir may have existed in the solar nebula either at the same time as the $^{16}$O-rich one, but in separate regions, or at a later time. Separate isotopic reservoirs in the nebula could have derived from materials with different nucleosynthetic origin ($^{16}$O-rich solids and $^{16}$O-poor gas [6,7,8]) or from heterogeneities produced locally by irradiation on the surface of the disk [*e.g.*, 9,10]. The formation of CAIs, chondrule precursors and nebular dust in a single isotopic reservoir is more consistent with the local production models, and supports the hypothesis that the initial isotopic composition of the solar system is ~5% more enriched in $^{16}$O than is preserved in the bulk Earth, Mars, or asteroids.

**References:** [1] Jones R. H. et al. (2004) *GCA*, 68, 3423-3438. [2] Kobayashi et al. (2003) *LPS XXXIV*, Abstract #1536. [3] Krot A. N. et al. (2002) *Science*, 202, 1051-1054. [4] Chakraborty S. (1997) *JGR*, 102, 4119-4128. [5] Gérard O. and Jaoul O. (1989) *JGR*, 94, 12317-12331. [6] Clayton R. et al. (1977) *EPSL*, 34, 209-224. [7] Scott E. R. D. and Krot A. N. (2001) *Meteoritics & Planet. Sci.*, 36, 1307-1319. [8] Yurimoto H. and Kuramoto K. (2002) *Meteoritics & Planet. Sci.*, 37, A153. [9] Clayton R. (2002) *Nature*, 415, 860-861. [10] Lyons J. R. and Young E. D. (2004) *LPS XXXV*, Abstract #1970.

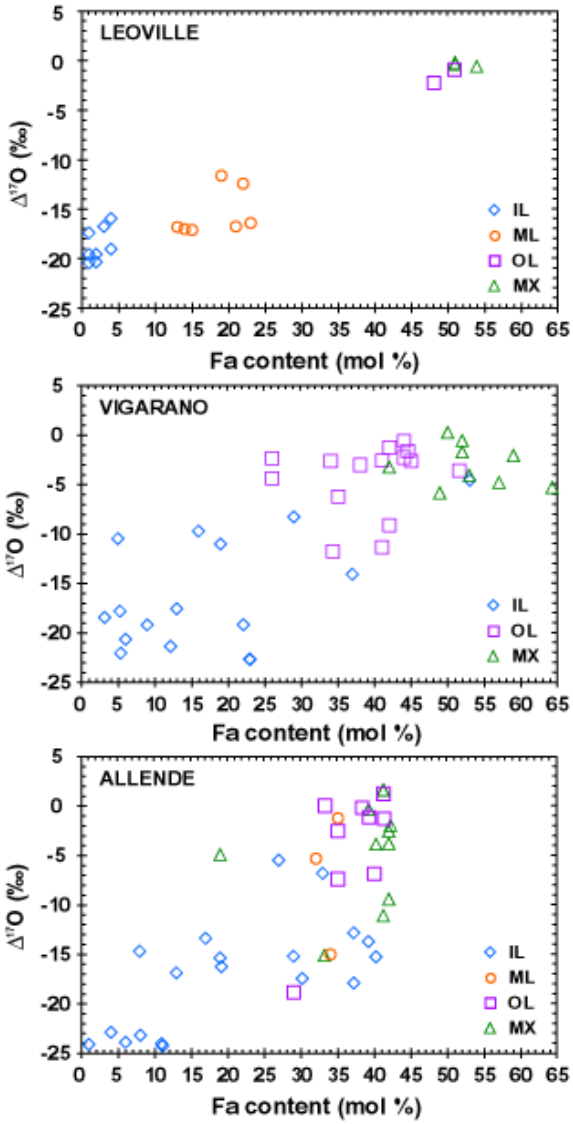


Fig. 1 Oxygen isotopic compositions vs. fayalite content of olivine from the AR (IL, inner layer; ML, middle layer; OL, outer layer) and matrix (MX) of the CV chondrites Leoville, Vigarano and Allende. 2σ errors on $\Delta^{17}$O are 2-3 ‰.

**HISTORY OF THERMALLY PROCESSED SOLIDS IN THE PROTOPLANETARY DISK: RECONCILING THEORETICAL MODELS AND METEORITICAL EVIDENCE** J. N. Cuzzi[1], M. Petaev[2], E. R. D. Scott[3], S. Weidenschilling[4], and F. J. Ciesla[5]; [1]Ames Research Center, NASA; Mail Stop 245-3, Moffett Field, CA 94035; jcuzzi@mail.arc.nasa.gov; [2]Dept. Earth and Planetary Sciences, Harvard University and Harvard-Smithsonian Center for Astrophysics; mpetaev@cfa.harvard.edu; [3]Hawai'i Institute of Geophysics and Planetology, University of Hawai'i at Manoa; escott@hawaii.edu; [4]Planetary Science Institute, Tucson, Az., sjw@psi.edu; [5]Ames Research Center, NASA; Mail Stop 245-3, Moffett Field, CA 94035; ciesla@cosmic.arc.nasa.gov

In this talk we assess theoretical models of the radial, temporal, and thermal evolution of nebula solids, and their ultimate accretion into planetesimals such as we see today, using meteorite evidence as a guide.

Each class of chondrites contains a characteristic suite of chondrules and CAIs that may have formed over a period of several Myr during which planetesimals were accreting in the disk. Details of the various models for transient melting of chondrules and igneous CAIs will be left to others. However, high-temperature processes of different kinds – evaporation, alteration, etc – did affect these constituents and their environment over this time span. Here we describe evolutionary scenarios consistent with a large time gap between CAI and chondrule formation and the presence of distinctive suites of chondrules and CAIs in each chondrite class.

Particle-gas dynamical processes transport particles of all relevant sizes (microns to many meters) within the nebula and affect their evolution in a variety of important ways. Turbulent radial diffusion spreads particles radially down their concentration gradients – as one example, it can prevent CAIs from being lost into the sun on several Myr timescales [1]. Vertical diffusion spreads the dense midplane particle layer, determining its volume density, which in turn affects the particle growth rate and even the dominant growth process [2-4]. Turbulent concentration selects aerodynamically sorted particles for orders-of-magnitude density enhancement, and is applicable to porous, fluffy particles of appropriate size as well as to solid chondrules [5]. Inward radial drift under gas drag brings a surprisingly large amount of material to regions where it evaporates; these evaporation fronts cause significant chemical modification of the nebula gas over a wide range of radii [6]. Radial transport by stellar winds can be important for small particles [7].

The basic physics of these processes will not be presented in detail. Instead we will concentrate on how scenarios of primary accretion which make use of this physics can be constrained by the meteorite record. We will discuss how models of the condensation-alteration sequence under non-equilibrium conditions might provide new insights into an extended nebula evolution of meteorite components. We will attempt to clarify how currently observed aspects of chondrite parent bodies can shed light on these issues, and will point out how future experimental studies of meteorite chemical and isotopic properties might better constrain these models or distinguish between them. We will assess the predictions of primary accretion models regarding observable physical, chemical, and isotopic properties, and accretion timescales, from the standpoint of meteoritic observations.

**References:** [1] Cuzzi JN, Davis S., and Dobrovolskis A. (2003) Icarus 166, 385; [2] Weidenschilling SJ (1997) Icarus 197, 290; [3] Cuzzi JN and Weidenschilling SJ (2005); Meteorites and the Early Solar System II; [4] Weidenschilling SJ and Cuzzi JN (2005); Meteorites and the Early Solar System II. [5] Cuzzi JN et al. (2001) Astrophys. J. 546, 496; [6] Cuzzi JN and Zahnle KJ (2004) Astrophys. J. in press (Oct 10 2004 issue). [7] Shu F. et al (1997) Science 277, 1475.

**EVAPORATION AND CONDENSATION DURING CAI AND CHONDRULE FORMATION.** Andrew M. Davis[1,2,3], Conel M. O'D. Alexander[4], Hiroko Nagahara[5], and Frank M. Richter[1,2], [1]Chicago Center for Cosmochemistry, [2]Department of the Geophysical Sciences, [3]Enrico Fermi Institute, University of Chicago, 5734 S. Ellis Ave., Chicago, IL 60637 (a-davis@uchicago.edu, richter@geosci.uchicago.edu), [4]Department of Terrestrial Magnetism, Carnegie Institution of Washington, 5241 Broad Branch Road, N.W., Washington, DC 20015 (alexande@dtm.ciw.edu), [5]Department of Earth and Planetary Sciences, University of Tokyo, Hongo, Tokyo 113-0033, Japan (hiroko@eps.s.u-tokyo.ac.jp).

**Introduction:** The most general argument for evaporation and condensation having played a significant role in determining the chemical properties of Solar System materials is based on the observation that all these materials are variously but systematically depleted in their more volatile elements relative to the bulk composition of condensable matter in the Solar System, generally accepted to be exemplified by CI chondrites. CAIs and chondrules are particularly valuable for gaining insight into condensation and evaporation, because they preserve isotopic, chemical and textural evidence of these processes. Coupled with modeling and laboratory experiments, the properties of CAIs and chondrules provide marvelous opportunities for understanding the conditions under which high temperature processes occurred in the early solar system.

**Theoretical background:** Condensation and evaporation are terms widely used to describe volatility fractionation processes, but they are incomplete. It is important to distinguish between equilibrium and kinetically controlled processes. Condensation is usually used as shorthand for equilibrium fractionation with falling temperature, and evaporation is often taken to mean a kinetically controlled fractionation with increasing temperature, but kinetically controlled condensation and near-equilibrium evaporation can also occur. Thermodynamic equilibrium condensation calculations have been widely applied for more than 30 years [e.g., 1–4]. Significant advances in understanding kinetically controlled evaporation processes are more recent [e.g., 1,5–15]. Volatility-based elemental fractionation can occur under equilibrium or kinetically-controlled conditions, whereas large isotopic mass fractionation effects can only occur under kinetic control under specifically favorable circumstances of departure from equilibrium PT conditions, gas composition, diffusion rates in solids and melts, etc. It is the presence or absence of isotopic fractionation effects in CAIs and chondrules coupled with the conditions necessary to preserve these effects that constrain early Solar System environments.

**Experiments:** Evaporation of CAI and chondrule compositions in the laboratory have confirmed much of the theoretical understanding of evaporation processes, but have also shown the need for experimentally determined parameters in models. A good example of this is isotopic fractionation of magnesium. It is predicted that the gas solid fractionation factor for magnesium should be given by the square root of the masses of the magnesium isotopes, e.g., $\sqrt{24/25}$, yet well-controlled experiments evaporating crystalline forsterite, liquid $Mg_2SiO_4$, melts of initially chondritic composition and CAI melts consistently give fractionation factors of about 2/3 of the expected value (all experiments summarized in [12]). In models relating degree of mass loss of magnesium with isotopic fractionation, the experimentally determined fractionation factor must be used.

**CAIs:** There is surprisingly little evidence for direct condensates among CAIs, as strong textural and petrologic arguments for subsequent melt crystallization can be made for some CAIs and for most others the mineralogy is too simple for strong petrologic constraints and textures are equivocal. In the 1970s, the best-known CAIs were the large Type A and B CAIs in CV chondrites. At the time, it was argued that most are condensates, because their mineralogy (spinel, melilite, fassaite and anorthite) matched that from condensation calculations and they are enriched in lithophile and siderophile elements by a factor of ~20 relative to CI chondrites [2,16]. It is now clear that although there may have been condensate precursors to these CAIs, the last event they experienced was one of heating and crystallization from a melt.

Careful determination of bulk chemical compositions of Type B CAIs have revealed that they are depleted in magnesium and perhaps silicon relative to compositions predicted from equilibrium condensation calculations [8]. These CAIs also have correlated enrichments in the heavy isotopes of silicon and magnesium [17], very similar to what has been measured in laboratory produced evaporation residues [6]. Both the elemental abundances and isotopic compositions of CAIs can be understood by evaporation of equilibrium condensates from a gas of solar composition [8] and the correlated elemental and isotopic fractionation effects have been reproduced in laboratory evaporation of CAI melts under plausible solar nebular conditions [12]. Type B CAIs have igneous textures indicating that they were once reheated to several hundred °C above their condensation temperatures for plausible nebular pressures and remained partially molten for at least several hours [18]. The duration of this high temperature event is such that significant evaporative loss of magnesium,

silicon and oxygen is to be expected given the evaporation kinetics of these elements from Type B CAI-like liquids in a low-pressure hydrogen-dominated gas [12]. A plausible source of the reheating is by the passage of a shock wave, and we will show that the temperature and pressure history of a CAI subject to Desch and Connolly's [19] canonical shock will fractionate the elemental and isotopic composition of a reasonable precursor (i.e., a condensate from a solar composition gas) so as to produce a very typical Type B CAI. An alternative model for formation of Type A and B CAIs involves single stage closed system evaporation of cold CI chondrite-like precursors under conditions at enhanced dust/gas ratios [15]. Partial back reaction reequilibrates isotopic compositions while permitting elemental fractionation. We will evaluate the strengths and weaknesses of both models.

**Chondrules:** Chondrules show a wide range of elemental compositions, which include large variations in Mg/Si ratios, FeO, Fe-metal, and alkali contents. Despite these variations, to date no large, systematic mass dependent isotopic fractionations (K, Fe, Mg, Si and O) have been found in chondrules [17,20-22]. Whatever process was responsible for the elemental fractionations must have occurred far from Rayleigh conditions.

There continues to be a vigorous debate about whether the variations were produced by differences in the chondrule precursors, evaporation and recondensation during chondrule formation, or modification after accretion onto the parent bodies.

Under the currently accepted conditions of chondrule formation, some evaporation of the alkalis, Fe and Si would be expected. Indeed, there is some petrologic evidence for recondensation of alkalis, Fe and Si onto chondrule rims [23,24], and alkalis and Si back into chondrules [25]. The fact that this evaporation and condensation did not also produce large isotopic fractionations has led some to suggest that chondrules formed at high partial pressures of $H_2$, perhaps as high as 1 bar [21]. However, such high partial pressures are difficult to reconcile with astrophysical models of planetary disks. An alternative is that while chondrules may have experienced evaporation and recondensation, the timescales were sufficiently long for them to approach isotopic equilibrium with the surrounding gas.

Comparison of chondrule compositions to kinetic evaporation and recondensation paths, and equilibrium and kinetic condensation paths suggest that the type A chondrules could have formed as either near-equilibrium melts through evaporation and recondensation, or direct condensation in CI-dust enriched (100-1000×solar) systems [4, 15, 24-27]. While direct condensation of some chondrules is possible, the presence of relict grains in many chondrules shows that most chondrules formed from solid precursors [28,29]. chondrules formed from solid precursors [28,29]. Type B chondrules and Al-rich chondrules probably need previously fractionated precursors. The physical separation of metal from chondrules and/or their precursor may also be needed to explain the full range of Fe contents of chondrules.

In conclusion, it seems likely that chondrules did experience some evaporation and/or condensation, but they formed under very dust enriched conditions that enabled them to approach equilibrium with the surrounding gas at high temperatures. Hence, the absence of mass dependent isotopic fractionation in them. However, equilibrium cannot have been maintained to low temperatures. Crystallization during cooling and the sluggish diffusion rates in the residual glass eventually prevented further chondrule-gas exchange [15].

**Summary:** Chondrules and CAIs have been evaporated, either from CI-like precursors or more refractory condensates, with chondrules having evaporated under more dust-enriched conditions than did CAIs.

**References:** 1. Davis A. M. and Richter F. M. (2003) In *Meteorites, Planets, and Comets* (Ed. A. M. Davis), Vol. 1 *Treatise on Geochemistry* (Eds. H. D. Holland and K. K. Turekian), Elsevier-Pergamon, Oxford, p. 407. 2. Grossman L. (1972) *GCA, 36*, 597. 3. Yoneda S. and Grossman L. (1995) *GCA, 59*, 3413. 4. Ebel D. S. and Grossman L. (2000) *GCA, 64*, 339. 5. Hashimoto A. (1983) *Geochem. J., 17*, 111. 6. Davis A. M. *et al.* (1990) *Nature, 347*, 675. 7. Alexander C. M. O'D. *et al.* (2000) *MAPS, 35*, 859 8. Grossman L. *et al.* (2000) *GCA, 64*, 2879. 9. Nagahara H. and Ozawa K. (2000) *Chem. Geol., 169*, 45. 10. Alexander C. M. O'D. (2001) *MAPS, 36*, 255. 11. Ozawa K. and Nagahara H. (2001) *GCA*, *65*, 2171. 12. Richter F. M. *et al.* (2002) *GCA, 66*, 521. 13. Grossman L. *et al.* (2002) *GCA, 66*, 145. 14. Richter F. M. (2004) *GCA*, in press. 15. Alexander C. M. O'D. (2004) *GCA*, in press. 16. Grossman L. (1973) *GCA, 37*, 1119. 17. Clayton R. N. *et al.* (1988) *Phil. Trans. R. Soc. London, A325*, 483. 18. Stolper E. and Paque J. M. (1986) *GCA, 50*, 1785. 19. Desch S. J. and Connolly H. C. Jr. (2002) *MAPS, 37*, 183. 20. Alexander C. M. O'D. and Wang, J. (2001) *MAPS, 36*, 819. 21. Galy A. *et al.* (2000) *Science, 290*, 1751. 22. Clayton R. N. (1993) *Ann. Rev. Earth Planet Sci.* 21, 115. 23. Alexander C. M. O'D. (1995) *GCA* 59, 3247. 24. Krot A. N. et al. (2004) *MAPS*, in press. 25. Nagahara H. et al. (1999) *Antarct. Met*. XIV, 113. 26. Nagahara H. and Ozawa K. (2004) *LPSC* CD#1793. 27. Blander M. et al. (2001) *J. Phys. Chem. B* 105, 11823. 28. Nagahara H. (1981) *Nature* 292, 135. 29. Jones R. H. (1996) In *Chondrules and the Protoplanetary Disk* (ed. R. H. Hewins, R. H. Jones, E. R. D. Scott) Cambridge Univ. Press, p 163.

**SHOCK HEATING: EFFECTS ON CHONDRITIC MATERIAL.** S. J. Desch[1], F. J. Ciesla[2], L. L. Hood[3], and T. Nakamoto[4]. [1]Department of Physics and Astronomy; Arizona State University; Tempe, AZ 85287; Steven.Desch@asu.edu; [2]NASA Ames Research Center; MS 245-3; Moffett Field, CA 94035; ciesla@cosmic.arc.nasa.gov; [3]Lunar and Planetary Laboratory; University of Arizona; 1629 E. University Blvd.; Tucson, AZ 85721; lon@lpl.arizona.edu; [4]Center for Computational Sciences; University of Tsukuba; Tsukuba 305-8577; Japan; nakamoto@rccp.tsukuba.ac.jp.

**Introduction:** At the 1994 Conference on Chondrules and the Protoplanetary Disk, shock waves were discussed as mechanisms that may have been responsible for forming chondrules, millimeter-sized igneous spheres which are significant components of chondritic meteorites [1, and references therein]. At the time, shock waves were appealing because they were thought to be brief, repetitive events that were quantitatively shown to be able to rapidly heat silicates to the appropriate temperatures for chondrule formation.

Since that meeting, more detailed models for the thermal processing of material in shock waves have been developed [2-4]. These models have tracked the thermal evolution of the silicates for longer periods of time and found that their cooling rates are also consistent with what has been inferred for chondrules. In addition to the thermal histories of these particles, shock waves may be able to explain a number of other features observed in primitive meteorites. Here, we review the recent work that has been done in studying the interaction of solids with shock waves in the solar nebula.

**Source of Shocks in the Early Solar System:** Shocks are ubiquitous in astrophysics, and many mechanisms have been suggested that could give rise to shocks in the early Solar System. One is bow shocks around planetesimals moving supersonically with respect to the gas [5]. The scale of these shocks would be roughly the size of the planetesimals. Another source is the accretion of material onto the disk [6]. These shocks would be large-scale but probably not process solids more than once. A promising source of shocks is gravitational instabilities within the disk [7]. These would be widespread and repeatable. Unfortunately, disk models are not yet to the point that we can conclusively identify a source of shocks. Analysis of how chondritic material is affected by shocks can help constrain this astrophysical unknown.

**Physics of Heating in Shock Waves:** A shock front is the supersonically moving discontinuity between cool, low-density, high-velocity gas and hot, high-density, slow-moving gas. As the fast-moving gas passes through the shock front, it is slowed, compressed and heated according to the Rankine-Hugoniot relations. But the motions of any solids in the gas are not initially affected by the shock front. Solids continue to move supersonically through the gas until they collide with roughly their own mass of gas. This supersonic drift velocity heats the solids just as meteoroids are heated as they pass through the atmosphere. In addition, the solids are heated by thermal exchange with the heated, compressed post-shock gas. Solids may also be heated by absorbing the infrared radiation emitted by other solids and gas molecules. Eventually, the solids come into dynamic equilibrium with the gas, and then also come into thermal equilibrium. The gas and solids return to their pre-shock temperatures. The physics of shock wave heating of solids is one in which heating is relatively sudden and short-lived. Experimental petrology has established that chondrules were heated in exacltly this manner, and the shock wave model has gained favor as the mechanism that melted the chondrules.

**Chondrule Formation in Shock Waves:** As stated above, three separate groups [2-4] have shown that the cooling rates of millimeter-sized particles suspended in nebular gas overrun by a shock wave can be consistent with those rates inferred for chondrules (10-1000 K/hr). Despite this agreement, the models differ slightly in their assumptions and the conclusions as to how particles are able to cool at these rates. The model of Iida et al. [2] assumed that the gas could cool itself effectively by emitting line radiation, infrared photons generated by transitions between the energy states of water and CO molecules. They assumed these photons could escape the shocked region with high efficiency, so the gas tended to cool rapidly. Since the gas does not stay warm for long, solids, which are mainly heated by frictional heating, stay hot only for as long as they are moving supersonically through the gas. The cooling rate of chondrules in such a model is > 100 K/hr. Desch & Connolly [3] and Ciesla & Hood [4], make the opposite assumption, that line photons cannot escape the shocked region before being absorbed by another water or CO molecule. In that case, the gas can stay warm for longer, and the solids are heated by the gas even after they slow to the gas velocity. Because more solids stay hot for longer, solids absorb more infrared radiation from other chondrules. In such models, chondrules tend to cool at rates of 10-100 K/hr, at rates

determined by how quickly the solids can travel several optical depths from the shock front.

Clearly line photons will escape the shocked region with some intermediate efficiency, not being perfectly trapped, but not escaping with perfect efficicency either. The resolution of the problem will come with more detailed modeling of the absorption of line photons by water and CO molecules in the gas. Likely inputs to this calculation will include the spatial distribution of water, which is perhaps influenced by the presence of a snow line [8]. Current solutions very likely bracket the real solution.

Cooling rates are not the only attribute of chondrules that may be explained in terms of the shock-wave heating model. One of the most prominent features of chondrules is that they formed through liquid spheres. However, if the ambient gas pressure is not high enough, liquid silicates, which have high vapor pressures, tend to boil, and they could hardly form chondrules. According to Miura et al. [9], the gas pressure in a region behind shocks is so high that the boiling of liquid particles is suppressed. It should be noted that a condition to heat and melt solids and a condition to keep the molten state stable are independent of each other, but the shock-wave heating model can meet these conditions consistently. Another interesting property of chondrules is their sizes. Susa & Nakamoto [10] pointed out that one of the mechanisms to which the chondrule size distribution may be attributed is the disruption of liquid particles in the high velocity gas flow. When the particles are liquid, those particles are exposed by the fast gas flow behind the shock. And the gas flow exerts the ram pressure on the partilces. When the ram pressure is stronger than the surface tension, which tends to keep the liquid particle spherical and is inversely proportional to the radius of the particle, the liquid particle is expected to break down. In the case of the shock-wave heating model, the maximal size of the liquid particle is estimated to be of the order of 1 mm [10], which is consistent with natural chondrules.

**Other Shock Wave Studies:** While most studies of shock waves in the solar nebula have focused on whether or not they could form chondrules, a variety of additional effects have also been studied. As some of the proposed shock generating mechanisms would operate on large scales, understanding how shock waves may have affected other objects is needed.

*Annealing Dust.* In addition to melting millimeter-sized particles, [11] showed that smaller particles can be brought to and maintained at elevated temperatures for extended periods of time. This would allow those grains that formed at large heliocentric distances to be annealed into crystalline grains, which are thought to be present in comets. This may also be important for understanding the structure of small grains that were present near the chondrule forming region.

*Chemical Reactions.* Associated with shock waves are large increases in gas pressure. These pressures may be larger than those expected at a given location in the nebula. In addition, if a volatile substance is present in the nebula in solid form, and at elevated concentrations, that substance may be vaporized and the resultant partial pressure may be at a value many orders of magnitude higher than is expected under canonical solar nebula conditions. Under such situations, the chemistry of the nebula can be affected. The chemical reactions which take place in the nebula will depend on the temperature, pressure, and concentration of the reacting species. Thus, a shock wave may provide a temporary environment in which chemical reactions can take place that would not otherwise have occurred.

This idea was explored in [12] in looking at the formation of fine-grained phyllosilicates in the solar nebula. The formation of these objects was originally thought to be kinetically inhibited in the solar nebula. However, if a shock wave were to occur in a region of the nebula with a significant ice enhancement beyond the snow line [8], then the temperature at which these objects could form would increase due to the increased pressure. This would allow them to form on very short timescales, provided the shocked gas did not dissipate before the reaction was completed.

**Discussion:** The occurrence of shock waves in the solar nebula may have played a major role in processing the primitive solids suspended in the gas. This processing may be seen in the thermal evolution of the solids, their chemical evolution, and their dynamical evolution. Understanding how these shock waves were created and operated, therefore, needs to be fully explored. Analysis of chondritic material may provide important constraints on the astrophysical sources of shocks in the solar nebula.

**References:** [1] Hewins R. H. et al. (1997) *Chondrules and the Protoplanetary Disk,* Cambridge University Press. [2] Iida A. et al. (2001) *Icarus 153,* 430-450. [3] Desch S. J. and Connolly, Jr. H. C. (2002) *Meteorit. Planet. Sci. 37,* 183-207. [4] Ciesla F. J. and Hood L. L. (2002) *Icarus 158,* 281-293. [5] Weidenschilling S. J. et al. (1998) *Science* 279, 681 [6] Ruzmaikina T. V. & Ip W. H. (1994) *Icarus 112*, 430 [7] Boss, A. P. (2001) *ApJ* 563, 367 [8] Cyr K. E. et al. (1998) *Icarus 135,* 537-548. [9] Miura H. et al. (2002) *Icarus 160,* 258-270. [10] Susa H. and Nakamoto T. (2002) *Ap. J. 564,* L57-L60. [11] Harker D. E. and Desch S. J. (2002) *Ap. J. 565,* L109-L112. [12] Ciesla F. J. et al. (2003) *Science 299,* 549-552.

**RHÖNITE-BEARING INCLUSIONS E201 AND E202 FROM EFREMOVKA: CONSTRAINTS FROM TRACE ELEMENT MEASUREMENTS.** C. Floss[1], M. A. Nazarov[2] and L. A. Taylor[3], [1]Laboratory for Space Sciences, Washington University, St. Louis, MO 63130, USA (floss@wustl.edu), [2]Vernadsky Institute of Geochemistry and Analytical Chemistry, Moscow 117975, Russia (nazarov@geokhi.ru), [3]Planetary Geosciences Institute, University of Tennessee, Knoxville, TN 37996, USA (lataylor@utk.edu).

**Introduction:** Inclusions containing rhönite are rare among CAIs and were known only from the Allende meteorite [e.g., 1-4] until [5] reported the discovery of two rhönite-bearing inclusions, E201 and E202, from the Efremovka CV chondrite. Unlike rhönite-bearing CAIs from Allende, these inclusions show little evidence of secondary alteration and, thus, are a good source of information about primary nebular processes. We are investigating the trace element and isotopic systematics of these inclusions in order to better understand their origin.

**Results:** Trace elements, including the REE, were measured by ion microprobe in the constituent minerals of both inclusions. The petrography of these CAIs was given by [5] and preliminary trace elements data for E201 was reported by [6].

*E201*: E201 is a type B1 inclusion whose core consists of subequal amounts of coarse-grained melilite and fassaite, often poikilitically enclosing spinel; however, there are also spinel-free islands of only melilite and fassaite. Minor rhönite and perovskite occur in the core, but no anorthite is present [5]. Surrounding the core is a mantle of mostly gehlenite-rich melilite, which is separated from the core of the inclusion by perovskite/melilite symplectites. The inclusion is surrounded by a thin rim of spinel and diopside. All of the minerals analyzed have modified group II REE patterns, which are depleted in an ultra-refractory component (Fig. 1). The LREE are enriched relative to the HREE and exhibit moderate volatility-controlled fractionations; positive Tm and Yb anomalies are also present [6]. Superimposed upon these patterns are variations typically associated with crystal chemical controls. Thus, melilite has a positive Eu anomaly and a more LREE-enriched pattern than fassaite. A small hibonite-bearing inclusion attached to the surface of E201 shows the same REE fractionations, indicating that it formed from a similar reservoir.

Fassaite in E201 is zoned, with decreasing Ti and Al and increasing Mg from the cores to rims of crystals [5]. Trace element abundances also vary, with REE and Y abundances increasing and Sc and V abundances decreasing with decreasing Ti. These variations are consistent with the trends expected from crystallization of type B melts [7]. One fassaite grain has REE abundances that are significantly higher (by an order of magnitude) than the others [6]. Core melilite REE compositions vary by a factor of five and are inversely correlated with Ak contents, as expected from partitioning experiments [8]. However, REE abundances are lowest in the more gehlenitic mantle melilite. This may reflect rapid cooling of the outer mantle, as [9] have noted that partition coefficients for melilite decrease with increased cooling rate.

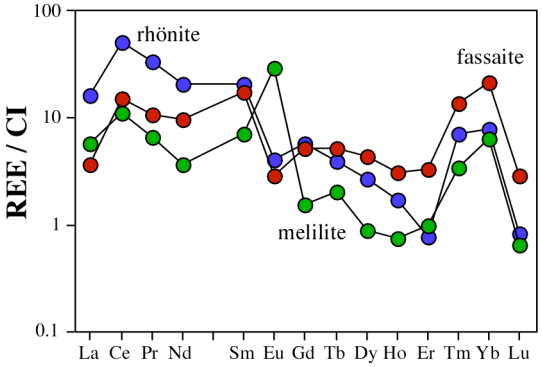


*Figure. 1. Representative CI chondrite-normalized REE patterns for minerals from E201.*

*E202*: E202 is a compact type A inclusion dominated by coarse-grained relatively gehlenitic melilite with minor fassaite, both of which poikilitically enclose spinel. Rounded rhönite grains are associated with fassaite and are surrounded by perovskite/melilite symplectites [5]. A rim containing spinel and perovskite surrounds one edge of the inclusion. The minerals in this inclusion have REE patterns that are largely unfractionated, but show some variations consistent with mineral/melt partitioning (Fig. 2). Melilite REE patterns are flat with small positive Eu anomalies; REE concentrations vary by a factor of three, but are not correlated with Ak contents. Both fassaite and rhönite REE patterns are HREE-enriched with negative Eu anomalies, and show little variation in abundance. REE concentrations are a factor of 5 higher in fassaite than rhönite. Perovskite has a slightly LREE-enriched pattern with a negative Eu anomaly and REE abundances of 600–900 x CI.

Preliminary Mg isotopic analyses suggest that both inclusions have $^{26}$Mg excesses due to the decay of $^{26}$Al, with $^{26}$Al/$^{27}$Al ratios consistent with the

canonical value of 5 x $10^{-5}$. Additional measurements are planned to confirm this, and to look for Mg isotopic fractionation in the mantle of E201 that may provide evidence for evaporative loss of Mg.

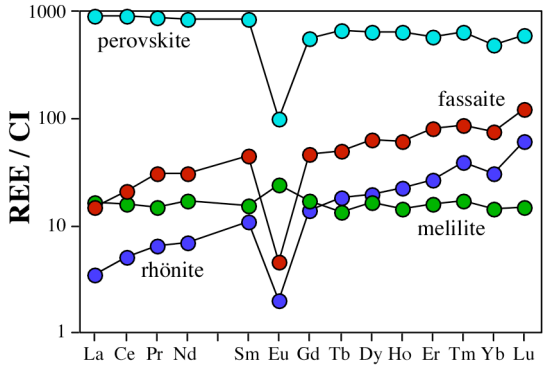


*Figure. 2 Representative CI-chondrite normalized REE patterns for minerals from E202.*

**Discussion:** The presence of rhönite in these inclusions and unusually Ti-rich fassaite in E201 may indicate high Ti/Si in their precursor materials [5], suggesting that the two inclusions originated in a similar region of the solar nebula. However, the trace element data indicate that they have experienced very different histories. In addition to the obvious differences in REE pattern types between the two inclusions, it is interesting to note that rhönite, which in E202 exhibits HREE-rich partitioning similar to fassaite, is in E201 much more strongly LREE-enriched than fassaite.

The modified group II REE pattern of E201 is unusual for type B1 inclusions [10] and indicates that its precursor material condensed after the fractionation and removal of an ultrarefractory component. The fact that an inclusion with similar REE patterns has accreted onto E201 suggests that melting of the E201 precursor material probably occurred in close spatial and/or temporal proximity to the original condensation event. E201 probably cooled rapidly under non-equilibrium conditions, as indicated by the absence of anorthite and the presence of rhönite [5], which is not predicted from equilibrium crystallization of type B CAI melts [11, 12]. Rapid cooling is also suggested by the low REE abundances in the mantle melilite, as noted above.

Spinel-free islands such as those seen in E201 have been interpreted as xenolithic components in some CAIs [13], but such an origin is unlikely in E201. Although the anomalously REE-rich fassaite grain noted above comes from a spinel-free region, two other fassaite grains from spinel-free areas have REE abundances in the range of those from spinel-rich areas. Moreover, [14] showed that REE concentrations for subliquidus fassaite extend to compositions that encompass such grains. Finally, it is not likely that xenolithic components would fortuitously have the same unusual fractionated REE patterns as the host CAI. The spinel-free regions may, however, represent unmolten or partially unmolten remnants of precursor material, which are not in complete equilibrium with the remainder of the CAI.

The origin of E202 is more enigmatic. Although compact type A inclusions are generally thought to have crystallized from liquids, their crystallization histories have been difficult to decipher. REE patterns in the minerals from E202 exhibit variations that are consistent with their formation from a melt, and [5] inferred a crystallization sequence of spinel followed by melilite, rhönite and fassaite for E202. However, melilite REE abundances are not correlated with Ak content as expected for igneous partitioning and fassaite REE and other trace element abundances show no systematic variations from one grain to another. E202 may have experienced later heating [e.g., 15] that obscured original igneous trends in melilite and homogenized fassaite REE compositions. However, the extent of metamorphism must have been limited, because major and trace element compositions in melilite are not homogeneous.

**Conclusions:** Trace element data show that E201 and E202 did not originate in the same part of the solar nebula. Both inclusions crystallized from melts of different precursor materials and E202 may have experienced some later metamorphism. The presence of rhönite in both CAIs could reflect crystallization kinetics [5], possibly coupled with elevated Ti/Si for E201, which contains Ti-rich fassaite in addition to rhönite.

**References:** [1] Fuchs L. H. (1971) *Am. Mineral.* **56**, 2053-2068. [2] Fuchs L. H. (1978) *Meteoritics* **13**, 73-88. [3] Allen J. M. et al. (1978) *PLPSC 9th,* 1209-1233. [4] Podosek F. A. et al. (1991) *GCA* **55**, 1083-1110. [5] Nazarov M. A. et al. (2000) *LPS. XXXI*, #1242. [6] Floss C. (2000) *MAPS* **35**, A53-A54. [7] Simon S. B. et al. (1991) *GCA* **55**, 2635-26455. [8] Beckett J. R. et al. (1990) *GCA* **54**, 1755-1774. [9] Davis A. M. et al. (1996) *LPS. XXVII*, 291-292. [10] Sylvester P. J. et al. (1992). [11] Stolper E. (1982) *GCA* **46**, 2159-2180. [12] Stopler E. and Paque J. M. (1986) *GCA* **50**, 1785-1806. [13] El Goresy A. et al. (1985) *GCA* **49**, 2433-2444. [14] Simon S. B. et al. (1991) *GCA* **55**, 2635-2655. [15] Teshima J. and Wasserburg G. J. (1985) *LPS. XXXVI*, 855-856.

**ELEMENT MAPPING IN ANHYDROUS IDPs: IDENTIFICATION OF THE HOST PHASES OF MAJOR/MINOR ELEMENTS AS A TEST OF NEBULA CONDENSATION MODELS.** G. J. Flynn[1], L. P. Keller[2], S. Wirick[3], and C. Jacobsen[3]. [1]Dept. of Physics, SUNY-Plattsburgh, Plattsburgh, NY 12901 (george.flynn@plattsburgh.edu), [2]NASA Johnson Space Center, Houston, TX 77058, [3]Dept. of Physics, SUNY-Srtony Brook, Stony Brook, NY 11794.

**Introduction:** Many anhydrous interplanetary dust particles (IDPs) are the most pristine samples of primitive solar system dust currently available for laboratory analysis. Their primitive nature is demonstrated by: 1) the high content of moderately volatile elements, indicating they have not been heated significantly since formation, 2) the absence of hydrated material, indicating they never experienced aqueous processing, 3) the presence of unequilibrated mineral assemblages, 4) the presence of large isotopic anomalies (e.g., D and $^{15}$N enrichment), in these IDPs.

**Measurements:** We have begun a project to identify the host phases of the major and minor elements in primitive IDPs, and compare the host of each element to predictions allowing us to test nebula condensation models. The project proceeds in three steps:

1) We map the spatial distributions of elements from K to Zn in ultramicrotome sections, each ~80 to 100 nm thick, using a zone plate focused X-Ray Microprobe (XRM) at Sector 2 of the Advanced Photon Source (APS) at Argonne National Laboratory. This XRM has an analysis beamspot ~150 nm in size, sufficient to resolve individual mineral grains in most primitive IDPs.
2) We map the spatial distribution of C, N, and O using a Scanning Transmission X-ray Microscope (STXM), which employs zone plate focusing to achieve an ~50 nm analysis beamspot, on ultramicrotome sections, and then determine the C, N, and O functional groups by X-ray Absorption Near-Edge Structure (XANES) spectroscopy.
3) Once the element hot-spots are identified using the XRM and STXM, we identify the host using a Transmission Electron Microscope (TEM).

We have analyzed 3 primitive, anhydrous IDPs, L2011*B2, L2010B10, and L2009*F3, using the XRM, and 3 primitive, anhydrous IDPs, L2005*A3, L2008H9, and L2011R11, using the STXM.

**XRM Results:** Some of the element maps we obtained in this project are shown in Flynn et al. [1]. Each of the elements that we mapped was found to be localized within each of the IDPs.

*K Results.* L2011*B2 is a cluster fragment that has a relatively high K concentration. The K is spatially correlated with the Si in this particle. TEM examination of other sections of this particle indicate the K-host is a pyroxene, while nebula condensation models predict that K should condense in feldspar.

*S Results:* Small S hot-spots were detected in all the IDPs examined. Most of the S is concentrated in Fe-sulfides, consistent with nebua condensation models.

*Zn Results:* The Zn is concentrated in small hot- spots co-located with both Fe and S, indicating that the Zn host is a Zn-rich, Fe-sulfide.

*Cu results:* The Cu in L2011*B2 is concentrated in small hot spots that are co-located with both Fe and S, suggesting the Cu is also in an Fe-sulfide.

*Ca Results:* The Ca is concentrated in a silicate phase, which has not yet been examined by TEM.

**STXM Results:** Because carbonate has a strong absorption at ~290.5 eV, the STXM is a particularly sensitive tool to searech for carbonate in the IDPs.

*Carbonate Results:* One IDP, L2011R11 shows a strong absorptions consistent with carbonate (see Fig. 1), suggesting carbonate may be a nebula condensate.

*Nitride Results:* The N concentrations in L2011R11 and L2005*A3 are so low that we have not mapped the N distribution in these IDPs, but we obtained N-XANES spectra consistent with amide or amine compounds. L2008H9 contains more N than the other two anhydrous IDPs. This N is concentrated in several small grains, and has an N-XANES spectrum consistent with nitrides (as described in Flynn et al. [2]). TEM examination of these N-rich grains is in progress.

**References:** [1] Flynn, G. J., Keller, L. P., and Sutton, S. R. (2004) Sub-Micrometer Scale Minor Element Mapping in Interplanetary Dust Particles, *Lunar & Planetary Science XXXV*, Lunar & Planetary Institute, Houston TX, CD-ROM, Abst. #1334. [2] Flynn, G. J., Keller, L. P., Wirick, S. and Jacobsen, C. (2004) Nitrogen Mapping and Nitrogen XANES Spectroscopy of IDPs, *Meteoritics & Planet. Science*, Abst. # 5092.

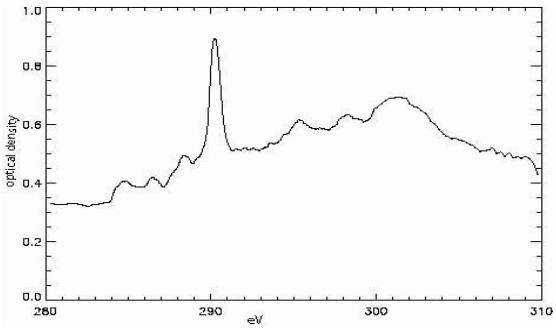


**Figure 1: XANES spectrum of selected areas on L2011R11 that show the large absorption at ~290.5 eV, characteristic of carbonate.**

**THEORETICAL STUDIES OF DISK EVOLUTION AROUND SOLAR MASS STARS.** C. F. Gammie[1] and B. M. Johnson[2], [1,2]Loomis Laboratory of Physics, 1110 West Green Street, Urbana, IL, 61801. gammie@uiuc.edu, bmjohnso@uiuc.edu .

**Introduction:** I will review current ideas about turbulence and the evolution of protoplanetary disks. Angular momentum conservation anchors disk gas and dust in its orbit about the young star. Turbulence is central to disk evolution because it is often, but not always, associated with angular momentum transport; this permits the development of slow radial flows and ultimately drives accretion onto the central star and overall evolution of the disk.

**Magnetorotational Instability:** One means of initiating turbulence in differentially rotating, highly conducting fluids is now well known: numerical experiments (e.g. [1]) and laboratory experiments (e.g. [2]) show that turbulence can be can be initiated and sustained by the magnetorotational instability (MRI) [3,4]. MRI driven turbulence has been shown to result in angular momentum exchange between annuli in the disk and thus accretion. The MRI likely drives accretion in many astrophysical disk systems, including cataclysmic variables, X-ray binaries, galactic nuclei, and even the central engine of gamma-ray bursts.

The MRI is effective only if the ionization fraction is large enough to couple the magnetic field to the disk fluid; the bulk of T Tauri disks is likely to be predominantly neutral [5,6]. At low ionization nonideal plasma effects enter, including Hall drift, Ohmic diffusion, and ambipolar diffusion. These nonideal effects complicate both analytic stability studies and numerical experiments. Nonideal effects alter the stability properties of the disk, but most of the disk at 0.1 AU < r < 30 AU is simply too poorly ionized for the MRI to be effective at promoting turbulence and angular momentum transport. We are thus motivated to look for other sources of turbulence, or else to conclude that the bulk of the disk is "dead" (laminar) and accretion occurs only in thin surface layers ionized by cosmic rays [6] or X-rays [7,8].

**Self-Gravity:** Gravitational instability can also drive turbulence in disks. Gravitational instability occurs when the self-gravity of the disk overcomes the stabilizing influences of pressure and rotation. In the language of planetary science, this happens when the disk central density exceeds the Roche density. What happens next depends on how rapidly the collapsing disk can dispose of its internal energy. If the disk cooling time is less than about half a rotation period, then bound objects (perhaps planets) form (e.g. [9]). If the disk cools more slowly, steady "gravito-turbulence," accompanied by angular momentum diffusion, follows. Massive disks, typically more than 1/10 the mass of the central star, are required for gravitational instability. Such conditions are only likely present in the outer disk (r > 2 AU) in the first ~$10^4$ years of the disk's existence.

**Baroclinic Instability:** Recent work has argued that a fluid instability related to radial stratification-- essentially radial convection-- (the "global baroclinic instability" [10]) may drive turbulence and angular momentum transport. This result is potentially important because protoplanetary disks will often have radial entropy gradients that are favorable for instability. Our recent work, however, shows no evidence of convective instabilities in our numerical experiments. Instabilities present in other contexts (such as baroclinic instability in planetary atmospheres) are strongly suppressed in disks by angular momentum conservation and by *differential* rotation.

**Other Mechanisms:** It is too early to conclude, however, that "dead" disks really exist. Most studies have used approximations that neglect the vertical structure of the disk. Vertical gradients in orbital velocity in the gas may lead to instabilities and the production of vortices; numerical studies indicate that anticyclonic vortices in disks can be long lived [11]. Interaction with the dust layer may play a crucial role [12]. And disk winds can also drive disk evolution (e.g. [13]).

Nevertheless it is interesting to ask what would happen if dead disks do exist. If accretion can continue in thin MRI-active surface layers, then matter naturally accumulates at certain radii in the disk (the location of the accumulation points depends on the opacity and other factors). If allowed to continue for long enough, the accumulation regions can become unstable, producing episodic accretion.

**References:** [1] Hawley, J.F. et al. (1996), *Ap. J.* 440, 742. [2] Sisan et al. (2004), physics/0402125. [3] Balbus, S.A., and Hawley, J.F. (1991), *Ap.J.* 376, 214. [4] Balbus, S.A., and Hawley, J.F. (1998), *Rev. Mod. Phys*. 70, 1. [5] Hayashi, C. 1981, *Prog. Theor. Phys.*, 70, 35. [6] Gammie, C.F. (1996), *Ap. J.* 457, 355. [7] Glassgold, A. et al. (1997) Ap.J. 480, 344. [8] Sano et al. (2000) *Ap.J.* 543, 486. [9] Gammie, C.F. (2001) Ap.J. 553, 174. [10] Klahr, H.H., and Bodenheimer, P. (2003) *Ap.J.* 582, 869. [11] Godon, P., and Livio, M. (1999) *Ap.J.* 523, 350. [12] Goodman, J. and Rafikov, R. (2001) *Ap.J.* 552, 793. [13] Wardle, M., and Konigl, A. (1993), *Ap.J.* 410, 218.

**CHEMICAL EFFECTS OF HIGH-TEMPERATURE PROCESSING OF SILICATES.** M. V. Gerasimov[1], E. N. Safonova[1], Yu. P Dikov[2], and O. I. Yakovlev[3]. [1]Space Research Institute, RAS, Profsoyuznaya, 84/32, Moscow, 117997, Russia, mgerasim@mx.iki.rssi.ru, , [2]Institute of Ore Deposits, Petrography, Mineralogy and Geochemistry, RAS, Moscow 109017, Staromonetny per., 35, [3]Vernadsky Institute of Geochemistry and Analytical Chemistry, RAS, Moscow 117975, GSP-1, Kosygin st., 19

**Introduction:** Hypervelocity collisions is a fundamental process which affect the evolution of solid material in the universe. Collisions of particles occur in dust clouds or protoplanetary disks. Planetesimals or meteorites impact large planetary bodies through the geological history. Solid material during an impact is subjected to high-temperature flash heating at highly compressed state which is followed by release of the pressure while temperature can remain rather high to cause vaporization of some portion of the material. The main reason of chemical differentiation here is the selective character of volatility of different elements, which can result in sufficiently different compositions of impact products (melted residua, vaporized/condensed stuff, etc.) while the bulk composition of the whole system remains unchanged. The process of star bursts also have some similarity to the evolution of initially high temperature and high-pressure impact-produced plumes. This supports the validity of the investigation of chemical differentiation of siliceous material during impact-related high-temperature flash processes. Here we present some basic results of our experimental investigation of evaporative chemistry under impact-simulated conditions.

**Experimental technique:** The simulation of impact-related high-temperature processing was performed using a laser pulse (LP) technique [1]. The Nd glass laser had the following parameters: the wavelength - 1,06 μm, the energy of a pulse 400÷600 J, the power density $10^6 \div 10^7$ W/cm$^2$, and a pulse duration ~$10^{-3}$ s. Typical temperature under such condition is 4000÷5000 K. The experiments were performed by vaporizing samples in a sealed cell which was usually filled by gas (helium, air, $H_2$, $CH_4$, etc.) at 1 atm. The laser beam was focused into a spot with diameter 3÷5 mm producing melting, evaporation, and dispersion of melted droplets into expanding plume. A copper foil was placed in the path of spreading of the vapor plume at a distance ~7 cm from the sample to collect condensed material. The glass spherules with diameters ranging from around one to several tens of microns were found on the surface of the condensed film. Chemical analysis of the spherules were performed using FESEM/EDS microprobe analyses.

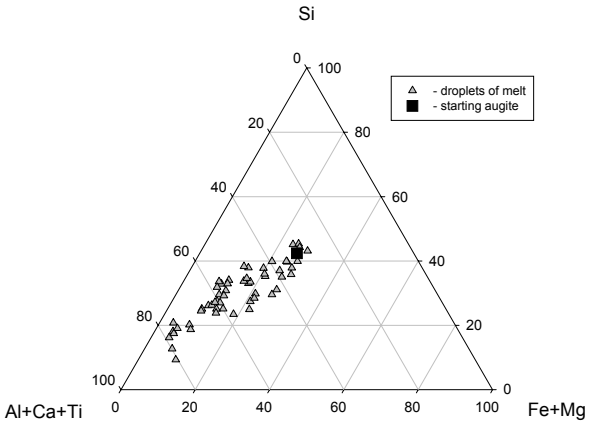


Fig. 1. Chemical composition (wt. %) of starting augite and of dispersed melted droplets which were produced in LP experiment. The field of droplets compositions indicate the trend of compositional changes of the augite melt during successive mass loss.

**Experimental results:** High-temperature impact-related treatment results in fundamental chemical changes of siliceous materials.

*Formation of refractory compositions*. Experimental investigation of differentiation of mafic melts shows that spherules in the beginning of a mass loss process are loosing Si, Fe, alkalis, and their composition enriches in Mg, Ca, Al, and Ti. With a developed mass loss spherules looses Mg while Si is still present in the system [2]. Even Na is not totally lost. Greater mass loss results in the enrichment of Ca, Al, and Ti in the system (Fig. 1). The end members of the mass loss process depends on the temperature of volatilization. Volatilization under 3000 K results in Al-rich spherules and volatilization at temperatures over 3000 K results in Ca-rich spherules.

*Reduction of iron.* An important effect of high-temperature processing is the reduction of iron. Two main mechanisms are responsible for the reduction: thermal and chemical. Thermal mechanism produces metallic iron nanoparticles through the body of high-temperature siliceous melts due to direct dissociation of iron oxide

$$FeO \rightarrow Fe + O$$

while chemical mechanism involve reducing components (C, H, etc.) in exchange reactions

$$FeO + C \rightarrow Fe + CO$$

Fig. 2 shows metallic iron nanoparticles (white points) inside the melt which were formed in LP experiment with olivine. Gray uniform body under the melt is the not melted starting olivine. Reduction of iron in olivine is a result of only thermal mechanism since no reducing components were present in the system. Generally both mechanisms are working in a multicomponent system making reduction rather efficient. Fig. 3 shows a melted spherule from LP experiment with Murchison. Its surface is heavily covered by Fe-metal and FeS particles. Due to immiscibility metallic particles are concentrated on the surface of melted droplets but some metallic particles can be present inside the melt. Siderophile elements have a noticeable trend of enrichment in the formed metallic particles.

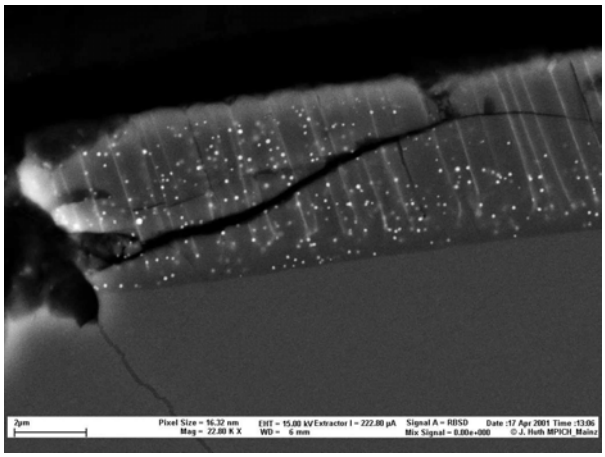

Fig. 2. SEM view of a cross-section of a piece of melt over a not melted olivine (gray) after a LP experiment. White points in the melt are iron-metal nanoparticles.

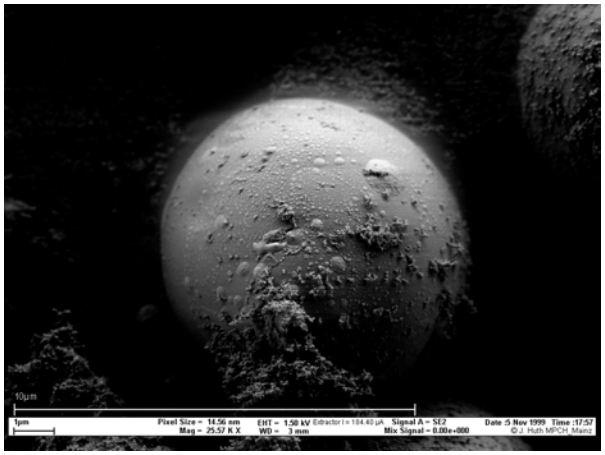

Fig. 3. SEM view of a melted spherule produced in LP experiment with Murchison. Its surface is covered by Fe-metal (small) and FeS (large) particles.

*Synthesis of complex organics*. We performed systematic experiments with samples containing inorganic carbon and hydrogen. In one set of experiments, carbon and hydrogen were incorporated into the sample in inorganic phases, in another, carbon and hydrogen free samples were vaporized in $CO_2$+$H_2O$ or $CH_4$ atmospheres. Experiments show the synthesis of a rather complex organic components (mainly hydrocarbons) even at oxidized conditions only if hydrogen and carbon is present in the system [3]. The possible mechanism here can be the Fischer-Tropsch-type of synthesis on the surface of forming condensed particles. Fig. 4 shows chromatograms of organic compounds obtained at oxidized conditions in LP experiment with a composite sample in atmosphere of air. Synthesis of organics at reduced conditions is sufficiently high [4]. Extracted organics were mainly PAHs with degree of polymerization up to $C_{20}$. X-ray photoelectron spectroscopy of obtained condensates indicate much higher concentration of carbon bound in C-C and C-H bonds than the amount of organic components extracted by solvents. It is probable that some organics are present in the form of a kerogen-like material.

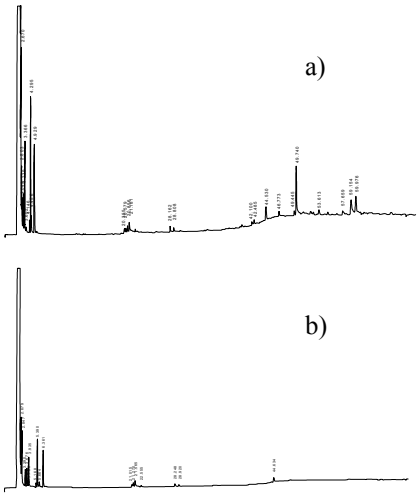


Fig.4 Chromatograms of organic compounds extracted from condensed material in LP experiment with peridotite(90%)+$MgCO_3 \cdot Mg(OH)_2$(10%) target (a) and from control analysis (b).

**References:** [1] M. V. Gerasimov (1998) *Earth, Moon, and Planets*, vol. 80, Nos. 1-3, pp.209-259. [2] M. V. Gerasimov et al., *GSA Special Paper, in press.* [3] M.V. Gerasimov et al. (2002) *Deep-Sea Research Part II*, v. 49, No 6, pp. 995-1009. [4] M. V. Gerasimov and E. N. Safonova (2003) *38th Vernadsky-Brown Microsymposium*, GEOKHI RAS, Moscow, CD-ROM, #MS022.

**Acknowledgment:** This research was supported by RFBR grant 02-05-64419.

**I-Xe AND THE CHRONOLOGY OF THE EARLY SOLAR SYSTEM**, J. D. Gilmour[1], O. V. Pravdivtseva[2], A. Busfield[1] and C. M. Hohenberg[2]. [1]University of Manchester, Manchester, M13 9PL, United Kingdom (jamie.gilmour@man.ac.uk). [2]McDonnell Center for Space Sciences, Washington University, St Louis, MO 63130, USA.

**Introduction:** The I-Xe system is based on the decay of $^{129}$I to $^{129}$Xe. The 16 Ma half life of $^{129}$I is sufficiently long to enable a wide variety of processes from the earliest chondrule formation to processes on sizable planetesimals. Here we examine how best to integrate data from this system into a wider timescale incorporating results from other chronometers.

**Calibration of Chronometers**: In addition to I-Xe, chronological information with the precision required to study the formation of the solar system can be obtained from systems based on the decay of $^{53}$Mn, $^{26}$Al and $^{235/238}$U (Pb-Pb). In order to maximize the return on these studies, it is necessary to calibrate the various chronometers against one another. Previous attempts have relied on single analyses of minerals in which more than one system can be accurately measured to determine a calibration[1,2]. However, sufficient data are now available in the case of some chronometer pairs to allow the consistency of the chronometers to be examined more closely. In what follows we adopt the arbitrary zeroes conventional within the I-Xe, Mn-Cr and Pb-Pb systems and examine the data for consistency and to establish a calibration.

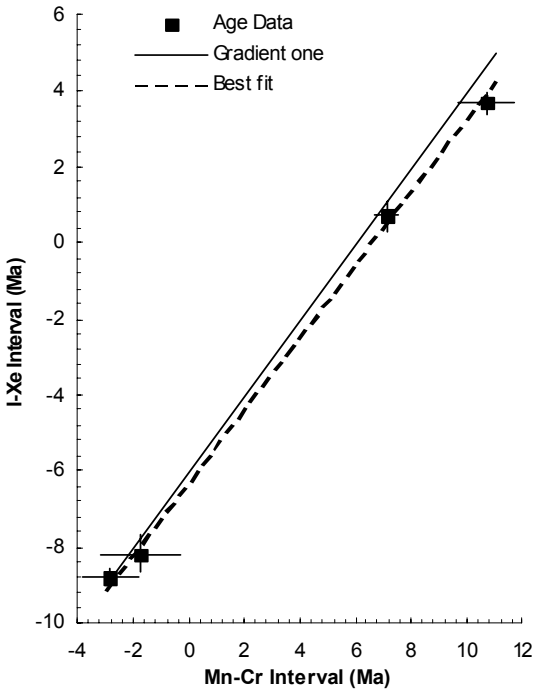


Fig 1. Comparison of relative ages of Acapulco, Richardton, Ste Marguerite and the earliest chondrules in the Mn-Cr and I-Xe systems. Data sources in text and reference [2]

*I-Xe vs Mn-Cr.* In Fig. 1 we present data from the Mn-Cr and I-Xe system measured in the chondrites Richardton and Ste Marguerite, in Acapulco and from chondrules. I-Xe data are normalized to Shallowater enstatite having a zero age, while the zero of the Mn-Cr system is defined by the angrite LEW86010.

The I-Xe measurement used here for Acapulco dates the closure of phosphate grains to xenon loss, while in the chondrites Ste Marguerite and Richardton it dates the closure of feldspar. I-Xe data for pyroxene from Richardton yield closure ages up to 10 Ma earlier than the feldspar data, testifying to the extended period of processing post-formation that the parent body of this meteorite experienced. The Mn-Cr system in Richardton and Ste Marguerite records the moment at which chromium ceased equilibrating between chromite and silicate phases, suggesting that identification of the Richardton Mn-Cr age with the feldspar I-Xe may be questionable. The final point is obtained from chondrules. In the Mn-Cr system chondrule data are sparse and tightly clustered. I-Xe chondrule data, in contrast, exhibit a wide spread that may be attributed to resetting or setting of the chronometer by parent body processes. However, dynamical considerations suggest that particles of the size of chondrules had to be sequestered on sizable bodies in the solar nebula on timescale short compared to the errors of isotope chronology, suggesting that the earliest parent body processes should approximate formation ages. Thus whether I-Xe ages are formation ages or alteration ages, the earliest chondrule data might be expected to be comparable to Mn-Cr (formation) ages.

There is a reasonable correlation between the two systems and the gradient of the best fit line (0.95) is close to 1. From the best fit line we would deduce that the I-Xe system closed in Shallowater enstatite 6.3 ± 0.3 Ma earlier than the Mn-Cr system closed in LEW86010.

*I-Xe (and Mn-Cr) vs Pb-Pb* .In Figure 2, we plot Pb-Pb ages vs I-Xe intervals for samples in which we would argue it is plausible that the two chronometers date the same event within the limits of the various techniques. Our first point stems from the identification of the oldest I-Xe chondrule age with the clustered chondrule Pb-Pb ages identified by Amelin et al.[3] We also include two previously unreported Richardton chondrules in which the Pb-Pb and I-Xe systems have

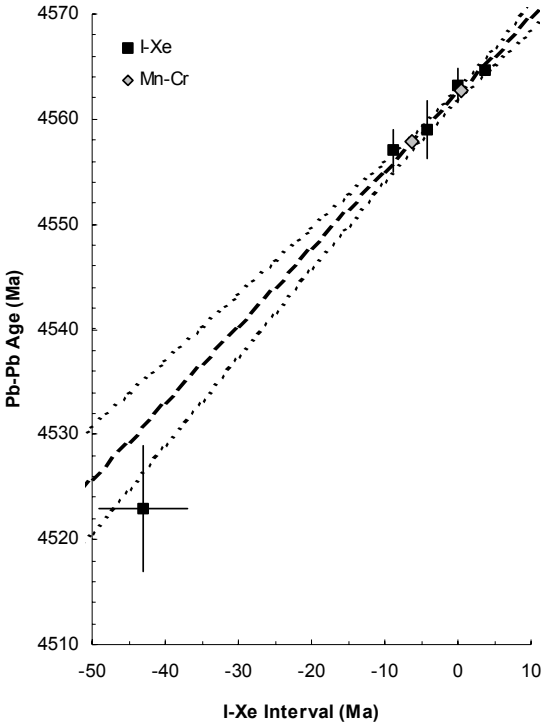


Fig. 2. Comparison of the I-Xe and Mn-Cr systems with the absolute Pb-Pb chronometer for samples from Acapulco, Richardton, Kernouve, LEW86010 and Ste Marguerite. Mn-Cr data have been converted to I-Xe intervals using the calibration of Fig. 1. Data sources in text and reference [2]

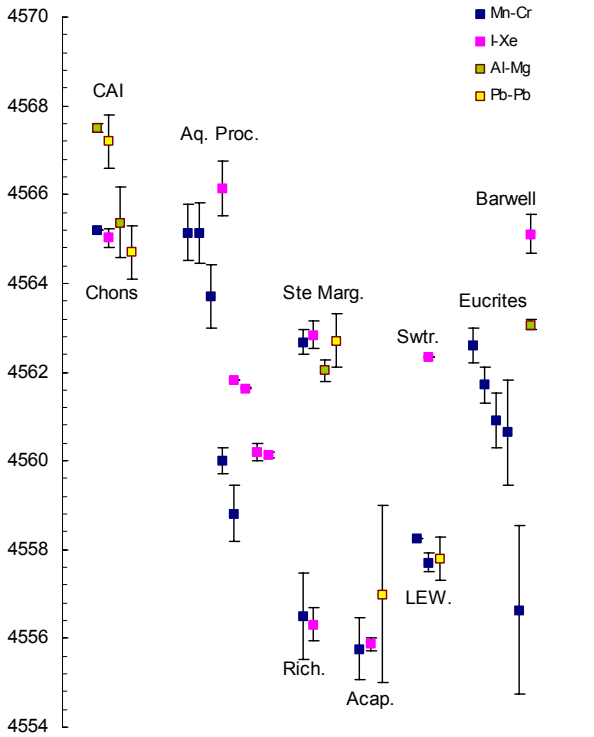


Fig. 3. Chronology derived from adopting the calibrations of Figs 1 and 2 for CAIs, Chondrules, Aqueous Processes Ste Marguerite, Richardton, Acapulco, Shallowater LEW86010, Eucrites and Igneous Clasts from Barwell *data sources in text and ref [2].

both yielded dates (O. V. Pravdivtseva, unpublished data). Data from the Pb-Pb and I-Xe chronometers from samples of Acapulo phosphate were reported by Nichols et al.[1] and are included, as is the data for the two systems from Kernouve reported by Brazzle et al.[4] In addition to these five points, we employ the calibration between Mn-Cr and I-Xe intervals advanced here to add equivalent I-Xe intervals derived from Mn-Cr intervals for the LEW86010 angrite[5] and Ste Marguerite[6]. The correlation line fixes the zero point of the I-Xe dating scheme, closure of Shallowater pyroxene to xenon loss, at 4562.3 +/- .4 Ma before the present. The gradient of the correlation line – 0.73 +/- 0.7 – is significantly different from 1, however, suggesting some error in the half lives of either $^{129}$I, $^{235}$U or both. Begemann et al.[7] have noted the need for improved determinations of the half lives of longer lived radionuclides and speculated that similar problems may exist among the shorter lived radioactives that form the basis of chronometers. Some indication that this is the case may be seen here, though the details of the calibration are dependent on the choice of samples included[8]

**Proposed Chronology:** the chronology of solar system formation produced by adopting the calibrations derived here is shown in Fig. 3. The sequence of events is perhaps more palatable that that produced in previous attempts at producing a unified chronology[2]; for instance, no parent body processes appear to definitively predate the earliest chondrule ages, though this has been achieved by adopting a calibration between short and long-lived chronometers requiring some revision of accepted half lives.

**References:**

[1] Nichols et al. (1994) GCA 58 2553. [2] Gilmour and Saxton (2001) Phil. Trans. R. Soc. Lond A 359 2037. [3] Amelin et al. (2002) Science 297 1678. [4] Brazzle et al. (1999) GCA 63 739 [5] Lugmair and Shukolyukov (1998) GCA 62 2863 [6] Polnau and Lugmair (2001) LPSC 32 abs #1527 [7] Begemann et al. (2001) GCA 65 111 [8] Busfield (2002) PhD Thesis, Univ. of Manchester.

**THE EFFECTS OF X-RAYS ON THE GAS AND DUST IN YOUNG STELLAR OBJECTS.**

A. E. Glassgold[1], E. D. Feigelson[2], T. Montmerle[3], and S. Wolk.[4], [1]Berkeley Astronomy Department, [2]Penn State University, [3]Observatoire de Grenoble,[4]Center for Astrophysics.

X-rays are emitted by essentially all young stellar objects (YSOs) and affect the circumstellar material of these systems. We will update the basic facts about YSO X-ray emission with recent observations from the Chandra and XMM/Newton satellite observatories, with emphasis on the flares of solar-mass stars recorded by the Chandra Orion Ultradeep Project (COUP). We will also discuss some of the important collateral effects of YSO X-rays on the circumstellar gas and dust.

A primary consequence of the detection of YSO X-rays is that particle acceleration must occur at early stages in the formation of sun-like stars. Extensive observations of the current Sun suggest that these particles included MeV nuclei that may have been responsible for the production of short-lived radionuclides in chondritic meteorites. This conclusion is supported by the detection of gyro-synchrotron radiation from some YSOs, providing direct evidence for the acceleration of electrons to MeV energies.

We will also relate the YSO X-ray observations to the particle fluences that are needed to account for the meteoritic measurements in the local irradiation scenario. We will discuss the limitations in making this connection due to gaps in our understanding of the nature of the flares.

The X-rays are also a source of ionization and heating for the gas and dust in the immediate environs of the YSO. One early suggestion was that hard X-rays penetrate deep into the disk and provide sufficient ionization to mediate the Balbus-Hawley instability, widely believed to be the origin of the turbulent viscosity underlying disk accretion. This idea is relevant in the context that the powerful winds generated by YSOs can blow away most of the galactic cosmic rays that would otherwise ionize the disk. Recent theoretical studies of disk ionization support the viability of this proposal.

The X-rays also help to heat the surface layers of protoplanetary disks to temperatures well above the midplane temperatures characteristic of the dust emission observed in the infrared. Even more important, the X-rays add an important ionic character to the chemistry of these layers that, together with their elevated temperatures, generates a wide variety of new diagnostics that have yet to be explored, especially for the inner disk region.

We will review some of the characteristic effects of X-rays on the condensed phases of the material near the YSO. During intense flares, X-rays may be an important thermal processing mechanism for pre-chondritic material. We will attempt to understand this possibility on the basis of simple theoretical considerations and the available laboratory data.

**ORIGIN OF SHORT-LIVED RADIONUCLIDES IN THE EARLY SOLAR SYSTEM.** J. N. Goswami[1], K. K. Marhas[2], M. Chaussidon[3], M. Gounelle[4] and B. Meyer[5]. [1]Physical Research Laboratory, Ahmedabad, India, [2]Max-Planck Institute for Chemistry, Mainz, Germany, [3]CRPG, Nancy, France, [4]CSNSM, University Paris XI, France, [5]Clemson University, South Carolina, USA.

Isotopic studies of early solar system objects such as CAIs and chondrules as well as of differentiated meteorites have revealed the presence of about a dozen short-lived now-extinct nuclides with half-life ranging from $10^5$ to $10^8$ years at the time of formation of these objects. The former presence of the now-extinct nuclides is based on the observation of excess abundances of their decay products in these samples. Correlation of such an excess with abundance of the stable isotope of the parent element conclusively establishes that the nuclide was incorporated "live" into the analyzed object at the time of its formation and decayed in-situ.

The origin of these nuclides has been debated over the last few decades. There are three viable sources: (i) continuous galactic nucleosynthesis, (ii) energetic particle interactions and (iii) freshly synthesized material from stellar objects. The possibility that continuous galactic synthesis, fuelled by supernova events occurring in the galaxy, may explain the observed abundance of the short-lived nuclide $^{129}$I (mean-life, = 23 Ma) was proposed soon after its discovery in 1960 [1-3]. The proposal for energetic particle production as well as of injection of freshly synthesized material from specific stellar objects were put forward soon after the discovery of the short-lived nuclide $^{26}$Al ( = 1Ma) in CAIs in mid-seventies [4-7]. The observational evidence for other short-lived radionuclides such as $^{41}$Ca ( = 0.15 Ma), $^{10}$Be and $^{60}$Fe ( =2.2 Ma) that cannot be explained in the continuous galactic synthesis scenario has now focussed most of the attention to the plausibility of either energetic particle production or injection from specific stellar objects as the potential sources of the short-lived nuclides present in the early solar system [see, e.g. 8 and references therein].

Several settings for energetic particle interactions have been proposed for the production of the short-lived nuclides. This could have happened within the natal presolar molecular cloud or later in a solar nebula environment. Although the source of energetic particles is difficult to pinpoint in the former case, significant flux of low energy particles are expected in a molecular cloud environment. In the solar nebula, the active early Sun acts as the source of the energetic particles; however, the setting in which interactions of solar energetic particles (SEP) with solar nebula material took place to produce the short-lived nuclides is currently a matter of debate. Irradiation of infalling material into the Sun along the nebular midplane by SEP very close to the Sun (the X-wind model [9, 10]) as well as SEP irradiation of nebular gas and dust of solar composition at the asteroidal belt region has been proposed. In the stellar origin models, nucleosynthetic yields of the short-lived nuclides from different stellar sources such as supernova, asymptotic giant branch (AGB) and Wolf-Rayet stars have been considered along with models for mixing of the freshly synthesized stellar material with material in the collapsing protosolar cloud for explaining the observed abundances of the short-lived nuclides in the early solar system [11-18]. Most of these approaches are successful in explaining only a subset of the meteorite data on abundances of the short-lived nuclides in the early solar system. The crucial test for identifying the most plausible source will be its ability to concurrently explain the data for a larger set of these short-lived nuclides.

The evidence for the presence of $^{10}$Be in the early solar system objects [19] clearly points towards the presence of an energetic particle produced component contributing to the inventory of the short-lived nuclides in the early solar system as $^{10}$Be is not a product of stellar nucleosynthesis. However, it is not clear if this irradiation took place in a presolar environment or a solar nebula environment [19-24]. On the other hand the presence of $^{60}$Fe in early solar system [25, 26] clearly hints at a contribution from a stellar source. Energetic particle irradiation is extremely inefficient in producing this nuclide due to the lack of suitable targets in material of solar composition. In contrast, $^{60}$Fe is produced copiously in supernova events and is also a product of nucleosynthesis in AGB stars.

If we consider the short-lived nuclides $^{26}$Al, $^{41}$Ca, $^{60}$Fe, and $^{182}$Hf, it appears that the abundances of these nuclides in the early solar system may be explained by considering injection of freshly synthesized material from the outer shells of a supernova [18]. On the other hand a thermally pulsating AGB star could be a source of the short-lived nuclides $^{26}$Al, $^{41}$Ca, $^{107}$Pd and $^{60}$Fe, even though it is difficult to match the inferred abundance of $^{60}$Fe concurrently with abundances of the other three short-lived nuclides [16]. It is also difficult to explain the abundance of the short-lived nuclide $^{53}$Mn by considering either of these stellar sources; it is not a product of AGB nucleosynthesis and is produced

in the inner regions of supernova and not in the outer shells. The possibility that this nuclide could be a product of continuous galactic nucleosyntheis has been proposed [27].

If we consider the standard composition and energy spectra of SEP seen in contemporary solar flares to be valid for flares from the early Sun, it is not possible to explain the observed abundances of the different short-lived nuclides in early solar system for any given combination of SEP flux, energy spectra and irradiation duration. This was shown in mid-eighties by considering abundances of $^{26}$Al and $^{53}$Mn [28] and is now extended to include the nuclides $^{41}$Ca and $^{10}$Be [21-23, 29]. A solution to this problem has been offered in the X-wind model by assuming that emission of energetic particles from the proto-Sun was dominated by $^{3}$He-rich impulsive flares. However, to obtain self-consistent data for $^{41}$Ca and $^{26}$Al abundances, additional assumptions on the composition of the irradiated refractory target material had to be invoked [10, 20]. Further, production of $^{60}$Fe in any significant amount may be ruled out by SEP interactions with solar system material.

Another potential problem of the solar energetic particle irradiation scenario is the recent experimental data that show presence of $^{10}$Be in early solar system objects that are devoid of $^{26}$Al [22, 30]. This would suggest that either the sources of $^{10}$Be and $^{26}$Al are decoupled or energetic particle production of $^{10}$Be did not co-produce significant amount of $^{26}$Al; this may be achieved by fine tuning the energy spectra of the SEP [22]. In this context the proposal for an irradiation in a presolar environment and/or trapping of cosmic ray $^{10}$Be by protosolar cloud as the source of $^{10}$Be also needs to be considered seriously [24].

At present it appears that more than a single source may be needed to explain the presence of the now-extinct short-lived nuclides present in the early solar system. Although the active early Sun is expected to be a source of copious flux of SEP, it is not clear whether SEP interactions with nebular material at asteroidal distances has effectively contributed to the inventory of the various short-lived nuclides present in the early solar system. Shielding of SEP by nebular gas and dust itself, during the very early stages of solar system evolution, could have reduced the effectiveness of SEP interactions. This was obviated in the X-wind model where SEP interactions takes place very close to the Sun. There has been recent suggestion for the presence of an extremely short-lived nuclide $^{7}$Be ( ~77d) in the early solar system [31]. If confirmed, it will provide a very important input to quantify the SEP production of short-lived nuclides as we can rule out other sources for this nuclide. Similarly a more quantitative and robust estimate of initial $^{60}$Fe abundance is needed that will hopefully allow us to pinpoint either a supernova or a AGB star as the source of this nuclide and make quantitative estimate of the contribution from this source to the inventory of the other short-lived nuclides in the early solar system.

**References:** [1] Reynolds, J. H. (1960) *Phys. Rev. Lett., 4*, 8. [2] Wasserburg, G. J. , Fowler, W. A. & Hoyle, F. (1960) *Phys. Rev. Lett., 4*, 112. [3] Cameron, A. G. W. (1960) *A.. J., 65*, 485. [4] Lee, T., Papanastassiou, D. A. & Wasserburg, G. J. (1976) *Geophys. Res. Lett., 3*, 109. [5] Heymann, D. & Dziczkaniec, M. (1976) *Science, 191*, 79. [6] Lee, T., Papanastassiou, D. A. & Wasserburg, G. J. (1977) *Ap. J. 211*, L107. [7] Cameron, A. G. W. & Truran, J. W. (1977) *Icarus, 30*, 447-461. [8] Goswami, J. N. (2004) *New Astron. Rev., 48*, 125. [9] Shu, F. H. et al. (1997) *Science, 277*, 1475. [10] Lee, T. et al. (1998) *Ap. J., 506*, 898. [11] Wasserburg, G. J. et al. (1994) *Ap. J., 424*, 412. [12] Wasserburg, G. J. et al. (1995) *Ap. J., 440*, L101. [13] Cameron, A. G. W. et al. (1995) *Ap. J., 447*, L53. [14] Arnould, M., Paulus, G. & Meynet, G. (1997) *A. & A,. 321*, 452. [15] Wasserburg, G. J., Gallino, R. & Busso, M. (1998) *Ap. J., 500*, L189. [16] Busso, M., Gallino, R. & Wasserburg, G. J. (2003) *Pub. Astron. Soc. Australia, 20*, 356. [17] Meyer, B. & Clayton, D. D., (2000) *Sp. Sci. Rev., 92*, 133. [18] Meyer, B. S. et al. (2004) *LPSC XXXV,* 1908.pdf. [19] McKeegan, K. D., Chaussidon, M. & Robert F. (2000) *Science, 289*, 1245. [20] Gounelle, M. et al. (2001) *Ap. J., 548*, 1051. [21] Goswami, J. N. , Marhas, K. K. & Sahijpal, S. (2001) *Ap. J.,* 549, 1151. [22] Marhas, K. K., Goswami, J. N. & Davis, A. M. (2002) *Science*, *298*, 2182. [23] Leya, I., Halliday , A. N. & Wieler, R. (2003) *Ap. J., 616*, 2003. [24] Desch, S. J., Srinivasan, G. & Conolly Jr., H. C. (2004) *Ap. J. 602*, 528. [25] Tachibana, S. & Huss, G. R. (2003) *Ap. J., 588*, L41. [26] Mostefaoui, S. et al. (2004) *New Astron. Rev., 48*, 155. [27] Wasserburg, G. J., Busso, M. & Gallino, R. (1996) *Ap. J., 466*, L109. [28] Wasserburg, G. J. & Arnould, M. (1987) In: *Lecture notes in Physics, 287*, Springer-Varlag p. 262. [29] Marhas, K. K. & Goswami, J. N. (2004) *New Astron. Rev., 48*, 139 [30] Marhas, K. K. & Goswami, J. N. (2003) *LPSC XXXIV*,1303.pdf. [31] Chaussidon, M., Robert, F. & McKeegan, K. D. (2004) *LPSC XXXV,* 1568.pdf.

**ON EARLY SOLAR SYSTEM CHRONOLOGY: IMPLICATIONS OF AN INITIALLY HETEROGENEOUS DISTRIBUTION OF SHORT-LIVED RADIONUCLIDES.** M. Gounelle[1,2] and S.S. Russell[2]. [1]Université Paris XI-CSNSM. Bâtiment 104, 91 405 Orsay, France (gounelle@csnsm.in2p3.fr). [2]Department of Mineralogy, The Natural History Museum, London, UK (sarr@nhm.ac.uk).

**Introduction:** Short-lived radionuclides (SR) with half-lives ~ Ma were alive in the early Solar System. Because their half-life is comparable to the timescales of early Solar System events such as CAI and chondrule formation, or planetary bodies differentiation, short-lived radionuclides can be used as chronometers [1]. Early Solar System chronology is usually built with the assumption that the distribution of short-lived radionuclides was homogeneous through the solar accretion disk [2]. This assumption leads to inconsistencies in the ages of several objects, such as CAIs, chondrules or the HED parent-body, especially for $^{53}$Mn and $^{26}$Al ages [3, 4]. The homogeneity assumption might be inappropriate. This would be the case if some of the SRs (e.g. $^{26}$Al and $^{53}$Mn) have been formed by irradiation, instead of being delivered by a late minute supernova [5]. In this paper, we explore a possible chronology based on an heterogeneous distribution of $^{26}$Al and $^{53}$Mn in the accretion disk.

**Model:** Our basic assumption is that the different abundances of extinct short-lived radionuclides in CAIs and chondrules are due to spatial rather than temporal differences. We develop a simple model where CAIs and chondrules form contemporaneously, in different spatial locations, and are characterised by distinct initial $^{26}$Al and $^{53}$Mn abundances. In this model, all unprimitive bodies are supposed to be originally chondritic, i.e. to be made of a mixture of CAIs, chondrules and matrix. This mixture determines the initial content in $^{26}$Al and $^{53}$Mn of a chondritic parent-body as a function of its CAI and chondrule abundance fraction. This approach enables us to calculate $^{26}$Al and $^{53}$Mn ages since the formation of the parent-body until the isotopic closure of $^{26}$Al and $^{53}$Mn. SR ages depend on the CAI and chondrule fraction of the precursor parent-body, as well as on its chemistry. We have explored three possible types of chemistry for the precursor parent-body: CV, CM and OC. Our aim is to identify *compatible* $^{26}$Al and $^{53}$Mn ages for a diversity of unprimitive objects, the d'Orbigny angrite, the Asuka-881394 eucrite, the H4 chondrites Sainte Marguerite and Forest Vale.

**Results and discussion:** We find compatible ages for realistic precursors chondritic parent-bodies, i.e. objects having similar or identical petrograpy to the existing chondrite groups. For example, for a CV precursor having 0 % CAI for the d'Orbigny parent-body, a compatible $^{26}$Al and $^{53}$Mn age of 3.4 Ma since chondrule-CAI formation is found if the chondrule fraction is ~ 60 %. These ages depend little on the precursor parent-body chemistry.

We anchor the calculated relative chronology to an absolute chronology using absolute Pb-Pb ages and relative Hf-W ages of the objects under scrutiny (Figure 1). Our model provides a compatible Al-Mg/Mn-Cr/Pb-Pb chronology, and is shown to be robust to any reasonable change in the input parameters.

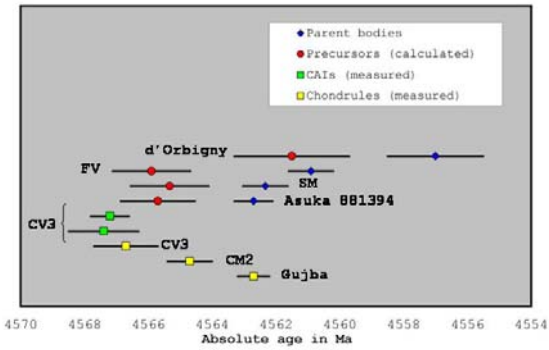


**Figure 1:** Absolute timescale for early Solar System events. Blue diamonds denote experimental Pb-Pb ages for D'Orbigny, the Forest Vale and Sainte Marguerite H4 chondrites, and a combined $^{182}$Hf-$^{182}$W/Pb_Pb age for the Asuka-881394 parent-body. The red circles are our calculated compatible $^{26}$Al and $^{53}$Mn ages for the precursors of d'Orbigny, the HED parent-body, and the H4 chondrites Forest Vale and Sainte Marguerite. Error bars are experimental error bars, and $\sqrt{\sigma_{\exp}^2 + \sigma_{calc}^2}$ when the age is the difference of a calculated and measured age. The green and yellow squares are experimental ages for the CAIs and chondrules respectively. Data from literature.

**References :**

[1]M. Wadhwa, et al., in: Protostars and Planets IV, V. Mannings, A.P. Boss, et al., Eds., Arizona University Press, Tucson, 2000, pp. 995-1018.[2]T.D. Swindle, et al., in: Chondrules and the protoplanetary disk, R.H. Hewins, R.H. Jones, et al., Eds., Cambridge University Press, Cambridge, 1996, pp. 77-86.[3]J.D. Gilmour, et al., *Phil. Trans. R. Soc. Lond. A* 359 (2001) 2037-2048.[4]K.D. McKeegan, et al., in: Treatise on geochemistry, H. Holland and K. Turekian, Eds., Meteorites, Planets, and Comets 1, Elsevier-Pergamon, Oxford, 2003, pp. 431-460.[5]S.S. Russell, et al., *Phil. Trans. R. Soc. Lond. A* 359 (2001) 1991-2004.

**THE ORIGIN OF SHORT-LIVED RADIONUCLIDES AND EARLY SOLAR SYSTEM IRRADIATION.**
M. Gounelle[1,2], F. H. Shu[3], H. Shang[4], A. E. Glassgold[5], K. E. Rehm[6] and T. Lee[7]. [1]Université Paris XI-CSNSM. Bâtiment 104, 91 405 Orsay, France (gounelle@csnsm.in2p3.fr). [2]Department of Mineralogy, The Natural History Museum, London, UK. [3]National Tsinghua University, Hsinchu, Taiwan (shu@mx.nthu.edu.tw). [4]Institute of Astronomy and Astrophysics, Academia Sinica, Taipei, Taiwan (shang@asiaa.sinica.edu.tw). [5]Department of Astronomy, University of California, Berkeley, CA 94720, USA (aeg@astro.berkeley.edu). [6]Physics Division, Argonne National Laboratory, Argonne IL 60431, USA (rehm@anph11.phy.anl.gov). [7]Institute of Earth Science, Academia Sinica, Taipei 115, Taiwan (typhoon@asiaa.sinica.edu.tw).

**Introduction:** Radionuclides with half-lives of the order of the Ma were present in the accretion disc when the components of chondrites, Calcium-Aluminium-rich Inclusions (CAIs) and chondrules, formed (see [1] for a recent review). Some short-lived radioanuclides such as $^{10}$Be, $^{26}$Al, $^{41}$Ca and $^{53}$Mn were present in early Solar System at levels above expectations from the continuous galactic nucleosynthesis, requiring therefore a special, last-minute, explanation for their origin (e.g. [1]). Two models have been proposed for the origin of these extinct short-lived radionuclides. The external stellar model stipulates that they were made in a supernova or an AGB star, and injected within the collapsing molecular cloud core that would eventually lead to the formation of our Sun, meteoritic components and planets (e.g. [2]). Alternatively, the internal irradiation model stipulates that short-lived radionuclides have been produced via *in situ* irradiation of accretion disc gas and/or dust by energetic particles (protons, $^{4}$He, $^{3}$He) accelerated by the protosun (e.g. [3-5]). Distinguishing between these two models has critical implications for low-mass star formation theories and the origin of chondrites.

Two recent experimental findings shed a new light on the origin of short-lived radionuclides and have urged us to revisit the irradiation model we proposed for the origin of short-lived radionuclides [3, 4, 6] in the context of the x-wind model [7]. In some rare hibonites from the CM2 chondrites, Mahras et al. [8] detected the past presence of $^{10}$Be while the decay product of $^{26}$Al is conspicuously absent. This decoupling between $^{10}$Be and $^{26}$Al was interpreted as contradicting irradiation models that simultaneously produce $^{10}$Be and $^{26}$Al. Chaussidon et al. [9] have made a strong case for the presence of $^{7}$Be in the early Solar System at a level $^{7}$Be/$^{9}$Be = (4.9 ± 1.3) x $10^{-3}$. This value is two orders of magnitude smaller than the one presented previously [10], and that we discussed last previously [11].

In this paper, we explore the possibility of bringing this new experimental data set in a coherent way within the framework of our irradiation model [3, 4, 6]. Compared to our 2001 calculations, no parameters were changed. Since the only modifications are the addition of $^{7}$Be to the list of calculated yields, and the use of better constrained nuclear cross sections, we refer the reader to our previous work for details of the irradiation model.

**Results:** Because of its short half-life (53 days) compared to typical irradiation timescales varying between a few years to a few 10s of years, $^{7}$Be yields need to be calculated at saturation. In other words, $^{7}$Be/$^{9}$Be = $f_7$ x $\tau$ instead of, for example, $^{10}$Be/$^{9}$Be = $f_{10}$ x $t_{irr}$, where $f_7$ and $f_{10}$ are the production rates of $^{7}$Be and $^{10}$Be respectively, $\tau$ is the mean-life of $^{7}$Be and $t_{irr}$ the irradiation time. For $^{7}$Be we consider p, $^{3}$He, $^{4}$He channels on $^{16}$O. Cross sections are taken from the compilation of [12] and completed with simulations. For the cross sections $^{24}$Mg($^{3}$He,p)$^{26}$Al and $^{4}$He($^{16}$O,x)$^{10}$Be, we used respectively the new measurement of [13] and previoulsy overlooked experimental data [14].

Figure 1 shows the calculated yields of short-lived radionuclides. We have distinguished between the two classes of flares occurring within the modern Sun: impulsive and gradual flares corresponding to $^{3}$He- and proton-rich events respectively [15]. The spectral parameters, as well as the relative abundance of cosmic-rays are identical to [3], i.e. p = 4, $^{3}$He/p = 0.3, $^{4}$He/p = 0.1 for impulsive flares and p = 2.7, $^{3}$He/p = 0, $^{4}$He/p = 0.1 for gradual flares, with p being defined as $dN = E^{-p}\,dE$, where N is the number flux of protons. We are in the case 2d of [3], where the core size distribution of protoCAIs range from 50 μm to 2.5 cm, similar to natural CAIs, and *M*, the effective number of passage of protons in the irradiation zone is 1.6.

Without changing any parameters, the yield of $^{7}$Be is in a very good agreement with the value found by [9]. The impulsive flares yield a value $^{7}$Be/$^{9}$Be = 7.5 x $10^{-3}$ to be compared to the experimental value $^{7}$Be/$^{9}$Be = (4.9 ±1.3) x $10^{-3}$ [9]. Gradual flares produce an even better agreement, with $^{7}$Be/$^{9}$Be = 6.2 x $10^{-3}$. Given the uncertainties discussed below, these differences between impulsive and gradual flares are insignificant. The main difference between the two types of flares is the ability of impulsive flares to produce the complete set of short-lived radionuclides at the meteoritic level.

**Discussion:** Because of its very short half-life (53 days) compared to the evolutionary timescales of protostars ($10^5$-$10^6$ yr), the presence of $^{7}$Be in CAIs is a smoking gun for evidence of in situ irradiation. Unless CAIs themselves formed outside the Solar System, it is not possible to make $^{7}$Be at a stage anterior to the CAI formation without having $^{7}$Be decay to negligible levels. Impulsive flares that can account for the abundance of $^{10}$Be, $^{26}$Al, $^{41}$Ca and $^{53}$Mn, can reproduce, within errors the observed abundance of $^{7}$Be in CAIs.

The rare CAIs containing $^{10}$Be and no $^{26}$Al can be accounted for by gradual flares that have the property of producing high levels of $^{10}$Be while underproducing $^{26}$Al and $^{41}$Ca (see Figure 1). Gradual flares are 100 times less abundant in the contemporary Sun than impulsive flares [15] in agreement with the rarity of FUN-like CAIs relatively to "normal" CAIs. The overproduction of $^{10}$Be by these flares (see Figure 1) can be accounted for by a combination of shorter exposure ages and lower luminosity for rare gradual flares in protostars. Because X-ray observations of protostars are still in their infancy, we cannot at the present time distinguish between the two possibilities. We note that a shorter exposure age is compatible with the origin of FUN-like CAIs proposed by [4]. According to these authors, FUN-like CAIs have retained some isotopic anomalies because they spent only short times in the reconnection ring where isotopic homogeneisation occurs [3].

We did not try to adjust our parameters (proton spectral shape, helium nuclei abundances...) to obtain a perfect match (see Figure 1) between our model and the experimental value. Indeed, the large uncertainties, mainly on the nuclear cross sections, but also on the cosmic-ray physics of protostars would make this attempt meaningless. We feel satisfied that our model can reproduce, the large diversity of new experimental data within a factor of a few. This is done with reasonable input parameters as the high abundance of $^{3}$He nuclei is now well established for impulsive flares [16], and since we scale our yields to the X-ray luminosity of protostars [17].

**Conclusions:** The wealth of new experimental data can be accounted for by our irradiation model. We note that we calculated in 2003 a value $^{7}$Be/$^{9}$Be ~ 3 x $10^{-3}$ [11], close to the value found experimentally some months later. Our model emphasizes the importance in distinguishing between impulsive and gradual flares. While impulsive flares can account for the distribution of short-lived radionuclides within normal CAIs, the rare gradual flares can account for the distribution of short-lived radionuclides in rare FUN-like CAIs. implications for our model of the discovery of $^{60}$Fe in ordinary chondrites [18].

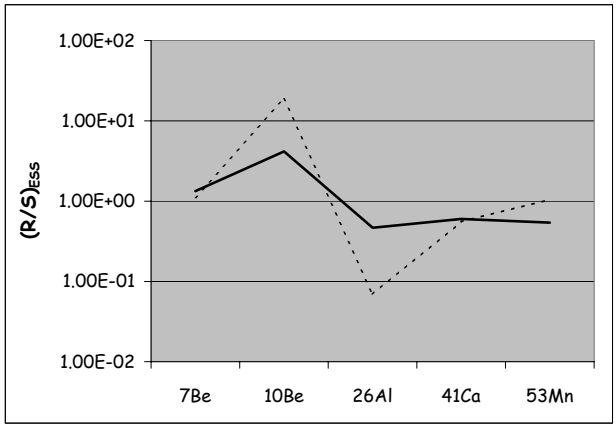


Figure 1: Yields of radionuclides normalised to their Early Solar System (ESS) values. Continuous line and dotted lines are impulsive and gradual flares respectively.

**References**: [1]S.S. Russell, M. Gounelle and R. Hutchison, *Phil. Trans. R. Soc. Lond. A* 359 (2001) 1991-2004. [2]M. Busso, R. Gallino and G.J. Wasserburg, *Publications of the Astronomical Society of Australia* 20 (2003) 356-370. [3]M. Gounelle, et al., *Astrophysical Journal* 548 (2001) 1051-1070. [4]T. Lee, et al., *Astrophysical Journal* 506 (1998) 898-912. [5]I. Leya, A.N. Halliday and R. Wieler, *Astrophysical Journal* 594 (2003) 605-616. [6]F.H. Shu, et al., *Astrophysical Journal* 548 (2001) 1029-1050. [7]F.H. Shu, et al., *Science* 277 (1997) 1475. [8]K.K. Marhas, J.N. Goswami and A.M. Davis, *Science* 298 (2002) 2182-2185. [9]M. Chaussidon, F. Robert and K.D. McKeegan, *Lunar Planet. Sci. Conf.* 35 (2004) #1568. [10]M. Chaussidon, F. Robert and K.D. McKeegan, *Meteoritics Planet. Sci.* 37 (2002) A31. [11]M. Gounelle, et al., *Lunar Planet. Sci. Conf.* 34 (2003) #1833. [12]Landolt-Börnstein, Springler-Verlag, 1994. [13]C. Fitoussi, et al., *Lunar Planet. Sci. Conf.* 35 (2004) #1586. [14]H.-J. Lange, et al., *App. Radiat. Isot.* 46 (1995) 83-112. [15]D.V. Reames, *Rev. Geophys. Supp.* 33 (1995) 585-589. [16]J. Torsti, et al., *Astrophysical Journal* 573 (2002) L59-L63. [17]E.D. Feigelson, G.P. Garmire and S.H. Pravdo, *Astrophysical Journal* 584 (2002) 911-930.

**DISEQUILIBRUIUM MELTING AND OXYGEN ISOTOPE EXCHANGE OF CAIs AND CHONDRULES IN THE SOLAR NEBULA.** James P. Greenwood, Earth & Environmental Studies Dept., Wesleyan University, Middletown, CT 06459-0139 (jgreenwood@wesleyan.edu).

**Introduction:** An empirical model for the melting rates of silicates and oxides is used (*1*), in conjunction with available diffusivity data, to assess exchange of oxygen isotopes in refractory, calcium-aluminum-rich inclusions (CAIs) during transient heating events in the early solar nebula. It is found that multiple heating events of short duration (seconds or less) with peak temperatures lower than the melting point of spinel (<2135˚C), subsequently followed by an anneal at temperatures of ~1000 to 1250˚C, are necessary to promote oxygen isotope exchange of melilite and anorthite relative to fassaite and spinel in CAIs. Oxygen isotope compositions of CAIs and chondrules can be explained as resulting from transient high-temperature events in the solar nebula.

**Disequilibrium melting kinetics:** Disequilibrium melting kinetics leads to melilite melting faster than fassaite during rapid, high-temperature, events (*1*).

**Oxygen isotope exchange in CAIs:** While melting is a rapid process, transport of oxygen in the molten minerals should be slower, and would seem to be the rate-limiting step. The observation that only oxygen isotopes are exchanged, that trace element signatures are not altered, and that major-element mineral zoning seems relatively unaffected (*2*), argues strongly that if the process is diffusive in nature, that oxygen diffusion was decoupled from cation diffusion. Oxygen must diffuse as a molecular species, such as $H_2O$, $O_2$, or CO in the molten CAIs. CO is the main oxygen-bearing gas in the early solar nebula, and $H_2O$ is expected to be an important product of photodissociation of CO in the solar nebula (*3*). Water diffusion in silicate melts is likely decoupled from network oxygen or cation diffusivities (*4*). Diffusivity of water in basaltic melts is 30 to 50 times faster than in granitic melts (*5,6*) and is a low activation energy (126 kJ/mol) process relative to the activation energies for diffusion of cations or oxygen in silicate melts (200-400 kJ/mol) (*4*). The small difference in $H_2O$ diffusivity between basalt and granite, relative to the three orders of magnitude difference in viscosity of these melts, suggests that the diffusivity of water will not be greatly different in melilitic or fassaitic melts. This points toward the importance of melting kinetics in this process, as variable diffusivity of water (and likely other volatile species) among the monomineralic melts is probably not a viable mechanism to explain the differences in the oxygen isotope compositions of the CAI minerals of CV chondrites. The diffusivity of $H_2O$ is slow enough to suggest that transport of the volatile oxygen-bearing species during remelting events may be via permeation. A high pressure gas pulse (as might be expected in bipolar outflows) may be necessary to exchange oxygen isotopes during melting. A subsequent anneal at lower gas pressures would lead to the loss of vesiculation features.

Anorthite liquid is more viscous than both melilitic and fassaitic liquids, and would be the slowest to exchange with an $^{16}$O-depleted volatile reservoir. The higher viscosity of anorthite melt also translates into more sluggish melting kinetics. The problem is that fassaite is generally $^{16}$O-rich and anorthite is generally $^{16}$O-poor, suggesting that short transient heating events cannot effectively exchange oxygen in anorthite and leave fassaite relatively unaltered. Anorthite is difficult to crystallize from CAI melts during controlled cooling rate experiments while melilite, spinel, and fassaite have little difficulty nucleating and crystallizing (*7*). This suggests that the multiple, short duration heating events will result in melilite and fassaite recrystallizing rapidly during cooling, while anorthite will stay molten until finally quenching to a glass at approximately 1000˚C (~2/3 Tm). Since atomic mobility is enhanced in liquids relative to solids, anorthite melt would have greater opportunity to exchange oxygen during cooling, relative to the newly crystallized fassaite and melilite. A subsequent high-temperature anneal would allow anorthite the time needed to nucleate and crystallize into blocky grains, as well as promote the 120˚ triple junctions observed in melilite grain assemblages (*8*).

**Proposed thermal history of CAIs and chondrules**. The thermal history of the CAIs involves at least three stages and is illustrated in Fig. 1. In stage 1, protoCAIs were formed by the condensation of a gas of solar composition (*9*), followed by remelting and slow cooling to produce igneous textures (*10*) and promote evaporation of Mg and Si (*11*). These protoCAIs were $^{16}$O-rich and their oxygen isotope composition resembled that of $^{16}$O-rich spinel in CAIs. In stage 2, these objects were heated in multiple, short duration, heating events to Tpeak < Tm of spinel (2135˚C), but above Tm of melilite and fassaite (~1500˚C), and then cooled quickly to a temperature below the solidus in the CAI system (~1230˚C; (*1 0*)) in an $^{16}$O-depleted environment. This episode of multiple heating events led to $^{16}$O-rich spinel and pyroxene and $^{16}$O-poor melilite and anorthite-rich glass. In stage 3, the

protoCAIs were heated above the glass transition of anorthite (~1000˚C), but below Tm of melilite or fassaite (~1260˚C) for a longer duration.

The rapid cooling in stage 2 from Tpeak to T<1230˚C for the multiple, short duration heating events is necessary so that fassaitic liquid does not exchange oxygen isotopes. Fassaite and melilite would be able to crystallize during the rapid cooling, while anorthite-rich melt would continue to exchange oxygen before quenching to a poorly-crystalline glass. This would be due to the greater ease in crystallization of fassaite and melilite (due to the higher fluidity of their melts) relative to anorthite. A fourth high-temperature stage would be necessary to form $^{16}$O-rich CAI rims (*12*), as rim formation likely takes place after oxygen isotope exchange of melilite in CAIs (*13*). The oxygen isotope compositions of the FUN inclusions (*14*) can be understood in the present model as well. Evaporation in stage 1 led to original $^{16}$O-rich spinel, olivine, and pyroxene having a mass-dependent fractionation array. The multiple transient heating events of stage 2 led to preferential oxygen isotope exchange of melilite, as in the large CAIs.

The homogeneous oxygen isotope compositions of the small CAIs of ordinary, enstatite, and CH chondrites (*14*) can also be explained by the present model (Fig. 1). The smaller CAIs were extensively heated due to their smaller size, and underwent greater degrees of melting. In stage 2, the multiple, short duration heating events likely lead to an assemblage of $^{16}$O-rich spinel and a fine-grained $^{16}$O-poor assemblage of melilite, fassaite and anorthite-rich glass. In stage 3, $^{16}$O-rich spinel was able to completely dissolve, albeit slowly, into the CAI melt derived from the $^{16}$O-poor components. This was followed by crystallization of this completely molten CAI with all mineral phases having the same oxygen isotope composition, but having an oxygen isotope composition that is intermediate between $^{16}$O-rich and $^{16}$O-poor minerals of CV chondrites, depending on the modal abundance of spinel. Spinel dissolved into these melts after the majority of oxygen isotope exchange with an ambient volatile reservoir, in order to explain the oxygen isotope distribution of these smaller CAIs.

This model can be extended to chondrules as well (Fig. 1). In stage 1, $^{16}$O-rich protochondrules are formed. The multiple transient heating events of stage 2 lead to protochondrules that are $^{16}$O-poor, with textures similar to those of the present chondrule population. Occasional $^{16}$O-rich olivine (and even rarer pyroxene) can survive as relict grains in chondrules, depending on the degree of heating. Stage 3 led to the further growth of large olivine and pyroxene crystals in porphyritic chondrules and the loss of glass in the barred olivine chondrules (*15*). The recent finding of $^{16}$O-rich olivine grains in microporphyritic chondrules (traditionally believed to be the least melted chondrules) (*16*) supports a model involving multiple melting events.

**References:** [1] Greenwood J. P. (2004) *LPSC* [2] H. Yurimoto, M. Ito, H. Nagasawa, *Science* **282,** 1874 (1998). [3] R. N. Clayton, *Nature* **415,** 860 (2002) [4] D. R. Cole, S. Chakraborty in *Stable Isotope Geochemistry, Reviews in Mineralogy and Geochemistry 43*, J. W. Valley, D. R. Cole, Eds. (Mineralogical Society of America, Washington, DC, 2001), pp. 83-223. [5] Y. Zhang, E. M. Stolper, *Nature* **351,** 306 (1991). [6] Y. Zhang, E. M. Stolper, G. J Wasserburg, *Geochim. Cosmochim. Acta* **55,** 441 (1991). [7] E. Stolper, J. M. Paque, *Geochim. Cosmochim. Acta* **50,** 1785 (1986). [8] A. J. Brearley, R. H. Jones, in *Planetary Materials, Reviews in Mineralogy 36*, J. J. Papike, Ed. (Mineralogical Society of America, Washington, DC, 2001), pp. 3-1-3-398. [9] L. Grossman, *Geochim. Cosmochim. Acta* **49,** 2433 (1972). [10] E. Stolper, *Geochim. Cosmochim. Acta* **46,** 2159 (1982). [11] R. N. Clayton, N. Onuma, L. Grossman, T. K. Mayeda, Earth Planet. Sci. Lett. 34, 209 (1977). [12] A. N. Krot, K. D. McKeegan, L. A. Leshin, G. J. MacPherson, E. R. D. Scott, *Science* **295,** 1051 (2002). [13] S. Itoh, H. Yurimoto, *Nature* **423,** 728 (2003). [14] K. D. McKeegan, L. A. Leshin in *Stable Isotope Geochemistry, Reviews in Mineralogy and Geochemistry 43*, J. W. Valley, D. R. Cole, Eds. (Mineralogical Society of America, Washington, DC, 2001), pp. 279-318. [15] A. Tsuchiyama, Y. Osada, T. Nakano, K. Uesugi, *Geochim. Cosmochim. Acta* **68,** 653 (2004). [16] R. H. Jones et al. (2004) *LPSC*.

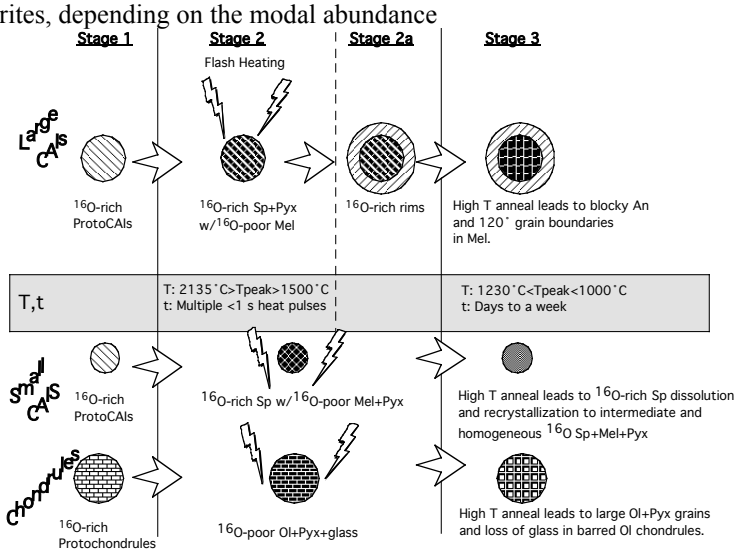

**MINERALOGY AND CHEMISTRY OF FINE-GRAINED MATRICES, RIMS, AND DARK INCLUSIONS IN THE CR CARBONACEOUS CHONDRITES ACFER/EL DJOUF 001 AND THE UNGROUPED CARBONACEOUS CHONDRITES ACFER 094 AND ADELAIDE.** Ansgar Greshake[1], Alexander N. Krot[2], and Klaus Keil[2], [1]Museum für Naturkunde, Institut für Mineralogie, Humboldt-Universität zu Berlin, Invalidenstr. 43, 10115 Berlin, Germany, email: ansgar.greshake@rz.hu-berlin.de, [2]Hawai'i Institute of Geophysics and Planetology, School of Ocean and Earth Science and Technology, University of Hawai'i at Manoa, Honolulu, HI 96822, USA.

**Introduction:** Apart from the relative coarse-grained high-temperature components – refractory inclusions [Ca,Al-rich inclusions (CAIs) and amoeboid olivine aggregates (AOAs)], chondrules, and Fe,Ni-metal – most carbonaceous chondrites contain abundant, very fine-grained (<1 μm) materials whose origin and genetic relationship to the coarse-grained components remain controversial. These fine-grained materials are observed in several textural occurrences: (*i*) as rims around coarse-grained components, (*ii*) as interstitial matrix, and (*iii*) as lithic clasts (dark inclusions). Due to the small grain size and high porosity, these materials are highly susceptible to aqueous alteration and thermal metamorphism – processes that operated on most chondrite parent asteroids and significantly modified or even erased solar nebular records in fine-grained materials. There are only a few carbonaceous chondrites which appear to have escaped thermal metamorphism and experienced small degree aqueous alteration; these include CR (Renazzo-like) and the ungrouped carbonaceous chondrites Acfer 094 and Adelaide. The primitive nature of Acfer 094 and CR chondrite North West Africa 530 is supported by the discovery of amorphous presolar silicates in these meteorites [1, 2]. In order to decipher the solar nebular records in fine-grained rims, matrix, and dark inclusions of these meteorites, we studied their mineralogy and chemistry using scanning electron microscopy (SEM), electron probe microanalyses (EPMA), and transmission electron microscopy (TEM).

**CR chondrites Acfer/El Djouf 001:** Fine-grained materials in Acfer/El Djouf 001 include dark inclusions, fine-grained clastic matrix, and rare fine-grained matrix-like rims around chondrules; the latter are texturally similar to those in CM chondrites [3]. Matrix appears to be very heterogeneous and consists of sub-μm sized mostly magnesian olivine and pyroxene, embedded into very fine-grained phyllosilicates interspersed with tiny Fe,Ni-metal and sulfide grains. Olivine is the most abundant anhydrous phase and sometimes occurs as clusters of several anhedral grains; pyroxene is less frequent and many grains are found to be intergrowths of ortho- and clinopyroxene, indicative of quenching at high temperatures (Fig. 1). Phyllosilicates are composed of saponite-serpentine intergrowths, textures commonly observed in CI1 chondrites [4]. Dark inclusions are much finer-grained, display a lower porosity, and contain higher abundances of saponite, serpentine, and magnetite and a lower abundance of anhydrous silicates (olivine and pyroxenes) than the CR matrix [5]. Fine-grained rims are mineralogically heterogeneous and contain regions in which anhydrous phases are more abundant than phyllosilicates. However, such regions are rare and the rims generally resemble the mineralogy of the matrix with abundant serpentine and saponite.

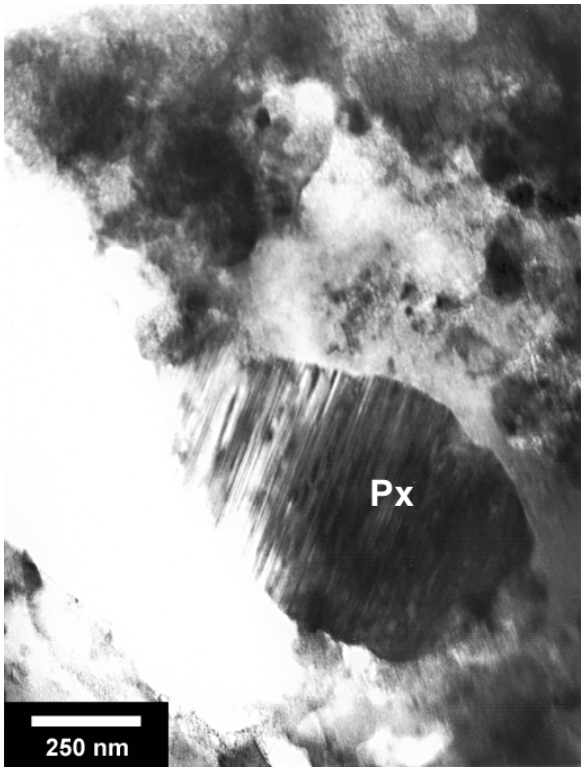


Figure 1. Bright field TEM image showing a Mg-rich pyroxene grain (Px) in the dominantly hydrous matrix of the CR2 chondrite Acfer 097.

Compositionally, matrix, dark inclusions, and rims are very similar; the matrix seems slightly enriched in Ca relative to rims and dark inclusions while the rims might be slightly depleted in Fe. Major deviations

from the CI values are observed for the most volatile elements with K being strongly enriched and Na and S being depleted in all fine-grained lithologies [e.g., 3]. The Ca/Al ratios vary from 1.54 in the matrix to 1.21 in the rims and 1.17 in the dark inclusions (CI=1.07; [6]); Ti/Al-ratios are 0.04 in the matrix and dark inclusions and 0.03 in the fine-grained rims (CI=0.05; [6]).

**Adelaide:** Our TEM study of the Adelaide matrix is consistent with observations of [7]. It predominantly consists of sub-µm-sized ferrous olivines set into an amorphous to microcrystalline anhydrous groundmass. The olivines commonly form clusters of anhedral grains; euhedral olivines, pyroxenes, and sulfides are less abundant. Some matrix regions are solely composed of tiny ferrous olivines. The bulk composition of the Adelaide matrix normalized to Si & CI shows a Ca depletion: the Ca/Al-ratio (0.16) is much lower relative to bulk Adelaide (0.69; [8]), whereas the Ti/Al-ratio (0.04) is less clearly below bulk Adelaide (0.08; [8]). K, Na, S are depleted, whereas Fe is enriched, possibly due to extensive terrestrial weathering of Adelaide.

**Acfer 094:** Matrix in Acfer 094 consists of Mg-rich olivine, magnesian low-Ca pyroxene, and Fe,Ni-sulfides all of rounded or elongated morphologies set into an amorphous ferrous silicate matrix (Fig. 2).

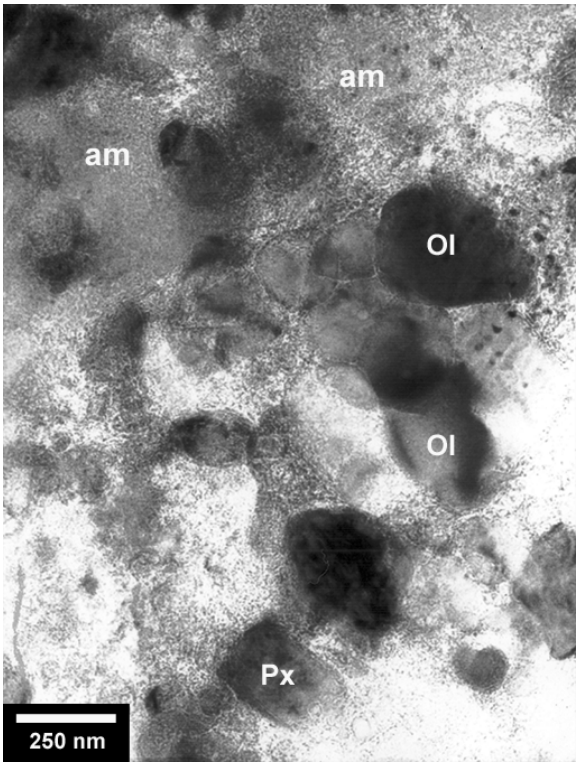


Figure 2. Bright field TEM image of the fine-grained material in Acfer 094 (after [9]). The matrix is dominated by small olivines (Ol) and pyroxenes (Px) embedded in an amorphous groundmass (am).

Phyllosilicates are exceptionally rare; they preferentially replace amorphous material and occasionally form tiny veins cutting through olivines. The bulk composition of the Acfer 094 matrix normalized to Si and CI is chondritic for most refractory and moderately volatile elements; only Ca seems slightly enriched and Ni slightly depleted. The Ca/Al-ratio of 1.6 is clearly superchondritic and the Ti/Al-ratio of 0.04 slightly below the chondritic value of 0.05 [6]. Probably due to terrestrial weathering, K is significantly enriched and Na slightly and S more strongly depleted.

**Discussion:** Fine-grained matrix, rims, and dark inclusions studied in Acfer/El Djouf 001 experienced aqueous alteration and contain no anhydrous amorphous material; crystalline material is dominated by magnesian olivine and pyroxenes which appear to have been quenched at high temperatures. Fine-grained matrix in Adelaide appears to have experienced thermal metamorphism resulting in formation of abundant crystalline ferrous silicates [7]. Matrix in Acfer 094 appears to be the most pristine; it largely escaped aqueous alteration and thermal metamorphism and contains abundant amorphous ferrous silicates and tiny crystalline magnesian silicates [9]. We infer that the primary components of fine-grained matrices are composed of crystalline magnesian silicates and amorphous ferrous silciates; crystalline ferrous silicates and phyllosilicates are secondary and resulted from aqueous alteration and thermal processing of primitive matrices most likely in an asteroidal setting.

**Acknowledgements:** We thank Dr. Allan Pring (South Australian Museum, Adelaide) for making the Adelaide sample available.

**References:** [1] Nguyen A. N. and Zinner E. (2004) *Science, 303*, 1496-1499. [2] Nagashima et al. (2004) *Nature, 428*, 921-924. [3] Bischoff et al. (1993) *GCA, 57*, 1587-1603. [4] Zolensky et al. (1993) *GCA, 57*, 3123-3148. [5] Endreß et al. (1994) *Meteoritics, 29*, 26-40. [6] Lodders K. and Fegley B. (1998) The Planetary Scientist's Companion, Oxford. [7] Brearley A. J. (1991) *LPSC XXII*, 133-134. [8] Davy et al. (1978) *Meteoritics, 13*, 121-140. [9] Greshake A. (1997) *GCA, 61*, 437-452.

**OXYGEN ISOTOPES OF ALUMINUM-RICH CHONDRULES FROM UNEQUILIBRATED ENSTATITE CHONDRITES.** Y. Guan[1], L. A. Leshin[1, 2], and G. J. MacPherson[3], [1]Department of Geological Sciences, [2]Center for Meteorite Studies, Arizona State University, Tempe AZ 85287-1404, USA, [3]Department of Mineral Sciences, National Museum of Natural History, Smithsonian Institution, Washington DC 20560-0119, USA. (yg@asu.edu).

**Introduction:** Al-rich chondrules, which commonly consist of primary anorthite or Al-rich glass, spinel, Al-rich diopside, and olivine, are rare in most unequilibrated enstatite chondrites (UECs). In a previous study of calcium-aluminum-rich inclusions (CAIs) in UECs [1], we incidentally analyzed the oxygen isotopic composition of an Al-rich chondrule from EET 87746 (EH3). The data showed that its oxygen isotopes fall outside the typical range for UEC ferromagnesian chondrules. In this report, we have measured oxygen isotopic compositions of additional Al-rich chondrules in UECs, with the goals of determining their relationship to UEC ferromagnesian chondrules and comparing them with Al-rich chondrules in unequilibrated ordinary chondrites (UOCs) and with CAIs in general.

**Samples and Experimental:** The Al-rich chondrules were identified from elemental X-ray maps of polished UEC thin sections by using a scanning electron microscope (SEM). One of the Al-rich chondrules was previously described [1]: E4642-1 from EET 87746 is ~100 μm in diameter and consists of euhedral spinel (up to ~20x50 μm), aluminous diopside, and two types of glass (CaO ~9-12%, Na2O ~3-4%; and CaO <2%, Na2O ~10-11%). The Al-rich chondrules L2003-1 and L2003-2 are from LEW 87220 (EL3). L2003-1 is ~420 μm in size and dominated by Na-Ca-rich glass that encloses dendritic Al-rich diopside laths. It also contains spinel, olivine, and enstatite grains (Fig. 1). L2003-2, a porphyritic chondrule of ~250 μm in diameter, is mainly composed of anorthite and enstatite, with minor amount of spinel and Al-rich diopside. E4640-2 is a small (~100 μm in diameter) compact pyroxene-anorthite Al-rich chondrule from EET 87746, with $Al_2O_3$ in diopside up to 33 wt%.

*In-situ* oxygen isotope analyses of the Al-rich chondrules were carried out using the Cameca IMS 6f ion microprobe at ASU. A 0.2-0.34 nA beam of $Cs^+$ was focused into a spot of ~20 μm in diameter in aperture illumination mode. Secondary ions were accelerated to -9 KeV and collected by peak-jumping into either a Faraday cup ($^{16}O^-$) or electron multiplier ($^{17}O^-$ and $^{18}O^-$) at a mass resolving power of ~6000, easily resolving the $^{16}OH^-$ interference on $^{17}O^-$. Uncertainties on individual analyses, taking into account the variation on repeated analyses of the standard, are ~3‰ (2σ). The magnitude of matrix effects is small (~1-2‰) under our analysis conditions. No correction for such effects has been made.

**Results and Discussion:** The oxygen isotope results from three Al-rich chondrules, plus data from the one analyzed previously [1], are plotted in Fig. 2. Shown for reference on the plot are the oxygen isotopic compositions of bulk ferromagnesian chondrules from enstatite chondrites [2].

The oxygen isotopic compositions of the four UEC Al-rich chondrules spread over a range of ~10‰. Data from the pyroxene-anorthite Al-rich chondrule E4640-2 falls within the range of the ferromagnesian chondrules of enstatite chondrites, whereas the other three Al-rich chondrules plot to the $^{16}O$-enriched direction, along the extension line defined by the ferromagnesian chondrules. E4642-1 is the most $^{16}O$-enriched Al-rich chondrule, with $\delta^{17}O$ = -5‰ and $\delta^{18}O$ = -3‰. All the data points from the Al-rich chondrules roughly determine a correlation line of slope 0.7±0.1, similar to the one defined by bulk ferromagnesian chondrules [2].

The observation that both Al-rich and ferromagnesian chondrules in UECs are approximately distributed on a single isotopic mixing line indicates that they are genetically related to each other. The oxygen isotopes of UEC CAIs [1, 3], however, do not fall on the same mixing line. Neither can UEC CAIs be linked to ferromagnesian chondrules of enstatite chondrites through the CCAM or Young and Russell lines [1]. There is no compelling evidence that the chondrule mixing line of slope 0.7±0.1 in enstatite chondrites might form from overprinting of a slope ~1 mixing line with mass-dependent fractionation processes. Therefore, the UEC CAIs apparently do not represent the $^{16}O$-rich end-member of the UEC chondrule mixing line. The Al-rich chondrules in UECs cannot be mixing products of CAIs and ferromagnesian chondrules. Similar relationship between Al-rich chondrules, ferromagnesian chondrules, and CAIs was also observed in ordinary chondrites [4].

Internal isotopic heterogeneities among minerals were exhibited in the Al-rich chondrules L2003-1 and L2003-2. In general, spinel and olivine are more $^{16}O$-enriched than other mineral phases, such as Al-rich diopside or anorthite. Because of the large uncertainties of the data and possible matrix effects, the origin

of these internal variations cannot be unequivocally determined. They could be produced either by mass-dependent isotopic fractionation or by partial isotopic exchange with an external reservoir, either in the nebular or on the parent body.

The entire oxygen isotopic range (~10‰) of UEC Al-rich chondrules observed in this study is significantly smaller than that of UOC Al-rich chondrules (~20‰) [4]. This could merely be a sampling bias due to the smaller dataset of this study. On the other hand, it might be another indication of the genetic relationship between Al-rich and ferromagnesian chondrules in enstatite chondrites. It has been known that the ferromagnesian chondrules in enstatite chondrites have a very restricted oxygen isotopic region, which is regarded as an indication of close approach to equilibrium between chondrules and the ambient nebular gas for enstatite chondrites [5]. Isotopic exchange at similar conditions would produce a narrow oxygen isotopic range for Al-rich chondrules as well. Furthermore, a larger degree of equilibration with the ambient nebular gas (higher temperature?) may well explain the difference in Al-Mg systematics between UEC and UOC Al-rich chondrules: In UOCs, about one third of those Al-rich chondrules measured contain $^{26}$Mg excesses from the *in situ* decay of $^{26}$Al [6], with inferred initial $(^{26}Al/^{27}Al)_o$ ratios ranging from ~$5\times10^{-6}$ to ~$1\times10^{-5}$. In UECs, out of the 14 UEC Al-rich chondrules analyzed so far [7, 8, and unpublished data], only one was found containing resolvable $^{26}$Mg excesses from the *in situ* decay of $^{26}$Al, with a $(^{26}Al/^{27}Al)_o$ ratio of ~$5\times10^{-6}$ [7].

**Conclusions:** The oxygen isotopic compositions of UEC Al-rich chondrules define a mixing line of slope ~0.7±0.1 that extends to the $^{16}$O-enriched direction from the ferromagnesian chondrule field of enstatite chondrites, suggesting that they are genetically related to ferromagnesian chondrules, but not to CAIs in enstatite chondrites. Therefore, similar to their UOC counterparts, UEC Al-rich chondrules were not simple mixtures of ferromagnesian chondrules and CAI material.

**References:** [1] Guan Y. et al. (2000) *EPSL, 181,* 271-277. [2] Clayton R. N. and Mayeda T. K. (1985) *LPS XVI,* 142-143. [3] Fagan T.J. et al (2001) *MAPS, 36,* 223-230. [4] Russell S. S. (2000) *EPSL, 184,* 57-74. [5] Clayton R. N. (1993) *Annu. Rev. Earth Planet. Sci. 21,* 115-149. [6] Russell S. S. et al. (1996) *Science, 273,* 757-762. [7] Guan Y. et al. (2002) *LPS, XXXIII,* Abstract #2034. [8] Grossman J. N. et al (1995) *Meteoritics, 30,* 514.

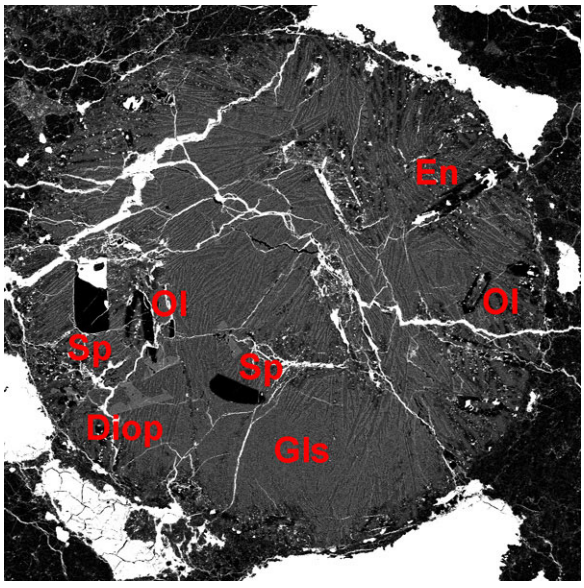


Fig. 1 Backscatter electron image of the Al-rich chondrule L2003-1 from LEW 87220. The chondrule is about 420 μm in diameter.

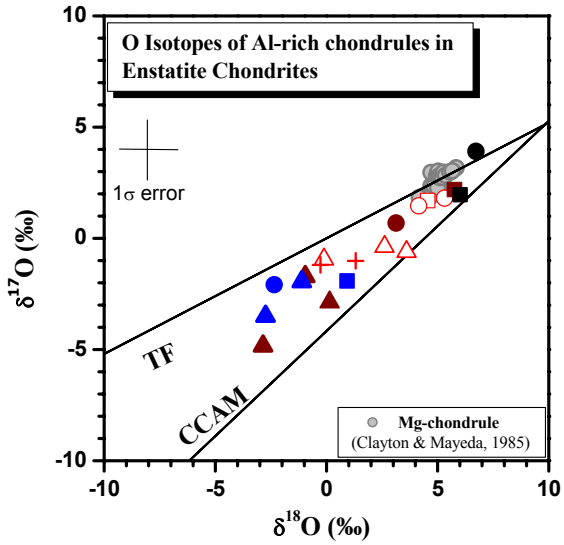


Fig. 2. Oxygen isotopic compositions of Al-rich chondrules in unequilibrated enstatite chondrites. Data points are color-coded for each individual chondrule. E4642-1 –blue; L2003-1 –red; L2003-2 –brown; E4640-2 –black. Triangle –spinel; Circle –anorthite or glass; Square –diopside; Cross –olivine.

**CATHODOLUMINESCENCE (CL) SPECTRAL STUDY OF EXPERIMENTALLY SHOCK-DEFORMED PLAGIOCLASE.** A. Gucsik[1], K. Ninagawa[2], H. Nishido[3], S. Toyoda[4], A. Tsuchiyama[5], A. Bidló[6] and K. Brezsnyánszky[7],[1]University of West Hungary, Bajcsy-Zs. u. 4., Sopron, H-9400, Hungary. E-mail:ciklamensopron@yahoo.com, [2]Okayama University of Science, 1-1 Ridai-cho, Okayama, Japan, [3]Okayama University of Science, 1-1 Ridai-cho, Okayama, Japan, [4]Okayama University of Science, 1-1 Ridai-cho, Okayama, Japan, [5]Osaka University, 1-1 Machikaneyama-cho, Toyonaka, Osaka, Japan, [6]University of West Hungary, Bajcsy-Zs. u.4., Sopron, H-9400, Hungary. [7]Geological Institute of Hungary, Stefánia út. 14., Budapest, H-1143, Hungary.

**Introduction:** Cathodoluminescence (CL) spectral properties of shocked plagioclase samples have previously been investigated in detail [1-4]. These authors observed that shock metamorphism causes peak shifts from green towards red wavelengths, peak broadening, decrease of luminescence intensity and disappearance of the crystal field sensitive $Mn^{2+}$ and $Fe^{3+}$-related peaks resulting from breakdown of the crystal structure (i.e., occurrence of diaplectic glass) at around 35 GPa. Here, we present the results of cathodoluminescence spectra, which were performed on experimentally shocked (shock pressures from 20 to 40 GPa) plagioclase specimens. The purpose of this study is to further investigate the capability of the CL technique to identify shock metamorphic effects in the shocked plagioclase.

**Experimental Procedure:** The samples (An20, An40 and An80) were subjected to shock pressures of 20, 30, 40, and 50 GPa (using the propellant gun at Institute for Material Research, Tohoku University, Japan). However, only the An40 samples were selected for this study, because they show better quality than the other grains. CL spectra were recorded (at Okayama University of Science, Japan) in the wavelength range of 300-800 nm, with 1 nm resolution by the photon counting method using a photomultiplier detector, Hamamatsu Photonics R2228.

**Results and Discussion:** Unshocked plagioclase shows a broad peak at around 580 nm related to Mn(II) activator, whereas both samples shocked at 20 and 30 GPa exhibit similar single broad peak at around 620 nm. But comparison of CL intensity among these samples might be difficult in such scheme due to a scanty CL measurement of the sample shocked at 20 GPa and the effect of surface condition on CL spectrum. The sample shocked at 40 GPa proves the reduction of CL intensity at around 620 nm and an enhancement of a peak at 450 nm is related to defect center (Fig. 1). A broad band at around 325 nm and a shoulder band of the Mn-related broad peak at 580 nm of the unshocked sample are related to the defect centers (Fig. 1). Decreasing of the luminescence, peak intensity and disappearance of the crystal field sensitive $Mn^{2+}$-related peaks at 30 and 40 GPa samples are in a good agreement with the previous studies indicating the formation of the shock-induced diaplectic glass. Consequently, changes in CL spectra of the shocked plagioclase, including peak broadening, peak disappearances or shifts, and decreases in peak intensities are related not only to local variations in the crystal field strength, such as distance changes between coordinated $-O^-$ and $Mn^{2+}$ activator ion, but also to changes (lacking or absence of recombination centers) of the distance between electron traps in the band gap between the conduction and valance bands. Moreover, this study can aid to determine whether or not CL effects in the shocked plagioclase are characteristic for particular shock pressure stages. This study might help to understand the nature of shock waves during the formation of chondrites and high-temperature-and pressure processes in the protoplanetary disk.

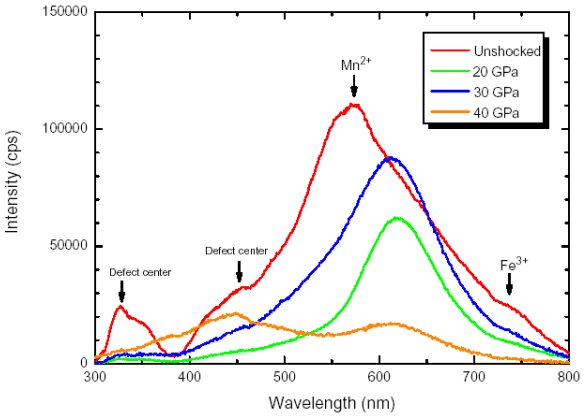


**Figure 1.** CL spectra of unshocked (An40-andesine) and shocked (20, 30, and 40 GPa) plagioclase samples (An40).

*Acknowledgement:* AG was supported by JSPS, Japan. We thank C. Koeberl (Univ. Vienna, Austria) for the helpful comments.

[1] Sippel R. F. and Spencer A. B. (1970) *Proc. Apollo 11 LPS, Geochim. Cosmochim. Acta, Suppl. 1,*Levinson A.A. (ed), Pergamon, New York, 2413–2426. [2] Götze et al. (1999) *Am. Miner., 84,* 1027-1032. [3] Kaus A. and Bischoff A. (2000) *Meteoritics and Planet. Sci.* 35, A86. [4] Marshall D.J. (1988) In: Marshall D.J (ed.) Allen and Unwin, London. p. 57.